


1-1-2010

# Characterization Of Arsd: An Arsenic Chaperone For The Arsab As(iii)-Translocating Atpase

Jianbo Yang  
*Wayne State University*

Follow this and additional works at: [http://digitalcommons.wayne.edu/oa\\_dissertations](http://digitalcommons.wayne.edu/oa_dissertations)

 Part of the [Biochemistry Commons](#), [Molecular Biology Commons](#), and the [Toxicology Commons](#)

---

## Recommended Citation

Yang, Jianbo, "Characterization Of Arsd: An Arsenic Chaperone For The Arsab As(iii)-Translocating Atpase" (2010). *Wayne State University Dissertations*. Paper 37.

This Open Access Dissertation is brought to you for free and open access by DigitalCommons@WayneState. It has been accepted for inclusion in Wayne State University Dissertations by an authorized administrator of DigitalCommons@WayneState.

**CHARACTERIZATION OF ArsD: AN ARSENIC  
CHAPERONE FOR THE ArsAB AS(III)-TRANSLOCATING ATPase**

by

**JIANBO YANG**

**DISSERTATION**

Submitted to the Graduate School

of Wayne State University,

Detroit, Michigan

in partial fulfillment of the requirements

for the degree of

**DOCTOR OF PHILOSOPHY**

2010

MAJOR: BIOCHEMISTRY AND MOLECULAR  
BIOLOGY

Approved by:

\_\_\_\_\_  
Advisor                      Date

\_\_\_\_\_

\_\_\_\_\_

\_\_\_\_\_

\_\_\_\_\_

**DEDICATION**

**To**

**My family**

## ACKNOWLEDGMENTS

I owe my deepest gratitude to my supervisor, Dr. Barry Rosen, whose encouragement, guidance and support from the initial to the final level enabled me to develop my project. I am also heartily thankful to my committee members, Dr. Douglas Ruden, Dr. Jianjun Wang and Dr. Timothy Stemmler who assisted me in the right direction of my graduate research.

I wish to recognize Dr. Hiranmoy Bhattacharjee and Dr. Yung-Feng Lin for their advice in my research, Dr. Jie Qin and Dr. Hung-Chi Yang for their helps on setting up ICP-MS experiment, Dr. Xiang Ruan and Dr. Hsueh-Liang Fu for helps on enzymatic assay, Dr. Jun Ye and Dr. Abdul Ajees Abdul Salam for the discussions on ArsD and ArsA structure, Dr. Timothy Stemmler and Ms. Swati Rawat for their help on EXAFS experiment. I would also like to thank all of my present and past laboratory colleagues: Dr. Yuling Meng, Dr. Zijuan Liu, Dr. Ashoka Kandegedara, Ms. Ju Sheng, Dr. Paul Kraft, Dr. Thiyagarajan Saravanamuthu, Dr. Yao Zhou, Dr. Yoshinaga Masafumi, Dr. Xuan Jiang, Dr. Kavitha Mannem and Mr. Jitesh Pillai. I want to express my thanks to all the faculties and staffs in our department who continuously supported me with advice and friendship. I also want to offer my regards and blessings to all alumni, friends and Chinese community at Wayne State University who supported me in any respect during the completion of the project.

Lastly, I am grateful to have strong support from my parents and my relatives in China during my study at Wayne State University.

## TABLE OF CONTENTS

Dedication .....	ii
Acknowledgements .....	iii
List of Tables.....	viii
List of Figures.....	ix
CHAPTER 1 – Review of the Literature .....	1
1.1 The toxicity of arsenic .....	1
1.1.1 Ubiquitous existence of arsenic in the environment.....	1
1.1.2 Health effect of arsenic .....	4
1.1.3 Medical application of arsenic.....	5
1.1.4 Mechanisms of arsenic toxicity .....	7
1.2 Arsenic detoxification .....	8
1.2.1 Arsenic uptake systems .....	8
1.2.2 Arsenic metabolism.....	10
1.2.3 Extrusion systems.....	13
1.3 ArsA and ArsD from <i>E. coli</i> R773 plasmid .....	15
1.3.1 Co-existence of ArsA and ArsD in <i>ars</i> operons.....	15
1.3.2 ArsA ATPase .....	16
1.3.3 Evidence of physical interaction between ArsD and ArsA.....	18
1.3.4 Cell biology of ArsD function .....	19
1.3.5 Biochemistry of ArsD function.....	21
1.3.6 Metalloid binding sites in ArsD.....	22
1.3.7 Proposed mechanism of metalloid transfer from ArsD to ArsA .....	24
1.4 Other metallochaperones.....	25

1.4.1	Copper chaperones .....	26
1.4.2	Iron chaperones .....	29
1.5	Summary .....	30
CHAPTER 2 - Arsenic binding and transfer by the ArsD As(III) metallochaperone .....		33
2.1	Introduction .....	33
2.2	Materials and methods.....	34
2.2.1	Strains, plasmids and media .....	34
2.2.2	DNA manipulation and mutagenesis.....	35
2.2.3	Protein expression and purification .....	36
2.2.4	Circular dichroism measurements.....	37
2.2.5	X-ray absorption spectroscopy (XAS).....	37
2.2.6	Fluorescence measurements.....	39
2.2.7	ATPase activity assays .....	40
2.2.8	Metalloid transfer assays .....	40
2.3	Results .....	41
2.3.1	Cys12, Cys13 and Cys18 form a three-coordinate As(III) binding site in ArsD .....	41
2.3.2	Tryptophan fluorescence reports trivalent metalloid binding by ArsD .....	42
2.3.3	Effect of cysteine substitutions on As(III) binding.....	44
2.3.4	Reduced glutathione increases the rate of binding of As(III) to ArsD but not ArsA <i>In vivo</i> .....	44
2.3.5	ArsD transfers As(III) directly to ArsA .....	47
2.3.6	Transfer of As(III) from ArsD to ArsA requires catalysis.....	48
2.4	Discussion .....	49

CHAPTER 3 - Correlation between ArsD dimerization and metallochaperone function.....	53
3.1 Introduction .....	53
3.2 Materials and methods.....	54
3.2.1 Strains, plasmids and media .....	54
3.2.2 DNA manipulation and mutagenesis.....	55
3.2.3 Protein expression and purification.....	56
3.2.4 Gel-filtration chromatography.....	56
3.2.5 ATPase activity assays .....	57
3.2.6 Generation of a random mutated library of PCR fragments.....	58
3.2.7 Yeast two-hybrid analysis .....	58
3.2.8 Sequencing of ArsD mutant genes in yeast colonies .....	59
3.3 Results.....	60
3.3.1 Dimerization equilibria of MBP-ArsD109 and His6-ArsD109.....	60
3.3.2 Mutations at the putative dimerization interface shift ArsD to a monomer .....	61
3.3.3 Generating an ArsD mutant with weaker dimerization .....	62
3.4 Discussion .....	64
 CHAPTER 4 – Mapping ArsA-ArsD interaction interface by genetic analysis .....	 68
4.1 Introduction .....	68
4.2 Materials and Methods.....	72
4.2.1 Reagents .....	72
4.2.2 Strains, plasmids and media.....	73
4.2.3 DNA manipulation and mutagenesis.....	74
4.2.4 Generation of a random mutated library of PCR fragments.....	74

4.2.5	Yeast two-hybrid analysis .....	75
4.2.6	Sequencing of ArsD and ArsA mutant genes in yeast colonies .....	76
4.2.7	Protein expression and purification .....	76
4.2.8	ATPase activity assays .....	77
4.2.9	Acetylation of lysine by Sulfo-NHS acetate .....	78
4.2.10	Metalloid binding assay .....	79
4.3	Results .....	79
4.3.1	ArsD mutants showing stronger interaction with ArsA .....	79
4.3.2	Lys37 and Lys62 are involved in interaction with ArsA .....	81
4.3.3	ArsD mutants showing weaker interaction with ArsA .....	84
4.3.4	ArsA mutants restoring interaction with ArsD mutants .....	86
4.3.5	ArsA mutants showing stronger interaction with ArsD .....	86
4.4	Discussion .....	87
	References .....	150
	Abstract .....	173
	Autobiographical Statement .....	177



## LIST OF TABLES

Table 2-1	Strains and plasmids used in CHAPTER 2 .....	93
Table 2-2	Oligonucleotide primers used in CHAPTER 2.....	95
Table 2-3	Summaries of the best-fit parameters from the ArsD <sub>1-109</sub> -As EXAFS fitting analysis.....	97
Table 3-1	Strains and plasmids used in CHAPTER 3 .....	98
Table 3-2	Oligonucleotide primers used in CHAPTER 3.....	100
Table 4-1	Summary of study of interaction between copper-chaperone proteins and their targets.....	102
Table 4-2	Strains and plasmids used in CHAPTER 4 .....	103
Table 4-3	Oligonucleotide primers used in CHAPTER 4.....	106
Table 4-4	ArsD mutations increasing or decreasing ArsA-ArsD interaction .....	110

## LIST OF FIGURES

Figure 1-1	Structure of R773 ArsA ATPase .....	111
Figure 2-1	Normalized XANES spectra of ArsD and its derivatives .....	112
Figure 2-2	ArsD EXAFS data and simulations .....	113
Figure 2-3	ArsD109 tryptophan mutants fold normally and have same activity as wild type.....	114
Figure 2-4	Protein fluorescence of single tryptophan derivatives T15W and V17W reports metalloid binding.....	116
Figure 2-5	Binding of As(III) by single tryptophan derivatives T15W and V17W and cysteine mutants.....	117
Figure 2-6	GSH accelerates binding of As(III) binding by V17W.....	118
Figure 2-7	As(GS) <sub>3</sub> is the metalloid donor to ArsD.....	119
Figure 2-8	As(GS) <sub>3</sub> does not activate ArsA.....	120
Figure 2-9	GSH helps cooperation of ArsA and ArsD .....	121
Figure 2-10	ArsD channels As(III) to ArsA .....	123
Figure 2-11	Metalloid transfer from ArsD occurs during ArsA catalysis .....	124
Figure 2-12	Model of transfer from As(GS) <sub>3</sub> to ArsD to ArsA.....	125
Figure 3-1	MBP-ArsD109 and His6-ArsD109 both stimulate ArsA ATPase activity .....	126
Figure 3-2	Dimerization equilibrium states of MBP-ArsD109 and His6-ArsD109 ....	127
Figure 3-3	ArsD dimerization interface in crystal structure.....	128
Figure 3-4	His6-tag ArsD109 <sub>S68A/R87A/R96A</sub> shifts equilibrium to monomer and still activates ArsA ATPase activity .....	129
Figure 3-5	Dimerization equilibrium of His6-ArsD109 <sub>G86E</sub> shifts to monomer.....	131
Figure 3-6	His6-ArsD109 <sub>G86E</sub> activates ArsA ATPase.....	132

Figure 3-7	Comparison of R773 ArsD structure and <i>Bacteroides vulgatus</i> ATCC 8482 ArsD.....	133
Figure 3-8	ArsD <sub>P52L</sub> dimerize more strongly with wild type ArsD in yeast two-hybrid.....	134
Figure 3-9	A hypothetical dimerization interface .....	135
Figure 4-1	ArsD mutants showing stronger interaction with ArsA .....	136
Figure 4-2	Mutating Lys37 and Lys62 to alanine abolishes ArsD function as an arsenic chaperone .....	137
Figure 4-3	Acetylation of Lys37 and Lys62 sabotages ArsD metallochaperone function .....	139
Figure 4-4	ArsD <sub>K2/104A-K37/62A</sub> still binds As(III) but does not interact with ArsA .....	140
Figure 4-5	ArsD mutants showing weaker interaction with ArsA and the corresponding complementary ArsA mutants .....	142
Figure 4-6	ArsA mutants showing stronger interaction with ArsD .....	144
Figure 4-7	Mapping mutations on ArsD structure.....	145
Figure 4-8	Mapping mutations on ArsA structure .....	146
Figure 4-9	Comparison of ArsA and Get3 structure .....	147
Figure 4-10	Structure model of ArsA-ArsD complex .....	149

## CHAPTER 1

### Review of the Literature

#### 1.1 The toxicity of arsenic

Arsenic (As) is a toxic metalloid that displays some of the properties of both metals and nonmetals. Arsenic has two biologically important oxidation states, As(V) and As(III). Arsenate is also called arsenic acid ( $\text{H}_3\text{AsO}_4$ ). And arsenite is called arsenous acid ( $\text{H}_3\text{AsO}_3$ ) or arsenic trioxide ( $\text{As}_2\text{O}_3$ ). Arsenic is widely distributed in the whole biosphere, which our life is dependent on. Human are exposed to arsenic by drinking water or eating food contaminated with arsenic. Antimony (Sb) is another toxic metalloid in the same group as arsenic in the period table. They share similar chemical properties. Chronic exposure to arsenic is related to skin lesions, neurological effects, high blood pressure, diabetes mellitus, diseases of the respiratory system, cardiovascular disease, and cancers typically involving the skin, lung, and bladder (Rahman et al., 2009).

##### 1.1.1 Ubiquitous existence of arsenic in the environment

Arsenic is widely distributed throughout the earth's crust at an average concentration of 2-3 mg/kg; arsenopyrite ( $\text{FeAsS}$ ) is the most abundant arsenic-containing mineral (Cullen and Reimer, 1989; Peters et al., 1996). Natural processes like weathering of rocks and volcanic emissions, and human activities such as combustion of fossil fuels, mining, smelting of ores or the application of arsenical pesticides, herbicides and wood preservatives, are the main sources which contribute to arsenic contamination in the environment.

Weathering of rocks leads to mobilization of the soluble oxoanions, arsenite and arsenate, and these are the dominant forms of arsenic in fresh water and in seawater. The concentrations of arsenic in fresh water vary between 1 to 100  $\mu\text{g/L}$  or even more. The concentration of arsenic in the world's oceans is at  $\sim 1\text{-}2 \mu\text{g/L}$  (Francesconi, 2005). Arsenic in ground water is largely the result of minerals dissolving from weathered rocks and soils. High concentrations of arsenic in ground water became a problem in recent years, due to the shortage of usable surface water. The use of deep tubewells for water supply in the Ganges Delta causes serious arsenic poisoning to large numbers of people in India (Kim et al., 2002). Arsenic contamination of ground water is prevalent in many countries throughout the world including India, Bangladesh, Thailand, Taiwan, and Mainland China.

Anthropomorphic sources include arsenical-containing fungicides, pesticides and herbicides, insecticides, rodenticides, wood-preserved, animal feeds, paints, dyes, and semiconductors. Lead arsenate was used to control the codling moth from the 1800s to the 1940s (when DDT became available). CCA (chromated copper arsenate) is the best known of the arsenical wood preservatives. The treated wood has a characteristic greenish tint. This wood has been widely used in decks and play structures. Arsenic is still being used in lawn and turf herbicides. Products with names like All-In-One Weed Killer, Crabgrass Killer, and Liquid Edger contain various arsenic compounds. Conventional poultry farmers often feed chickens roxarsone, one of many drugs approved by the Food and Drug Administration for the purpose to kill microbes but actually containing arsenic. Arsenic helps remove impurities during glass making. It is also used as a colorant in fireworks and a doping material in semiconductor

manufacturing. In the end, all of these arsenics will end up somewhere, usually in topsoil and water, where arsenic could be enriched by crops and enters the food chain.

Arsenic will accumulate in crops if the crops are irrigated with arsenic contaminated water or grown in the soils contaminated by arsenic from herbicide or insecticide. As one of the most popular crops in the world, rice is of particular concern (Williams et al., 2005). Flooded soils, in which paddy rice is cultivated, lead to rapid mobilization of arsenite (As(III)), which becomes available for rice to take up (Xu et al., 2008). Among the cereals, rice accumulates relatively high proportions of arsenic in its edible parts. Rice grain contains arsenic that range from 0.08 to 0.20 mg/kg if grown on non-contaminated soils (Zavala and Duxbury, 2008). It could be as high as 2.0 mg/kg if rice is grown in contaminated areas (Tripathi et al., 2007).

Arsenic contamination of drinking water is a serious environmental problem worldwide because of the large number of contaminated sites that have been identified and the large number of people at risk (Chappell et al., 1997). An estimated 100 million people in more than 70 countries are at risk of exposure to unacceptable arsenic levels in either well water or ground water. This has become a major public health issue in the developing world, primarily Bangladesh and surrounding countries, where many thousands of individuals are suffering from precancerous arsenic-related disease. In 2001, the US Environmental Protection Agency lowered the Maximum Contaminant Level (MCL) in drinking water from 50 µg/L to 10 µg/L. The World Health Organization (WHO) standard is also 10 µg/L. There are many locations in the United States where groundwater contains arsenic concentrations in excess of the new standard of 10 µg/L <<http://water.usgs.gov/nawqa/trace/arsenic/>>.

As a consequence of its environmental pervasiveness, exposure and health effects, arsenic ranks first on the United States Government's Comprehensive Environmental Response, Compensation, and Liability (Superfund) Act Priority List of Hazardous Substances. <<http://www.atsdr.cdc.gov/cercla/05list.html>>

### 1.1.2 Health effect of arsenic

Humans are exposed to arsenic mainly through either oral or inhalation routes. Oral exposure occurs via consumption of contaminated water, food and drugs. Occupational exposure occurs mainly through inhalation via semiconductor and glass manufacturing, or power generation by the burning of arsenic-contaminated coal (Yager and Wiencke, 1993). Large dose of arsenic exposure will cause acute toxicity including gastrointestinal discomfort, vomiting, diarrhea, bloody urine, anuria, shock, convulsions, coma, and death. The toxicity of arsenic is related to the chemical form and its oxidative state. Dimethyl arsenate (DMAs(V)) and methylarsenate (MAs(V)) are less toxic, than As(V). The sequence is as the following, DMAs(V),MAs(V)<As(V)<As(III)<MAs(III) (Hughes, 2002). General noncarcinogenic symptoms of chronic arsenic poisoning in humans are weakness, loss of appetite and energy, loss of hair, hoarseness of voice, loss of weight, and mental disorders (Hindmarsh and McCurdy, 1986). Following absorption of trivalent or pentavalent arsenic compounds, arsenic is initially accumulated in the liver, kidney, lung, spleen, aorta, and skin. One of the hallmarks of chronic toxicity in humans from oral exposure to arsenic are skin lesions, which are characterized by hyperpigmentation, hyperkeratosis, and hypopigmentation (Cebrian et al., 1983). In Taiwan, Blackfoot Disease, a peripheral vasoocclusive disease which leads to gangrene of the extremities, is also observed in individuals chronically exposed

to arsenic in their drinking water (Tseng, 1977). Other targets include nervous system (peripheral neuropathy) (Valentine et al., 1982), and vascular system (Wu et al., 1989).

Inorganic arsenic is classified by the International Agency for Research on Cancer (Higginson and DeVita, 1980) and the U.S. Environmental Protection Agency (EPA, 1988) as a human carcinogen. Epidemiological studies have revealed an association between arsenic concentrations in drinking water and increased incidences of skin cancers (including squamous cell carcinomas and multiple basal cell carcinomas), as well as cancers of the liver, bladder, respiratory and gastrointestinal tracts (Chen et al., 1985; Chen et al., 1986; Smith et al., 1992). In the past few decades, arsenic exposure has attracted great interest, due to occupational disease of lung cancer among copper smelter workers, and the connection with increased risk of skin, lung and bladder cancers.

### **1.1.3 Medical application of arsenic**

Although arsenic is toxic, few things in this world are completely evil. Arsenic compounds have also been used to treat diseases like trypanosomiasis and promyelocytic leukemia. Roughly a century ago, arsenic formed the structural centerpiece of arsphenamine, known as Salvarsan or Compound 606, this molecule was the first wonder drug: the cure for syphilis. Arsphenamine was soon followed by neoarsphenamine, which was water-soluble and easier to administer (Sneader, 1985). These drugs were used for syphilis chemotherapy for forty years, until the advent of penicillin rendered them obsolete.

In the realm of inorganic arsenic, arsenic trioxide ( $As_2O_3$ ), solubilized as the arsenite salt of an alkali metal, is a prominent medicinal compound. In the 18th century,



Dr. Thomas Fowler developed a therapeutic agent known as Fowlers solution by combining arsenic trioxide with potassium bicarbonate (Scheindlin, 2005). Throughout the 19th century Fowler's Solution was deemed a useful alternative to quinine for malaria, and there were also claims of beneficial effects in syphilis and sleeping sickness. It was also sporadically tried for the treatment of leukemia and found effective for inducing remission in chronic myelogenous leukemia (CML). In the early 1970s, some Chinese physicians, analyzing a number of traditional preparations used in treating cancer, found  $As_2O_3$  to be a common component of these products. They proceeded to test the compound in a variety of cancers, and obtained remission rates of 90% in relapsed acute promyelocytic leukemia (APL) (Niu et al., 1999). Recent studies show that arsenic directly targets to cysteine residues in zinc fingers within PML-RARalpha and PML. Arsenic binding induces PML oligomerization, which increases its interaction with the small ubiquitin-like protein modifier (SUMO)-conjugating enzyme UBC9, resulting in enhanced SUMOylation and degradation (Zhang et al., 2010). Further research on anticancer activity of arsenic is still going on. Preliminary results have been reported on various diseases such as multiple myeloma (MM), acute lymphoblastic leukemia (ALL) and myelodysplastic syndrome (MDS) (Verstovsek and Estrov, 2004).

There are also organic arsenic derivatives under development. Organic phenylarsenic acid (PAA) compounds with potent *in vitro* activity against human acute lymphoblastic leukemia cells showed 50% inhibition of cell growth (Liu et al., 2003). S-dimethylarsino-glutathione has been identified as a lead compound among more than 100 derivatives and is currently being developed for clinical use by ZIOPHARM

Oncology, Inc. A Phase II trial is nearing completion in patients with primary liver cancer and advanced myeloma, a Phase II trial is ongoing in patients with lymphomas, and a Phase I oral trial is in progress.

#### 1.1.4 Mechanisms of arsenic toxicity

Arsenic occurs predominantly in inorganic form as arsenate (As(V)) and arsenite (As(III)). Pentavalent Arsenate is an analogue of phosphate and thus interferes with essential cellular processes such as oxidative phosphorylation and ATP synthesis. For example, arsenate reacts *in vitro* with glucose to form glucose-6-arsenate, which resembles glucose-6-phosphate, can inhibit hexokinase (Lagunas, 1980). At both the substrate and mitochondrial level, arsenolysis diminishes *in vitro* formation of ATP by the replacement of phosphate with arsenate in the enzymatic reactions. Depletion of ATP by arsenate has been observed in cellular systems (Gresser, 1981). ATP levels are reduced in rabbit (Delnomdedieu et al., 1994b) and human erythrocytes (Winski and Carter, 1998) after *in vitro* exposure to arsenate.

The toxicity of trivalent arsenite is due to its propensity to bind to sulfhydryl groups, with consequent detrimental effects on general protein functioning. A main target is pyruvate dehydrogenase (PDH), which is a multi subunit complex that requires the cofactor lipoic acid, a dithiol, for enzymatic activity. Arsenite inhibits PDH (Szinicz and Forth, 1988), perhaps by binding to the lipoic acid moiety. Lipoate is needed in the formation of acetyl-CoA from pyruvate and in the formation of succinyl-CoA from alpha-ketoglutarate. Therefore, arsenic blocks the Krebs Cycle and interrupts oxidative phosphorylation, resulting in a marked depletion of cellular ATP and eventually death of the metabolizing cell. Other targets include numerous other cellular enzymes, which are

involved in cellular glucose uptake, gluconeogenesis, fatty acid oxidation and production of glutathione. The binding of arsenite to the critical sulfhydryl groups in these enzymes, interferes the normal protein function and lead to toxicity.

Reactive oxygen species can be induced by arsenite that can eventually alter the redox status of the cell and present a stressful and toxic situation and induce large deletion mutations in hamster-human hybrid cells (Hei et al., 1998). Many mechanism of arsenic carcinogenicity have been proposed, including genotoxicity, cell proliferation, altered DNA repair and DNA methylated oxidative stress, co-carcinogenesis, and tumor promotion (Hughes, 2002). DMAs has the potential to promote rat urinary bladder carcinogenesis and one of the mechanisms involved is its stimulation of cell proliferation in the urinary bladder epithelium (Wanibuchi et al., 1996). A significant dose-dependent decrease in activity of a DNA repair enzyme, poly-(ADP-ribose)polymerase by arsenite was observed (Yager and Wiencke, 1997).

## **1.2 Arsenic detoxification**

In response to the ubiquity of arsenic in the environment and to counteract the deleterious effects of arsenic, nearly every organism, from *E. coli* to human, evolved resistance strategies, including arsenite oxidation or methylation into less toxic species, as well as active extrusion of arsenite from the cell (Rosen, 2002).

### **1.2.1 Arsenic uptake systems**

In solution at neutral pH, arsenic acid exists as the arsenate oxyanion. Since arsenate is very similar with phosphate, the phosphate transporters are usually hijacked to catalyze the arsenate uptake. In the prokaryote *E. coli*, there are two phosphate transporters, Pit and Pst (Rosenberg et al., 1977). Both catalyze arsenate uptake, but

the Pit system appears to be the predominant system for arsenate (Willsky and Malamy, 1980). Similarly, in the eukaryote *Saccharomyces cerevisiae* several phosphate transporters, such as PHO84 (Bun-Ya et al., 1992), PHO86 and PHO87 (Bun-ya et al., 1996), participate in arsenate uptake. Specific arsenate transporters have been identified in plant that are believed to mediate a large part of the observed arsenate influx and these include the *A. thaliana* Pht1;1 and 1;4 high and medium affinity phosphate uptake systems (Shin et al., 2004). Human AQP9 expressed in *Xenopus laevis* oocytes increased the uptake of MAs(V) and DMAs(V), two major pentavalent arsenic cellular metabolites (McDermott et al., 2010).

The pKa of arsenous acid is 9.2. At neutral pH, it is present in solution primarily as neutral  $\text{As}(\text{OH})_3$  (Ramirez-Solis et al., 2004), which might be considered an inorganic equivalent of glycerol. Recently, arsenite uptake was found through aquaglyceroporins in bacteria, yeast and mammalian cells. A screen of a random mutagenesis *E. coli* library turned up that mutation in GlpF leads to resistance to Sb(III) (Sanders et al., 1997). The chemical properties of Sb(III) and As(III) are very close, and, even though the mutant did not exhibit increased arsenite resistance, GlpF was shown to increase As(III) uptake if it is overexpressed in *E. coli* (Meng et al., 2004). *S. cerevisiae* cells with *FPS1* gene deleted are more sensitive to arsenite, indicating that the glycerol channel Fps1p mediates uptake of arsenite and antimonite (Wysocki et al., 2001). *Xenopus laevis* oocytes microinjected with either mouse AQP7 or rat AQP9 cRNA exhibited increased transport of As(III), which suggests that AQP9 and AQP7 may be major routes of arsenite uptake into mammalian cells (Liu et al., 2002). The ability of the four known human members of the aquaglyceroporin family, hAQP3, hAQP7, hAQP9, and

hAQP10, to facilitate  $\text{As}(\text{OH})_3$  movement in *Xenopus* oocytes was also examined. The order of effectiveness as an  $\text{As}(\text{III})$  transporter was found to be hAQP9 > hAQP7, with little or no transport by hAQP3 or hAQP10 (Liu et al., 2004b). AQP9 was also shown to be able to transport  $\text{MAs}(\text{III})$  (Liu et al., 2006b). In *S. cerevisiae* cells, hexose permeases are found to be involved in arsenite uptake (Liu et al., 2004a). Human and rat GLUT1 catalyzed uptake of both  $\text{As}(\text{OH})_3$  and  $\text{CH}_3\text{As}(\text{OH})_2$  in oocytes (Liu et al., 2006a). Plants take up arsenite significantly if they are grown in reducing environments such as paddy-grown rice and aquatic species. It was hypothesized that plants also take up arsenite through aquaporins (Meharg and Jardine, 2003), although the molecular identity of the proteins that participate in uptake, efflux, compartmentation and long-distance transport of  $\text{As}(\text{III})$  is largely unknown. Heterologous expression of NIPs, a subfamily of plant aquaporins, in yeast, confirmed the arsenite transport capacity of AtNIP7;1 and OsNIP2;1, but in addition showed that all group II NIPs are capable of arsenite transport (Bienert et al., 2008).

### 1.2.2 Arsenic metabolism

After arsenic is taken up into the cells, usually it is metabolized intentionally or adventitiously by reduction, oxidative methylation and glutathione conjugation, and then it is pumped out of the cell or sequestered in intracellular organelles.

When the pentavalent oxyanion arsenate is taken up, it is reduced to  $\text{As}(\text{III})$  prior to extrusion or sequestration. Three independently evolved families of arsenate reductase enzymes have been recognized (Mukhopadhyay et al., 2002). The product of *arsC*, the last gene of the *ars* operon of *E. coli* plasmid R773 is an arsenate reductase, which belongs to the first family. R773 ArsC uses glutaredoxin as the reducing agent

and only has one cysteine residue participating in the reaction. The crystal structure of the 16-kDa R773 ArsC has been reported with bound substrate (arsenate) and product (arsenite) (Martin et al., 2001). A second family of arsenate reductases also widely distributed in bacteria is represented by the *arsC* gene product of *Staphylococcus aureus* plasmid pI258 (Ji and Silver, 1992). The pI258 enzyme uses thioredoxin as the source of reducing potential (Ji et al., 1994) and has two intramolecular cysteine residues that participate in the catalytic cycle (Messens et al., 1999). The crystal structure of the pI258 ArsC has been solved and this enzyme is related to low molecular-weight protein tyrosine phosphatases and exhibits low-level phosphatase activity (Zegers et al., 2001). The third family of arsenate reductases is related to the superfamily of protein phosphatases that includes CDC25a, a cell cycle phosphatase. Yeast Acr2p and Leishmania LmACR2 both belong to this family. Acr2p has a single active site cysteine residue and uses glutaredoxin and glutathione as reductants (Mukhopadhyay et al., 2000). LmACR2 is a bifunctional protein with both protein tyrosine phosphatase activity and pentavalent antimony reduction activity. It's proposed that the physiological function of LmACR2 is to dephosphorylate phosphotyrosine residues in leishmanial proteins but not to reduce the pentavalent antimony for detoxification (Zhou et al., 2006). Specific arsenate reductases have been identified in many plant species including Arabidopsis (Dhankher et al., 2006), *P. vittata* (Ellis et al., 2006), and rice (Duan et al., 2007). Many plant arsenate reductases are also bifunctional and show tyrosine phosphatase activity. They are homologous to the human cell-cycle dual-specificity phosphatase CDC25.

Metabolic conversion of inorganic arsenic into methylated products is a multistep process that yields mono-, di-, and trimethylated arsenicals. The methylation is proposed to occur by a series of reductions of pentavalent to trivalent arsenicals coupled to oxidative methylations (Challenger, 1945). In recent years, it has become apparent that formation of methylated metabolites of inorganic arsenic is not necessarily a detoxification process, since intermediates and products formed in this pathway may be more reactive and toxic than inorganic arsenic. Toxicity of the arsenic metabolites is  $\text{DMAs(III)} > \text{MAs(III)} > \text{As(III)} > \text{As(V)} > \text{DMAs(V)} > \text{MAs(V)} > \text{TMAOs}$  (Akter et al., 2005). But the final major pentavalent products,  $\text{DMAs(V)}$  and  $\text{TMAOs}$  are approximately a hundred-fold and a thousand-fold less toxic than  $\text{As(III)}$ , respectively (Hirano et al., 2004). Arsenic methylation by fungi and other eukaryotes has been well documented (Bentley and Chasteen, 2002). In rat liver, a novel SAM-dependent pathway has been discovered that involves a 42-kDa methyltransferase (designated *cyt19*) linked to thioredoxin-thioredoxin reductase system (Thomas et al., 2004; Zakharyan et al., 1995). Only recently its homolog, *ArsM*, has been identified in 125 bacteria and 16 archaea, and was characterized in *Rhodopseudomonas palustris*. *ArsM* not only conferred arsenic resistance, but also generates trimethyl arsine gas ( $\text{TMA(III)}$ ). Reduced glutathione was used as the electron donor (Qin et al., 2006). *Cyanidioschyzon sp. isolate 5508* oxidized  $\text{As(III)}$  to  $\text{As(V)}$ , reduced  $\text{As(V)}$  to  $\text{As(III)}$ , and methylated  $\text{As(III)}$  to form  $\text{TMAOs}$  and  $\text{DMAs(V)}$ . Two arsenic methyltransferase genes, *CmarsM7* and *CmarsM8*, were cloned from this organism and demonstrated to confer resistance to  $\text{As(III)}$  in an arsenite hypersensitive strain of *Escherichia coli*. The two recombinant *CmArsMs* were purified and shown to transform  $\text{As(III)}$  into  $\text{MAs(V)}$ ,  $\text{DMAs(V)}$ ,  $\text{TMAOs}$ ,

and TMAs(III) gas, with an optimum temperature around 60-70<sup>0</sup>C (Qin et al., 2009). Since ArsM homologues are widespread in nature, arsenic methylation by microbes is proposed to have an important impact on the global arsenic cycle.

### 1.2.3 Extrusion systems

There are two basic mechanisms of arsenite extrusion. One is carrier-mediated efflux via an arsenite carrier protein, and the other by an arsenite-translocating ATPase (Dey and Rosen, 1995). The most common mechanism of arsenite resistance is efflux from cells catalyzed by members of two different and unrelated families of permeases, ArsB and Acr3.

Majority of bacteria use ArsB, which is found in most *ars* operons, to extrude arsenite. By itself, ArsB is a secondary efflux protein coupled to the protonmotive force and confers a moderate level of arsenite resistance (Kuroda et al., 1997). ArsB transports As(III) but has higher affinity for Sb(III). ArsB is an antiporter that catalyzes the exchange of trivalent metalloid for protons, coupling arsenite efflux to the electrochemical proton gradient (Meng et al., 2004). When ArsA is co-expressed with ArsB, an ArsAB complex is formed that is obligatorily coupled to ATP. ArsB associates with the ArsA ATPase to form a pump that confers high level resistance. ArsB is unique in that it exhibits a dual mode of energy coupling depending on the subunit composition (Dey and Rosen, 1995). Some bacteria have three-gene *arsRBC* operons and extrude arsenite by ArsB alone, while others have five-gene *arsRDABC* operons and use the ArsAB pump (Rosen, 1999). It has been proposed that the five-gene operons arose by insertion of the *arsDA* genes into a three-gene operon (Rosen, 1999, 2002). Recently, ArsD was shown to be an arsenic chaperone. ArsD sequesters the free arsenite in the



cell cytosol, delivers it to the ArsAB pump for extrusion thus confers higher resistance to arsenite than ArsAB pump alone (Lin et al., 2006).

The Acr3 family includes members found in bacteria, archaea and fungi. Unfortunately, many members of the Acr3 family have been given the name ArsB even though they exhibit almost no sequence similarity to ArsB. The first identified member is from in the SKIN element of *B. subtilis* (Sato and Kobayashi, 1998). *S. cerevisiae* Acr3p confers arsenite resistance (Ghosh et al., 1999; Wysocki et al., 1997). Yeast Acr3p favors As(III) as substrate rather than Sb(III). *C. glutamicum* ATCC 13032 has been shown to have three genes for Acr3 homologues, each of which contribute to the high level of arsenite resistance in this organism (Ordonez et al., 2005). Expression of *C. glutamicum* or *Alkaliphilus metalliredigens* *acr3* genes in an arsenite-hypersensitive strain of *E. coli* in which all *ars* genes were deleted confers resistance to As(III). This heterologously expressed Acr3 catalyzes efflux of arsenite from *E. coli*. It exhibits significant differences from R773 ArsB. While ArsB exchanges As(III) with protons, Acr3 does not, but how it is coupled to the proton-motive force is unknown at this point. Like the yeast Acr3p, the *C. glutamicum* Acr3 is also more specific for As(III) than Sb(III), in contrast to ArsB, which has higher affinity for Sb(III) than As(III) (Fu et al., 2009).

In eukaryotic cells, arsenite resistance is mainly conferred by members of the MRP (multidrug resistance-associated protein) group of the ABC superfamily of transport ATPases (Cole et al., 1994; Deeley et al., 2006), which physiologically catalyze export of GS-conjugates such as leukotriene C4 (LTC4) (Leier et al., 1994). MRP1-catalyzed export of glutathione from cells was increased by arsenite, suggesting that MRP1 functions as an As(GS)<sub>3</sub> carrier (Zaman et al., 1995). In the liver MRP2

extrudes arsenic glutathione complexes into bile and may be a major route of arsenic detoxification in humans (Kala et al., 2000). PgpA, another MRP homolog, was also demonstrated to transport  $\text{As}(\text{GS})_3$  in *Leishmania* (Legare et al., 2001). In *S. cerevisiae*, an MRP homolog, Ycf1p, has been shown to transport  $\text{As}(\text{GS})_3$  into the vacuole and confers arsenite resistance in yeast (Ghosh et al., 1999).

### 1.3 **ArsA and ArsD from *E. coli* R773 plasmid**

In bacteria, the genes for arsenic detoxification are usually encoded by arsenic resistance (*ars*) operons. Nearly every sequenced bacterial genome contains an *ars* operon. Many *ars* operons have only three genes, *arsRBC*, where *ArsR* is an As(III)-responsive transcriptional repressor, *ArsB* is a  $\text{As}(\text{OH})_3/\text{H}^+$  antiporter that extrudes As(III), conferring resistance (Meng et al., 2004), and *ArsC* is an arsenate reductase that converts As(V) to As(III), the substrate of *ArsB*, hence extending the range of resistance to include As(V) (Mukhopadhyay and Rosen, 2002). Some *ars* operons have two additional genes, *arsD* and *arsA*, such as the *arsRDABC* operon in *E. coli* plasmid R773, and cells expressing the *arsRDABC* operon are more resistant to As(V) and As(III) than those expressing *arsRBC* operons because *ArsA* forms a complex with *ArsB* that catalyzes ATP-driven As(III)/Sb(III) efflux. While *ArsD* exhibits weak repressor activity (Chen and Rosen, 1997; Wu and Rosen, 1993), its primary function has recently been shown to be as an arsenic metallochaperone that delivers As(III) to the *ArsA* ATPase (Lin et al., 2006). Interaction with *ArsD* increases the affinity of *ArsA* for As(III), producing increased efflux and resistance at environmental concentrations of arsenic.

#### 1.3.1 **Co-existence of *ArsA* and *ArsD* in *ars* operons**

Nearly every sequenced bacterial genome contains an *ars* operon. Although the majority is three-gene *arsRBC* operons, to date, there are more than fifty bacterial and archaeal arsenic resistance operons and gene clusters that contain *arsA* and *arsD* genes. It is striking that *arsA* and *arsD* genes are always found together in *ars* operons. The order of the genes in those operons may differ from each other, but the *arsD* gene nearly always precedes an *arsA* gene. The linkage of these two genes suggests first, that *ArsD* and *ArsA* co-evolved before their association with *ArsB*, second that the *arsDA* genes moved laterally into an *ars* operon as a unit and third, that *ArsD* has a biochemical function related to *ArsA* in arsenic detoxification.

### 1.3.2 *ArsA* ATPase

The 583-residue *ArsA* ATPase is a member of a family of ATPases that probably arose from GTPases (Leipe et al., 2002). It is normally bound to *ArsB* (Dey et al., 1994), but, in the absence of *ArsB*, *ArsA* is found in the cytosol and can be purified as a soluble protein. *ArsA* has two halves, A1 and A2, that are connected by a 25-residue linker (Li and Rosen, 2000). The crystal structure of the enzyme has been determined (Zhou et al., 2000). Three types of domains can be resolved. First, there are two nucleotide-binding domains (NBDs). The NBDs are folded structures that both contain residues from both A1 and A2. A metalloid binding domain (MBD) that binds three As(III) or Sb(III) is located about 20 Å from the NBDs. This is an allosteric site at the opposite end of the protein from the NBDs (Figure 1-1). Of the three Sb(III), one is connected to Cys113 and Cys422 (MBS1), a second to Cys172 and His453 (MBS2), and the third to His148 and Ser420 (MBS3) (Zhou et al., 2000). Each metalloid is bound by two *ArsA* residues. The highest affinity site is composed of Cys-113 and Cys-422

(Ruan et al., 2006), and a third cysteine, Cys-172, can participate in high affinity binding (Ruan et al., 2008). Binding of As(III) or Sb(III) brings the two halves of ArsA together, activating ATP hydrolysis. Connecting the single MBD to the two NBDs are two signature sequences that serve as signal transduction domains (STDs), D<sup>142</sup>TAPTGH<sup>148</sup>TIRLL in A1 (STD1) and D<sup>447</sup>TAPTGH<sup>453</sup>TLLLL in A2 (STD2), that corresponds to the Switch II region of many other nucleotide binding proteins and have been proposed to be involved in transmission of the energy of ATP hydrolysis to metalloid transport (Zhou and Rosen, 1997). In the ArsA structure these sequences are seen as extended stretches of residues physically linking the NBDs through Asp142 and Asp447 at the N-terminal end to the MBD through His148 and His453. Asp142 and Asp447 are Mg<sup>2+</sup> ligands in NBD1 and NBD2, respectively, and His148 and His453 are Sb(III) ligands in the MBD (Zhou et al., 2000). This physical connection between the domains allows ATP hydrolysis at the NBDs to alter the affinity for As(III), and, reciprocally, allows metalloid binding at the MBD to alter the affinity for and rate of hydrolysis of ATP.

Specific spectroscopic probes, single tryptophan residues, were introduced into strategic locations in ArsA. The fluorescent properties of these tryptophan residues change in response to nucleotide binding, hydrolysis and/or conformational changes in domains. The intrinsic fluorescence of Trp159 has allowed real time monitoring of the conformation of ArsA during the individual steps of the catalytic cycle and has allowed modeling of the reaction cycle (Walmsley et al., 1999, 2001). The results suggest that the rate-limiting step in the overall reaction in the absence of metalloid activation is the

isomerization of a longlived conformation of the enzyme, and that binding of metalloid overcomes this rate-limiting step, increasing the rate of hydrolysis.

In the crystal structure NBD1 is occluded and has ADP bound. NBD2 is more open, and ATP can be exchanged into the site (Zhou et al., 2000). This gives the appearance of an alternation of sites, and alternating site mechanisms are found in other transport ATPases. There is good evidence to suggest non-equivalence of the two sites. NBD1 hydrolyzes ATP in the absence of activation while NBD2 does not (Kaur, 1999). For this reason, basal hydrolysis has been termed unisite catalysis. In the presence of metalloid, both sites hydrolyze ATP and participate in multisite catalysis. Two single tryptophan residues, Trp141 and Trp446, had been used to study either NBD1 or NBD2. Trp141 is adjacent to NBD1 and to the N-terminal Asp142 of the A1 signature sequences. Trp446 is in the equivalent position in NBD2, next to Asp447 of the A2 signature sequence. The fluorescent properties of these two mutants allow measurement of the rate of hydrolysis in each site singly. The fluorescent properties of Trp141 clearly show that NBD1 hydrolyzes ATP during unisite catalysis (Zhou and Rosen, 1997). In contrast, Trp446 fluorescence indicates that NBD2 is catalytically inactive until metalloid is bound, that is, only under multisite conditions (Zhou et al., 2002). Although the two NBDs are not equivalent in all respects, the existing data cannot yet distinguish between different functions for the two or alternating sites catalysis.

### **1.3.3 Evidence for physical interaction between ArsD and ArsA**

Yeast two-hybrid analysis demonstrates that ArsD and ArsA physically and specifically interact (Lin et al., 2006). Among the four soluble proteins encoded by the

R773 *arsRDABC* operon, ArsA was found to interact with ArsD but not with the ArsR repressor or the ArsC arsenate reductase; ArsD interacted with ArsA and with itself, which would be expected since ArsD is a homodimer (Chen and Rosen, 1997), but not with ArsR or ArsC; ArsR, which is a homodimer, also interacts with itself, but not with the other proteins. Since there is no arsenic or antimony in yeast cells, ArsD and ArsA must interact in the absence of metalloid. However, when Cys12, Cys13 or Cys18, the residues in ArsD that form the metalloid binding site (described in more detail below), were mutated to serines, the serine-substituted ArsD mutants neither activate ArsA ATPase activity nor bind Sb(III) in this mutated site (Y.F. Lin and B.P. Rosen, unpublished), consistent with the idea that it is the metalloid-bound form of ArsD that activates ArsA. These data suggest that ArsD interacts with ArsA with high affinity when metalloid is bound but with low affinity in the absence of metalloid such as in the yeast cytosol in the two-hybrid assays.

Direct physical interaction between ArsD and ArsA was observed by chemical crosslinking with dibromobimane (dBBr), a fluorogenic, homobifunctional thiol-specific crosslinking reagent that becomes highly fluorescent when its two alkylating groups react with cysteine residues within 3 to 6 Å of each other (Kosower et al., 1980). When the mixture of ArsD and ArsA was reacted with dBBr, a crosslinked species was detected that reacted with both anti-ArsA and anti-ArsD antibodies. MgATP is required for the formation of ArsD-ArsA crosslinked product. These results suggest first that ArsD and ArsA interact at their cysteine-rich metalloid binding sites and second that ArsD interacts with nucleotide-bound form of ArsA.

#### 1.3.4 Cell biology of ArsD function

That *arsD* and *arsA* genes are nearly always found together in *ars* operons implies co-evolution for a common function, most likely arsenic detoxification. Cells co-expressing *arsDAB* were more resistant to high concentrations of As(III) compared to cells expressing only *arsAB*, consistent with interaction of ArsD with ArsA increasing the efficiency of the ArsAB pump (Lin et al., 2006). The concentration of arsenic in such growth experiments is usually in the millimolar range, which might be found in a volcanic area such as Yellowstone National Park, but such concentrations are much greater than would be found under most environmental conditions. To examine whether the presence of a functional *arsD* gene conferred an growth advantage to cells at lower levels of arsenic, two batches of cells of an *E. coli* strain in which the chromosomal *ars* operon had been deleted were mixed together and grown at equal amount in the presence of 10  $\mu$ M sodium arsenite, a concentration present in many deep tube wells in Bangladesh. One batch of cells had a plasmid with only the *arsAB* genes, and the other had the *arsDAB* genes. After a little more than a week, the cells with *arsDAB* had largely replaced those with only *arsAB*, demonstrating that ArsD provides a competitive advantage for growth in soil or water with moderate amounts of arsenic contamination.

Examination of As(III) accumulation in intact cells revealed that ArsD enhances the ability of the pump to extrude As(III) and reduces the intracellular arsenic concentration to subtoxic levels. Cells expressing only *arsB* were able to lower the intracellular level of As(III) compared to a strain with no *ars*, reflecting the ability of ArsB to catalyze  $\text{As(OH)}_3/\text{H}^+$  exchange (Meng et al., 2004). When *arsA* and *arsB* were co-expressed, the cells have more efficient As(III) extrusion than with *arsB* alone (Dey and Rosen, 1995). When *arsD* was co-expressed with *arsAB*, the cells exhibited a further

reduction in As(III) accumulation (Lin et al., 2006). These lines of evidence support the idea that ArsD increases the efficiency of the ArsAB pump. The competitive advantage provided by direct interaction of ArsD with ArsA provides a driving force for the co-evolution of the two genes.

### 1.3.5 Biochemistry of ArsD function

The hallmark of metallochaperones is delivery of metal ions directly to target proteins (Rosenzweig, 2002). The ability of ArsD to transfer Sb(III) to ArsA was shown by mixing Sb(III)-loaded ArsD with ArsA, separating the two proteins and determining how much Sb(III) was bound to ArsA. In the presence (but not the absence) of magnesium and a nucleotide, ArsA was able to extract Sb(III) from ArsD.

Metalloid transfer studies of the transfer of As(III) or Sb(III) from ArsD to ArsA are consistent with a mechanism in which this metallochaperone accelerates the rate of transfer to its partner. However, for ArsD and ArsA, this transfer process is thermodynamically unfavorable because ArsD has higher affinity for metalloid than does ArsA. However, if the metalloid bound to the ArsAB pump is pumped out of the cell, mass action will provide the directionality of the reaction. This suggests that ArsD might not only serve a role in protecting the cell from free metalloid but also in loading ArsA for metalloid extrusion. Indeed, because ArsD has higher affinity for metalloid than ArsA, it can 'scavenge' the cytosol for free metalloid for delivery to ArsA, allowing the ArsAB pump to confer resistance at significantly lower concentrations of As(III). The  $K_m$  of ArsB as a secondary carrier is 0.14 mM (Kuroda et al., 1997), but natural waters range in concentration of total inorganic arsenic from 7 nM to 70  $\mu$ M, and concentrations of arsenic in drinking water in worst arsenic-contaminated wells in West Bengal and



Bangladesh are approximately 40  $\mu\text{M}$  (Smedley and Kinniburgh, 2002). By lowering the concentration of substrate at which the pump functions efficiently, ArsD and ArsA provide cells with a mechanism to respond to environmental concentrations of metalloid.

ArsD not only delivers metalloids to ArsA but also enhances its ATPase activity at low metalloid concentrations. In the presence of ArsD, the apparent affinity of ArsA for As(III) is largely increased but the  $V_{\text{max}}$  remains unchanged in ATPase reactions (Lin et al., 2006). ArsD makes the enzyme more effective at low concentrations of metalloid, a property expected for a metallochaperone. As(III) or Sb(III) activates the ATPase activity of ArsA, so that the increase in affinity of ArsA for metalloids in the presence of ArsD can simply be attributed to the higher affinity of ArsD in the ArsD-ArsA complex, that is, ArsD allows for activation of ArsA ATPase at lower metalloid concentrations. This explains how cells expressing *arsDAB* can rapidly replace cells expressing only *arsAB* at a subtoxic concentration of As(III).

In summary, the increase in ArsA efficiency resulting from interaction with ArsD leads *in vitro* to augmented activity of the ArsAB extrusion pump, to greater resistance in organisms with the *arsDAB* genes, and finally to increased fitness for growth in the low but ubiquitous levels of environmental arsenic.

### 1.3.6 Metalloid binding sites in ArsD

R773 ArsD has three vicinal cysteine pairs, Cys12-Cys13, Cys112-Cys113 and Cys119-Cys120. Alignment of the primary sequence of homologues of R733 ArsD indicates that the cysteine pair Cys12-Cys13 and a single additional cysteine, Cys18 are conserved in homologues. Two other cysteine pairs, Cys112-Cys113 and Cys119-Cys120, are found in some homologues but not others. A series of cysteine mutants

and truncations of ArsD were constructed, purified and studied for the metalloid binding (Lin et al., 2007a). Mutants or truncations with only a single vicinal cysteine pair can still bind to a phenylarsine oxide affinity column, which indicates indirectly that each cysteine pair can form an independent metalloid binding site (Li et al., 2001). In more recent experiments, binding of Sb(III) was measured directly (Lin et al., 2007a). Wild-type R773 ArsD binds three Sb(III) per monomer. If two of the three cysteine pairs were changed to alanine or serine residues, or if the C-terminal vicinal pairs were removed by construction of truncated versions, variants with only a single vicinal pair were found to bind one Sb(III) per monomer, showing directly that each cysteine pair forms an independent metalloid binding site. If the conserved cysteine Cys18 was mutated, the mutant with the only first cysteine pair, Cys12-Cys13, was unable to bind Sb(III). This suggests that the cysteine pair Cys12-Cys13 and Cys18 form a 3-coordinate thiolate metalloid binding site, which has been termed MBS1. The metalloid binding sites formed by cysteine pairs Cys112-Cys113 and Cys119-Cys120 are designated MBS2 and MBS3, respectively. All three binding sites have similar affinity to Sb(III), approximately 1  $\mu$ M.

A truncated ArsD lacking both MBS2 and MBS3 (ArsD<sub>1-109</sub>), still interacted with ArsA in the yeast-two-hybrid assay and had the same stimulatory effect on ArsA ATPase activity as wild-type ArsD (Lin et al., 2007a). In contrast, an ArsD derivative lacking MBS1 but retaining MBS2 (ArsD<sub>1-118,C12A/C13A</sub>) was unable to interact with ArsA in yeast-two-hybrid assay and did not stimulate ArsA activity. These results suggest that MBS1, but not MBS2 or MBS3, participate in metalloid transfer to ArsA and in activation of ArsA ATPase activity. Cells expressing a mutated *arsD*<sub>1-118, C112A/C113A</sub> gene, which

encodes an ArsD derivative having only MBS1, in trans with *arsAB* accumulated As(III) to nearly the same extent as those expressing wild type *arsDAB*. These cells also have a modest reduction in arsenite resistance compared to cells expressing wild type *arsDAB*. However, the cells expressing other ArsD mutants lacking MBS1 (*arsD<sub>C12/C13A</sub>* or *arsD<sub>C18A</sub>*) accumulate slightly more As(III) than cells with only *arsAB* and were no more resistant to As(III) than cells with only *arsAB*. These *in vivo* results strongly support the hypothesis that MBS1 (Cys12, Cys13 and Cys18), but not MBS2 or MBS3, is required for metallochaperone activity.

### 1.3.7 Proposed mechanism of metalloid transfer from ArsD to ArsA

The fact that the MBSs in ArsA and MBS1 in ArsD appear to be involved in interaction suggests that metalloid binding sites in both proteins are brought into close proximity, allowing transfer of metalloid directly from the binding site on ArsD to the binding site on ArsA. It is plausible that this interaction destabilizes the metalloid binding sites on ArsD, reducing its affinity, while stabilizing the metalloid binding sites on ArsA by occluding the metalloid within the complex, thus enabling transfer of metalloid to ArsA. In this manner, the thermodynamically unfavorable process of transferring the metalloid from a high to a low-affinity site could be overcome, although, as mentioned above, this might not be a concern if the transferred metalloid is rapidly extruded from the cell. While the details of metalloid transfer from ArsD to ArsA are unknown at this time, the mechanism of transfer of copper from the metallochaperone CCS to the superoxide dismutase SOD1 is instructive (Lamb et al., 2001; Torres et al., 2001). The cysteine residues of CCS project into the active site of SOD1. By doing so, Cu(I) bridges the donating cysteine residues of CCS and the receiving histidine residues,

stabilizing the heterodimer and facilitating metal transfer. In effect, transfer of copper between the Atx1 and Ccc2p is 'catalyzed' by the metallochaperone. We propose a similar mechanism of As(III) transfer from ArsD to ArsA in which there is a step-wise exchange of sulfur ligands from ArsD cysteines to ArsA cysteines (Figure. 2-12). The MBS1 (metalloid binding site 1) of ArsD and MBSs of ArsA come close to each other, then the As(III) bound by ArsD will be released by one cysteine of ArsD and coordinated by the cysteine of ArsA to form an As(III) intermediated complex. Through step by step change of the thiol-ligands of As(III) from ArsD to ArsA, finally As(III) is coordinated by the three cysteines from ArsA.

#### 1.4 Other metallochaperones

Arsenic is a non-essential element in any organism. ArsD functions to sequester toxic arsenic and deliver it to the extrusion pump. Similar metal-chaperones have been found for essential but toxic metals such as copper and iron. They sequester free metal in cells and specifically deliver to target proteins. Though copper and iron are essential, both Cu(I) and Fe(II) could undergo Fenton or Fenton-like chemistry to generate highly toxic hydroxyl radical. Accumulation of free Cu(I) and Fe(II) is detrimental to the cell. On one hand, the metal-chaperone could sequester the metal and keep the concentration of free metal at very low concentration. On the other hand, the chaperones specifically deliver metal to the target proteins, which could be the enzyme requiring the metal as cofactor, the extrusion pump or the metal-storage protein.

Metal-chaperones deliver metals to the target proteins. Usually without a metal, the chaperone protein does not interact with the target protein or does so very weakly. In the presence of metal, the interaction is strengthened. After the metal is delivered,

the chaperone protein dissociates from the target protein, and a new cycle starts. For this cycle to be efficient, the chaperone-target interaction should be transient and weak. This is one reason that it's difficult to study how chaperone proteins interact with their target proteins.

#### 1.4.1 Copper chaperones

Copper chaperone has been found from prokaryotic cells to eukaryotic cells. *In vitro*, most copper enzymes easily acquire their metal without the help of any auxiliary proteins. However, in living cells such as yeast, the cytoplasmic free copper concentration is estimated to be less than  $10^{-18}$  M since SOD1 cannot get Cu(I) even though the total copper concentration is very high. Almost no free copper exist in the cells, and copper chaperone proteins are required for the maturation of the enzyme (Rae et al., 1999).

*Enterococcus hirae* has a *copYZAB* operon encoding proteins involved in copper homeostasis. CopA and CopB are P-type ATPase pumps, importing and exporting copper, respectively. CopY is a operon repressor in the absence of Cu(I). CopZ is required for delivery of Cu(I) to CopY to activate transcription of the operon (Odermatt and Solioz, 1995). Through gel-filtration, Cu(I)-CopZ transfer Cu(I) to CopY. But these two proteins do not come off the gel-filtration column as a complex (Cobine et al., 1999). The interaction between CopZ and CopY was suggested to be mediated by charged residues. MNKr2, a homolog of CopZ, the second copper binding site of human Menkes ATPase, can be engineered to gain the function similar of CopZ to transfer Cu(I) to CopY through changing the different charged residues (Cobine et al., 2002), suggesting CopZ and CopY interact through these charged residues. Surface Plasmon Resonance

show that CopZ specifically interacts with CopA immobilized on the chip. Cu(I) increased the affinity of interaction between CopZ and CopA 15-fold by decreasing the dissociation rate of the two proteins. Mutation of Cys to Ser of the N-terminal copper binding motif CXXC of CopA abolishes the modulation of interaction affinity by Cu(I), but the mutant still binds to CopZ as well as wild-type CopA in the absence of Cu(I) (Multhaupt et al., 2001). Recent studies show that N-terminal copper binding site of CopA may only serve as a regulatory site, while CopZ is able to directly transfer Cu(I) to TM-MBS, the transmembrane copper binding site (Gonzalez-Guerrero and Arguello, 2008).

CopZ homologues are Atx1 in yeast and HAH1 in human. Ccc2 in yeast and Menkes (ATP7A) and Wilson (ATP7B) ATPase in humans are CopA homologues that also have several copies of CopZ-like copper binding motif in their N-termini. These MBDs (metal binding domain) have been proposed to accept Cu(I) from chaperone proteins. Atx1 interacts with the N-terminal MBD of Ccc2 in the yeast two-hybrid system (Pufahl et al., 1997). The transfer from Atx1 to the MBD of Ccc2 is reversible, which suggests the transfer from Atx1 to Ccc2 is not due to higher affinity for Cu(I). But Atx1 can protect Cu(I) from other copper scavengers in the cell such as glutathione, and directly bring Cu(I) to the target protein through protein-protein interaction (Huffman and O'Halloran, 2000). The binding interface between Atx1 and the first MBD of Ccc2 has been characterized by NMR. By following the  $^{15}\text{N}$  and  $^1\text{H}$  chemical shifts, a new species is detected. This species is in fast exchange with the parent species on the NMR time scale. Nuclear relaxation data are consistent with the formation of an adduct (Arnesano et al., 2001). Based on NMR chemical shift mapping information, a structure model of

the transient complex was proposed through *in silico* docking. The model shows that the interaction is mainly of an electrostatic nature with hydrogen bonds stabilizing the complex (Arnesano et al., 2004). Coupling site-directed mutagenesis and NMR study, the contribution of copper and cysteine residues of the binding site was studied. The copper is essential for the weak and transient metal-mediated interaction (Banci et al., 2006). Recently, a new target protein, copper amine oxidase Cao1 is also shown to accept Cu(I) from Atx1. And these two proteins were shown to interact with each other in yeast two-hybrid system (Peter et al., 2008).

Hah1 compensates for the function of Atx1 in *atx1Δ* yeast (Hung et al., 1998). Coimmunoprecipitation experiments revealed that HAH1 interacts with both the Wilson (ATP7B) and Menkes (ATP7A) proteins and that this interaction depends on available copper. This provides a mechanism for the function of HAH1 as a copper chaperone in mammalian cells to transfer to ATP7A and ATP7B (Hamza et al., 1999). Yeast two-hybrid experiments show copper-dependent interaction between HAH1 and the 2<sup>nd</sup> or 4<sup>th</sup> MBD of ATP7B (van Dongen et al., 2004), also with 2-6 MBD of ATP7A (Larin et al., 1999). The interaction between HAH1, and the second or the fifth soluble domains of ATP7A (MNK2 and MNK5, respectively), was investigated in solution using heteronuclear NMR. The copper-transfer properties of MNK2 and MNK5 are similar, and differ significantly from those previously observed for the yeast homologous system. No stable adduct is formed between either of the MNK domains and HAH1. The copper(I) transfer reaction is slow on the time scale of the NMR chemical shift, and the equilibrium is significantly shifted towards the formation of copper(I)-MNK2/MNK5 (Banci et al., 2005). NMR titration show the formation of an adduct by Cu(I)-HAH1 with

WLN4 that is in fast exchange on the NMR time scale with the isolated protein species as confirmed by  $^{15}\text{N}$  relaxation data. A similar interaction is also observed between Cu(I)-HAH1 and WLN2; however, the relative amount of the adduct in the protein mixture is lower. In both cases the interaction interface can not be mapped by NMR (Achila et al., 2006).

Another example of a copper chaperone is the chaperone protein involved in the maturation of superoxide dismutase (SOD1). In *Saccharomyces cerevisiae*, it's LYS7 and in human it's CCS. They are responsible for the delivery of copper to copper/zinc superoxide dismutase (Culotta et al., 1997). Interaction of the yeast copper chaperone yCCS in complex with its partner protein, superoxide dismutase (SOD1), has been elucidated crystallographically using a mutant SOD1 (Lamb et al., 2001). In this mutant SOD1, His48, one of the ligand for copper was mutated to Phe. yCCS, and this mutant SOD1 form a stable complex (Lamb et al., 2000).

#### 1.4.2 Iron chaperones

Frataxin, the protein lacked in the neurological disease Friedreich's ataxia, functions as a mitochondrial iron chaperone for iron-sulfur cluster and heme biosynthesis. Frataxin interacted with aconitase in a citrate-dependent fashion, reduced the level of oxidant-induced inactivation, and converted inactive  $[3\text{Fe-4S}]^{1+}$  enzyme to the active  $[4\text{Fe-4S}]^{2+}$  form of the protein. Thus, frataxin is an iron chaperone protein that protects the aconitase  $[4\text{Fe-4S}]^{2+}$  cluster from disassembly and promotes enzyme reactivation (Bulteau et al., 2004). Yeast frataxin was shown to interact with ferrochelatase by NMR (He et al., 2004). This model was proposed based on the structural information to show the channel of iron transfer from frataxin to ferrochelatase



for the heme synthesis (Bencze et al., 2007). Yeast frataxin Yfh1 binds to the central Fe/S-cluster (ISC)-assembly complex, which is composed of the scaffold protein Isu1 and the cysteine desulphurase Nfs1. Association between Yfh1 and Isu1/Nfs1 was markedly increased by ferrous iron, but did not depend on ISCs on Isu1. Functional analyses *in vivo* showed an involvement of Yfh1 in *de novo* ISC synthesis on Isu1 (Gerber et al., 2003). The iron-bound form of ISU is viable for assembly of holo ISU, either by subsequent addition of sulfide or by NifS-mediated sulfur delivery. Without sulfur delivery, isothermal titration calorimetry (ITC) shows that holo human frataxin forms a complex with ISU with sub-micromolar binding affinities, while apo frataxin does not bind to ISU, suggesting an important role for iron in cross-linking the two proteins and/or stabilizing the structure of frataxin that is recognized by ISU (Yoon and Cowan, 2003). In *Drosophila*, holo frataxin also forms a complex with ISU that can be trapped without the sulfide delivery and can be detected by ITC (Kondapalli et al., 2008).

Ferritins are the main iron storage proteins found in animals, plants, and bacteria. The capacity to store iron in ferritin is essential for life in mammals. Human ferritins expressed in yeast contain little iron. Human poly (rC)-binding protein 1 (PCBP1) increased the amount of iron loaded into ferritin when expressed in yeast. Coimmunoprecipitation shows PCBP1 binding to ferritin. *In vitro*, PCBP1 binds iron and facilitates iron loading into ferritin (Shi et al., 2008).

## 1.5 Summary

Arsenic is widely distributed throughout the earth's crust and is brought into water and soils due to natural weathering process and human activities. Severe health effects have been observed in populations exposed to arsenic, which include cancer,

cardiovascular disease, peripheral neuropathies and diabetes mellitus. Because of the prevalence of arsenic in the environment, nearly every organism, from *E. coli* to humans, has genes for arsenic detoxification.

The ArsAB pump in *E. coli*, encoded by the *ars* operon of plasmid R773, confers resistance to arsenicals and antimonials. ArsA is the catalytic subunit of the pump that hydrolyzes ATP in the presence of arsenite or antimonite. ArsB is a membrane protein containing arsenite-conducting pathway. ArsA forms complex with ArsB, therefore ATP hydrolysis is coupled to extrusion of As(III) or Sb(III) through ArsB. Upon overexpression, ArsA exists primarily as a soluble protein in the cytosol. Purified ArsA is an As(III)/Sb(III)-stimulated ATPase.

ArsD is an arsenite chaperone for ArsA. ArsD sequesters free As(III) in the cell and then delivers to ArsA. ArsD increases the apparent affinity of ArsA for As(III) by about 60 fold from 1.2mM to 20 $\mu$ M (Lin et al., 2006). This effect is more significant at 'physiological' concentration of As(III) in the cell. There is no data of the maximum concentration of free As(III) inside the cells, at which the cells can tolerate. Most likely it is less than 50 $\mu$ M suggested by measuring growth of *E. coli* cells, lacking arsenic resistance operon, with addition of As(III) in the medium. 50 $\mu$ M As(III) inhibits cell growth. The free As(III) inside the cell should not be higher than outside of the cell (Hung-Chi Yang, Barry Rosen, unpublished). By increasing affinity of ArsA for As(III), ArsD also increased ArsA ATPase activity at the 'physiological' concentration of As(III). Therefore, ArsAB pump efficiency is increased and less As(III) will be accumulated in the cells. On the other hand, since ArsD is a protein with higher affinity for As(III), there is less chance for free As(III) to bind to other proteins interfering their function after the

formation of ArsD-As(III) complex. So ArsD also confers the cell with the advantage of low availability of free As(III), therefore decreasing the deleterious effect of free As(III).

ArsD has been shown to transfer Sb(III) to ArsA in the presence of  $Mg^{2+}$  and ATP. ArsD and ArsA can be crosslinked by dibromobimane, a homofunctional cysteine crosslinker with arm length about 6Å. The N-terminal metal binding site of ArsD, formed by Cys12, Cys13 and Cys18, is required for the metallochaperone function. From ArsA crystal structure, three cysteine residues, Cys113, Cys172 and Cys422 are found to near each other and involved in As(III) binding. Since both ArsD and ArsA use cysteine residues as ligands for As(III), all these results suggest that ArsD interacts with ArsA through their arsenic binding sites. However, the interaction detail is not known yet and the process of arsenic transfer is also not known. I approached the answers from three directions in chapters 2, 3 and 4. In chapter 2, the binding affinity of ArsD for As(III) was determined, and ATP hydrolysis was shown to be required for As(III) transfer from ArsD to ArsA. The results suggest that ATP hydrolysis changes ArsA to a conformation with higher affinity for As(III), and As(III) is transferred at this step. In chapter 3, the relation between ArsD dimerization and metallo-chaperone function was studied. In chapter 4, yeast two-hybrid analysis was used to select mutations affecting the interaction between ArsD and ArsA, which shed light on the interface between ArsD and ArsA.

## CHAPTER 2

### Arsenic binding and transfer by the ArsD As(III) metallochaperone

#### 2.1 Introduction

In bacteria and archaea various *ars* operons encode ArsAB ATPases that pump the trivalent metalloids As(III) or Sb(III) out of cells. In these operons, an *arsD* gene is almost always adjacent to the *arsA* gene, suggesting a related function. Most transition and heavy metal ions do not exist as free ions in the cytosol but are sequestered by a variety of proteins variously called metal ion chaperones, scaffolds or intracellular carriers (Field et al., 2002). ArsD was recently shown to be a chaperone for transfer of cytosolic As(III) to the 583-residue ArsA ATPase, the catalytic subunit of the efflux pump (Lin et al., 2006; Lin et al., 2007a). ArsD is a 120-residue protein with three conserved cysteine residues, Cys12, Cys13 and Cys18 required for chaperone activity (Lin et al., 2007a). ArsA exhibits a low, basal rate of ATPase activity in the absence of As(III) or Sb(III) and a higher, activated rate in their presence. ArsA has a high affinity metalloid binding site composed of Cys113 and Cys422 (Ruan et al., 2006), and a third residue, Cys172, that participates in high affinity binding and activation of ATP hydrolysis (Ruan et al., 2008). In analogy with the mechanism of copper transfer from chaperones to copper pumps or enzymes (Boal and Rosenzweig, 2009), we previously proposed a step-wise transfer from the cysteines of ArsD to the cysteines of ArsA (Lin et al., 2007b). ArsD increases the affinity of ArsA for As(III), permitting detoxification of environmental concentrations of arsenic.

In this study the properties of As(III) binding by ArsD and subsequent transfer to ArsA were examined. X-ray absorption spectroscopy was used to show that As(III) is

coordinated with three sulfur atoms, consistent with Cys12, Cys13 and Cys18 forming the As(III) binding site. Assays with single-tryptophan derivatives of ArsA have been informative about As(III) or Sb(III) binding properties and catalysis (Walmsley et al., 1999, 2001; Zhou et al., 2001; Zhou and Rosen, 1997; Zhou et al., 2002), so an assay using intrinsic protein fluorescence was developed as a probe of metalloid binding to ArsD. Two single tryptophan derivative of ArsD were constructed by changing either Thr15 or Val17 to tryptophan in a tryptophan-free background. Both exhibited quenching of fluorescence upon binding of As(III) or Sb(III), from which the apparent affinity for metalloid could be estimated. Since it is likely that cytosolic As(III) is bound to reduced glutathione (GSH), the effect of GSH on binding to ArsD was examined. GSH greatly increased the rate of binding As(III) to ArsD, suggesting that ArsD accepts metalloid from the As(GS)<sub>3</sub> complex. In contrast, GSH did not affect the As(III)-stimulated ArsA ATPase activity, suggesting that As(III) is directly transferred from ArsD to ArsA, as opposed to release from ArsD, binding to GSH and then interaction of ArsA with the As(GS)<sub>3</sub> complex. To differentiate between these two possibilities, the effect of the As(III) chelator dimercaptosuccinic acid (DMSA) was examined. The chelator did not affect transfer, indicating channeling of As(III) from ArsD to ArsA. Transfer occurs only under conditions where ArsA hydrolyzes ATP, suggesting that ArsD transfer As(III) to an ArsA conformation transiently formed during catalysis and not simply to the closed conformation that ArsA adopts when As(III) and MgATP are bound (Zhou et al., 2001).

## **2.2 Materials and Methods**

### **2.2.1 Strains, plasmids and media**

*E. coli* cells were grown in Luria-Bertani (LB) medium (Sambrook et al., 1989) at

37°C. Ampicillin (100 µg/ml) or kanamycin (40 µg/ml) was added as required. *E. coli* strain JM109 [*recA1 supE44 endA1 hsdR17 gyrA96 relA1 thiΔ(lac-proAB)* F' (*traD36 proAB<sup>+</sup> lacI<sup>q</sup> lacZΔM15*)] was used for molecular cloning. *E. coli* strain BL21(DE3) [*F-ompT hsdS<sub>B</sub> (r<sub>B</sub>-m<sub>B</sub>-) gal dcm* (DE3 [*lacI lacUV5-T7 gene1 ind1 Sam7 nin5*])] was used for protein expression and purification. ArsA with a C-terminal 6-histidine tag was expressed from plasmid pAlter-dAhB (Li and Rosen, 2000). ArsD contains three vicinal cysteine pairs, of which the last two are not required for chaperone activity, so the last 11 residues containing those two cysteine pairs were removed, creating the ArsD<sub>1-109</sub> truncation. N-terminal MBP-fused ArsD<sub>1-109</sub> (henceforth designated MBP-ArsD109) was expressed from plasmid pMAL-ArsD109 (Lin et al., 2007a). ArsD<sub>1-109</sub> with an N-terminal six-histidine tag (henceforth designated as wild type ArsD109) was expressed from plasmid pET28a-ArsD109. The codons for the two native ArsD tryptophan residues, Trp35 and Trp97, were mutated to tyrosine codons by site directed mutagenesis in plasmid pET28a-ArsD109, generating pET28a-ArsD109<sub>W35/97Y</sub>. In this plasmid Thr15 and Val17 codons were mutated to tryptophan codons, generating pET28a-ArsD109<sub>T15W</sub> and pET28a-ArsD109<sub>V17W</sub>, respectively. The codon for Cys12, Cys13 and Cys18 was individually mutated to glycine codons in pET28a-ArsD109, generating pET28a-ArsD109<sub>C12G</sub>, pET28a-ArsD109<sub>C13G</sub> and pET28a-ArsD109<sub>C18G</sub>, respectively. The codons for Cys12, Cys13 and Cys18 were mutated to glycine codons in pET28a-ArsD109<sub>T15W</sub>, generating pET28a-ArsD109<sub>C12G,T15W</sub>, pET28a-ArsD109<sub>C13G,T15W</sub> and pET28a-ArsD109<sub>C18G,T15W</sub>. Growth in liquid culture was estimated from the absorbance at 600 nm. The strains and plasmids are listed in Table 2-1.

## 2.2.2 DNA manipulation and mutagenesis

Plasmid extraction, DNA restriction endonuclease analysis, ligation and other general molecular biological procedures were performed as described (Sambrook et al., 1989). Transformation of *E. coli* cells was carried out using a BIO-RAD MicroPluser (BIO-RAD, Hercules, CA). DNA purification kits were obtained from QIAGEN (Valencia, CA). Either a Qiaprep Spin Miniprep kit or a Qiaquick gel extraction kit (QIAGEN) was used to prepare plasmid DNA for restriction enzyme digestion, sequencing, and recovering DNA fragments from agarose gels. The sequence of new plasmid constructs was confirmed by DNA sequencing of the entire gene. Site-directed mutagenesis was performed using Quick-change Site-Directed Mutagenesis kit (Stratagene, La Jolla, CA) and confirmed by sequencing. DNA sequencing was performed using a CEQ2000 DNA sequencer (Beckman Coulter, Brea, CA). The primers used are listed in Table 2-2.

### **2.2.3 Protein expression and purification**

Cells bearing the indicated plasmids were grown in LB medium overnight at 37°C and then diluted 50-fold into 1 L of the same medium. Proteins were expressed by induction with 0.3 mM isopropyl- $\beta$ -D-thiogalactopyranoside at  $A_{600}$  of 0.6-0.8 for 3 hrs. MBP-ArsD109 was purified from *E. coli* strain BL21(DE3) bearing plasmid pMAL-ArsD109 as described (Lin et al., 2006). Cells were harvested by centrifugation and washed once with a buffer containing 50 mM MOPS, pH 7.5, 0.5 M NaCl, 5 mM DTT and 10 mM 2-mercaptoethanol (Buffer A). The cells were suspended in 5 ml of Buffer A per gram of wet cells and lysed by a single passage through a French press at 20,000 psi. Diisopropyl fluorophosphate (DIFP) (Sigma) was added at 2.5  $\mu$ l/g wet cells immediately following French press. Unbroken cells and membranes were removed by centrifugation at 150,000 x *g* for 1 hr at 4°C. The supernatant was loaded to 10 ml

amylose column (New England Biolabs, Ipswich, MA) pre-equilibrated with Buffer A. Unbound proteins were washed by 200 ml of buffer A, and MBP-ArsD109 was eluted with Buffer B (50 mM MOPS, pH 7.5, 0.5 M NaCl, 5 mM DTT, 10mM maltose and 10 mM 2-mercaptoethanol), followed by addition of 0.25 mM EDTA and 5 mM DTT to each fraction. MBP-ArsD109 containing fractions were identified by sodium dodecyl sulfate polyacrylamide gel electrophoresis (SDS-PAGE), pooled, concentrated by Amicon Ultra-15 Centrifugal Filter Unit with Ultracel-10 membrane (Millipore), mixed with 10% glycerol, aliquoted and stored at  $-80^{\circ}\text{C}$  until used. ArsA with a six histidine tag at the C-terminus was purified from cells of strain BL21(DE3) expressing pAlter-1-dAhB plasmid, as described (Zhou and Rosen, 1997). Basically similar procedure was used as purification of MBP-ArsD109, but with different buffer and column. Probond Ni-column (Invitrogen) was used. Buffer A(50 mM MOPS, pH 7.5, 0.5 M NaCl, 30 mM Imidazole and 10 mM 2-mercaptoethanol) and Buffer B(50 mM MOPS, pH 7.5, 0.5 M NaCl, 300 mM Imidazole and 10 mM 2-mercaptoethanol) were used. ArsD and its derivatives with a six histidine tag at the N-terminus were purified similarly. Purified proteins were stored at  $-80^{\circ}\text{C}$  until use, and their concentrations were determined according to the method of Bradford (Bradford, 1976) or from the absorption at 280 nm (Gill and von Hippel, 1989).

#### **2.2.4 Circular dichroism measurements**

Circular dichroism (CD) spectra from 190 to 260 nm were acquired with a spectrometer from Olis Inc. (Bogart, GA) at  $20^{\circ}\text{C}$  using a 0.2-cm path-length cell at 1.75-nm intervals. Three scans were averaged for each spectrum. ArsDs were assayed at  $10\ \mu\text{M}$  in 10 mM potassium phosphate buffer, pH 7.5.

#### **2.2.5 X-ray absorption spectroscopy (XAS)**



XAS samples were prepared in 50 mM MOPS, 0.5 M NaCl and 30% glycerol, pH 7.5. For wild-type ArsD109, 4 mM protein was incubated with 3.2 mM sodium arsenite for 1 hr on ice, and unbound As(III) was removed with a Bio-Gel P-6 column. For C12G, C13G and C18G, 4mM protein was incubated with 1 mM As(III) for 1hr. A higher protein:ligand ratio was used since unbound As(III) was not removed by gel filtration due to weak binding by the mutant proteins. Solution samples were loaded in Lucite cells, wrapped in Kapton tape and flash frozen in liquid nitrogen.

XAS data were collected at the Stanford Synchrotron Radiation Laboratory (SSRL) on beamline 9-3, equipped with Si[220] double crystal monochromator equipped with a harmonic rejection mirror. Samples were maintained at 10 K using Oxford Instruments continuous-flow liquid helium cryostats. Protein fluorescence excitation spectra were collected using a 30-element Ge solid-state array detector. A germanium filter (0.6 mm in width) and solar slits were placed between the cryostat and detector to filter scattering fluorescence not associated with protein bound arsenic signals. XAS spectra were acquired in 5 eV steps in the pre-edge region (11,625-11,825 eV), 0.25 eV steps in the edge region (11,850-11,900 eV) and 0.05 Å<sup>-1</sup> increments in the extended x-ray absorption fine structure (EXAFS) region out to a *k* range of 13 Å<sup>-1</sup>. The data were integrated from 2 to 20 s in a *k*-weighted manner in the EXAFS region for a total scan length of 45 min. X-ray energies were calibrated using an arsenic foil absorption spectrum collected simultaneously with the protein data. The first inflection point for the arsenic foil edge was assigned to 11,867 eV. Each fluorescence channel of each scan was examined for spectral anomalies prior to averaging and spectra were closely monitored for photodegradation. The data represent an average of 6 to 7 scans.

XAS data were processed using the Macintosh OS X version of the EXAFSPAK software suite (available on the World Wide Web) integrated with the Feff v7 software (Ankudinov and Rehr, 1997) for theoretical model generation. Data reduction followed a previously published protocol for a spectral resolution in bond lengths of 0.13 Å (Lieberman et al., 2006). EXAFS fitting analysis was performed on raw/unfiltered data. Protein EXAFS data were fit using single scattering Feff v7 theoretical models, calculated for carbon, oxygen, sulfur and copper coordination to simulate arsenic-ligand environments, with values for the scale factors ( $S_c$ ) and  $E_0$  calibrated by fitting crystallographically characterized arsenic model compounds. Criteria for judging the best-fit EXAFS simulations utilized both the lowest mean square deviation between data and fit, corrected for the number of degrees of freedom ( $F'$ ), and reasonable Debye-Waller factors ( $\sigma^2 < 0.006 \text{ \AA}^2$ ).

### 2.2.6 Fluorescence measurements

Fluorescence measurements were conducted with a QuantaMaster™ UV VIS QM-4 Steady State Spectrofluorometer (Photon Technology International, Birmingham, NJ) at room temperature. For time based measurements, the excitation wavelength was 295 nm, and the emission wavelength was 345 nm. Emission scans were acquired between 310 and 390 nm. As(III) or Sb(III) was added as sodium arsenite or potassium antimonyl tartrate, respectively, at the indicated concentrations to a cuvette containing 2 ml of 1  $\mu\text{M}$  ArsD in a buffer consisting of 50 mM MOPS-KOH, pH 7.5, 0.25 mM EDTA. GSH was added to the indicated concentrations. Additions were made from concentrated solutions, and fluorescence was corrected for dilution. To examine the effect of pH, buffers containing 50 mM sodium acetate, pH 4.0, 50 mM sodium acetate,

pH 5.0, 50 mM MES, pH 6.0, 50 mM MOPS, pH 7.0, 50 mM Tris, pH 8.0 or 50 mM CHES, pH 9.0, were used.

### **2.2.7 ATPase activity assays**

ATPase activity was estimated using a couple assay (Vogel and Steinhart, 1976), as described (Hsu and Rosen, 1989). ArsA was added at a final concentration of 0.3  $\mu$ M into an assay mixture containing 5 mM ATP, 1.25 mM phosphoenolpyruvate, 0.25 mM NADH, 10 units of pyruvate kinase and lactate dehydrogenase with or without the indicated concentrations of potassium antimonyl tartrate or sodium arsenite, in the buffer containing 50 mM MOPS-KOH, pH 7.5, 0.25 mM EDTA. ArsD was added at the indicated concentrations. The mixture was pre-warmed to 37°C, and the reaction was initiated by addition of 2.5 mM MgCl<sub>2</sub> and measured at 340 nm. The linear steady state rate of ATP hydrolysis was used to calculate specific activity. The reaction volume was 0.2 ml each in 96-well microplates, and the reactions were monitored by microplate reader SPECTRA max 340PC (Molecular Devices). GSH or DMSA was added as indicated.

### **2.2.8 Metalloid transfer assays**

Transfer assays were performed as described (Lin et al., 2007b) except that purified MBP-ArsD109 was used in place of cytosol fractions containing MBP-ArsD109. A 0.5 ml amylose column pre-equilibrated with 4 ml of buffer consisting of 50 mM MOPS-KOH, 0.5 mM NaCl, pH 7.5 (column buffer) was used. Purified MBP-ArsD109 was dialyzed against column buffer supplemented with 5 mM  $\beta$ -mercaptoethanol and 0.5 mM dithiothreitol and loaded to the column, which was then washed with 1 ml of column buffer. Next 0.5 ml of 1 mM sodium arsenite was added to the column, which

was then washed with 4 ml of column buffer. BSA or purified ArsA (0.5 ml of 20  $\mu$ M of either protein) was applied to the columns with 5 mM MgATP, MgADP or MgATP $\gamma$ S, as indicated. The column was eluted with 1 ml of column buffer supplemented with the appropriate nucleotide and then 2 ml of column buffer. Finally the column was eluted with 1.5 ml of 10 mM maltose. Ten fractions of 0.5 ml were collected and analyzed by sodium dodecyl sulfate (SDS) polyacrylamide gel electrophoresis (PAGE) (Laemmli, 1970). For assays conducted at 4°C, everything was pre-cooled to 4°C for 30 min. The protein concentration of each fraction was determined according to the method of Bradford (Bradford, 1976). The arsenic concentration was quantified by inductively coupled plasma mass spectroscopy (ICP-MS).

## 2.3 Results

### 2.3.1 Cys12, Cys13 and Cys18 form a three-coordinate As(III) binding site in ArsD

R773 ArsD has three cysteine pairs, Cys12-Cys13, Cys112-Cys113 and Cys119-Cys120, plus an additional cysteine at residue 18. However, only cysteine residues 12, 13 and 18 are conserved in known homologues, and truncation of the last two vicinal pairs had no effect on ArsD chaperone activity, and this variant, with a N-terminal six-histidine tag was used as the wild type ArsD109 for further analysis (Lin et al., 2007a). (It should be pointed out that six-histidine tags do not bind As(III) (Qin et al., 2007)). The nature of the binding site was investigated in structural detail using XAS using wild type and mutant ArsD109s lacking individual cysteine residues (C12G, C13G and C18G). XANES analysis indicated arsenic in both the wild type and mutant proteins is As(III) (Figure 2-1). The observed value for the first inflection point energy is 11868 eV,

consistent with observed values for As(III) in protein and model systems (Ramirez-Solis et al., 2004). XANES spectra for wild type ArsD109 are unique from those observed for the three mutant proteins, indicating the distinctive structural environment that coordinates As(III) in the wild type sample is different from that seen in the mutant samples. On the other hand, the structural environment of each mutant sample is closely related to the other mutant samples.

The EXAFS fitting results are most consistent with trivalent arsenic being maintained in a 3-coordinate all-sulfur structural environment in wild type ArsD109 (Figure 2-2). This environment is different in the mutants. The structural environment for the wild type protein is dominated by a symmetric three sulfur coordination environment to the As(III) at an average bond length of 2.24 Å. Addition of a small oxygen/nitrogen scattering contribution to the As-S<sub>3</sub> fits for the wild type suggests a possible low percentage partial dissociation of the bound metalloid (Table 2-3). There was no sulfur ligation in any of the three cysteine mutants. EXAFS analysis of C18G suggests an average nearest neighbor coordination environment constructed of three As-O interactions at 1.79 Å. In the remaining two mutants, the data are best fit with two independent As-O/N environments constructed of two oxygen ligands at 1.79 Å and a third oxygen/nitrogen ligand interaction between 2.13 and 2.16 Å. The most likely explanation for these results is that As(III) is bound to the thiolates of Cys12, Cys13 and Cys18 in the wild type, but that, in the mutants, binding to the two remaining cysteines is weak, and most of the arsenic is present as As(OH)<sub>3</sub>.

### 2.3.2 Tryptophan fluorescence reports trivalent metalloid binding by ArsD

Previous assays to quantify arsenic binding by wild type and mutant ArsDs used

ICP-MS (Lin et al., 2006; Lin et al., 2007a). To develop a real-time assay for arsenic binding, single tryptophan derivatives of ArsD109 were constructed. ArsD has two native tryptophan residues, Trp35 and Trp97. Trp35 does not respond to As(III), but the fluorescence of Trp97 is quenched when As(III) binds to the vicinal pair, Cys112-Cys113 but not to the Cys12-Cys13-Cys18 As(III) binding site (Li et al., 2001; Li et al., 2002). A tryptophan-free derivative lacking the last two vicinal cysteine pairs was constructed (W35/97Y). Two derivatives with single tryptophan residues near the As(III) binding site were then constructed by changing Thr15 or Val17 to tryptophan. Introduction of either tryptophan residue had no apparent effect on ArsD structure or function. The overall secondary structure of these two mutants, T15W and V17W, were similar to wild-type ArsD109, as determined by circular dichroism (Figure 2-3A), and both stimulated ArsA ATPase activity nearly as well as wild-type ArsD109 (Figure 2-3B; data not shown for V17W). Tryptophan-free W35/97Y showed very low background fluorescence (Figure 2-4A). Both single tryptophan derivatives exhibited considerable intrinsic protein fluorescence compared with W35/97Y, with emission maxima of approximately 340 nm compared with an emission maximum of approximately 355 nm for free tryptophan in solution. Denaturation of the proteins with guanidine red shifted the emission maxima to approximately 352 nm. The fluorescence of either T15W or V17W was quenched approximately 50% by addition of high concentrations of As(III) or Sb(III) (Figure 2-4B).

In the absence of added thiols, the rate of fluorescence quenching, presumably proportional to the rate of As(III) binding, was very slow, requiring more than 0.5 hr to attain a steady-state level of fluorescence when 1  $\mu$ M protein was mixed with 5  $\mu$ M

As(III) (Figure 2-5A). From the As(III) concentration dependence of fluorescence quenching, apparent binding constants for the two single tryptophan proteins could be calculated from the relationship  $k_{\text{obs}} = k_{\text{off}} + k_{\text{on}}[\text{As(III)}]$  (Tamerler et al., 2006), where  $k_{\text{obs}}$  is the rate of quenching fitted with SigmaPlot 9.0 (Figure 2-5B). For V17W,  $k_{\text{off}}$  was calculated as  $(4 \pm 2) \times 10^{-4} \text{ s}^{-1}$ , and  $k_{\text{on}}$  was calculated as  $(2 \pm 0.06) \times 10^{-4} \text{ s}^{-1} \cdot \mu\text{M}^{-1}$ . From the ratio  $k_{\text{off}}/k_{\text{on}} = k_{\text{d}}$ , a binding affinity of  $2 \pm 1 \mu\text{M}$  was calculated. For T15W,  $k_{\text{off}}$  was estimated as  $(3 \pm 1) \times 10^{-4} \text{ s}^{-1}$ , and  $k_{\text{on}}$  as  $(2 \pm 0.05) \times 10^{-4} \text{ s}^{-1} \cdot \mu\text{M}^{-1}$ , and  $k_{\text{d}} = 1.5 \pm 0.5 \mu\text{M}$ . Thus, the values for the two single tryptophan derivatives are in agreement.

### 2.3.3 Effect of cysteine substitutions on As(III) binding

Substitutions of the three cysteines in ArsD were previously result in loss of Sb(III) binding ability by gel filtration assays (Lin et al., 2007a). As noted above, no sulfur ligation was observed with any of the three cysteines mutants in the EXAFS experiments. However, neither EXAFS nor binding assays by gel filtration are as sensitive as fluorescence assays and cannot measure low affinity binding. As(III) binding parameters were estimated from quenching of T15W fluorescence of each cysteine mutant (Figure 2-5B). C18G/T15W, which retains the Cys12 and Cys13 vicinal pair, has  $k_{\text{on}} = (5 \pm 0.1) \times 10^{-5} \text{ s}^{-1} \cdot \mu\text{M}^{-1}$ ,  $k_{\text{off}} = (1.4 \pm 0.1) \times 10^{-3} \text{ s}^{-1}$  and  $k_{\text{d}} = 28 \pm 3 \mu\text{M}$ . C12G/T15W, which retains Cys13 and Cys18, has  $k_{\text{on}} = (5 \pm 0.1) \times 10^{-5} \text{ s}^{-1} \cdot \mu\text{M}^{-1}$ ,  $k_{\text{off}} = (2.4 \pm 0.1) \times 10^{-3} \text{ s}^{-1}$  and  $k_{\text{d}} = 48 \pm 3 \mu\text{M}$ . C13G/T15W, which retains Cys12 and Cys18, has  $k_{\text{on}} = (4 \pm 0.2) \times 10^{-5} \text{ s}^{-1} \cdot \mu\text{M}^{-1}$ ,  $k_{\text{off}} = (2.7 \pm 0.1) \times 10^{-3} \text{ s}^{-1}$  and  $k_{\text{d}} = 68 \pm 6 \mu\text{M}$ . Thus, the affinity of each of the three cysteine mutants decreased by 20-fold or more compared with the parental protein containing Cys12, Cys13 and Cys18.

### 2.3.4 Reduced glutathione increases the rate of binding of As(III) to ArsD but not

### **ArsA *In vivo***

As(III) is nearly completely complexed with GSH (Delnomdedieu et al., 1994a). As GSH is the major intracellular thiol in *E. coli*, cytosolic As(III) would be expected to be primarily in the form of As(GS)<sub>3</sub> (Apontoweil and Berends, 1975). For that reason, the effect of 5 mM GSH on the rate of binding of 50 μM sodium arsenite to 1 μM V17W was examined over a pH range of 4.0 to 9.0 (Figure 2-6). The rate of fluorescence quenching increased with increasing pH with or without GSH. In the absence of GSH, the rate of fluorescence quenching was about 10-fold faster at pH 9 than at pH 7. Addition of GSH accelerated the rate by 10-fold at pH 7.5, and the rate was too fast to measure accurately at pH 8 or higher. The pH dependence in the absence of GSH indicates binding of As(III) by thiolates of the three ArsD cysteines but could also reflect dissociation of As(OH)<sub>3</sub> to As(OH)<sub>2</sub><sup>-1</sup> (pK<sub>a</sub> of 9.23). Acceleration by GSH is consistent with binding of As(III) by thiolates of GS<sup>-1</sup> (pK<sub>a</sub> of 8.7), which is highly pH dependent (Yehiayan et al., 2009), consistent with intermolecular transfer of metalloid from As(GS)<sub>3</sub> to ArsD.

The effect of GSH was investigated in more detail. In the absence of GSH, fluorescence of V17W decreased very slowly when 50 μM sodium arsenite was added at pH 7.5 (Figure 2-7A). Addition of 0.2 mM GSH had little effect, but 5 mM GSH increased the rate substantially. Addition of 5 mM of either β-mercaptoethanol or L-cysteine also increased the rate of quenching with As(III) (Figure 2-7B). While ArsD might be able to accept As(III) from complexes with other monothiols, but only GSH is present intracellularly in concentrations high enough to be involved physiologically. In contrast, 2.5 μM potassium antimonyl tartrate rapidly quenched fluorescence in the



absence of added monothiols (Figure 2-7B), consistent with the fact that ArsD has higher affinity for Sb(III) than As(III) (Li et al., 2002). Addition of 5 mM tris(2-carboxyethyl)phosphine (TCEP), which is a stronger reductant than GSH but is not a monothiol, did not increase the rate of quenching (Figure 2-7A), indicating that the effect of GSH is not simply to protect either ArsD or As(III) from oxidation. Since formation of As(GS)<sub>3</sub> is slow at pH 7.5 (Yehiayan et al., 2009), 4 mM sodium arsenite was pre-incubated with 16 mM GSH for 10 min to allow for formation of the complex. When preformed As(GS)<sub>3</sub> was added at 50 μM, the rate of quenching was too fast to quantify (Figure 2-7A), supporting our hypothesis that As(GS)<sub>3</sub> is a direct donor of metalloid to ArsD.

To examine whether GSH also facilitates As(III) binding to ArsA, the stimulation of ArsA activity by As(III) was determined in the presence or absence of GSH (Figure 2-8). ArsA exhibited an apparently affinity of around 0.6 mM for As(III) with or without GSH. These results indicate that ArsA accepts either free As(III) or from As(GS)<sub>3</sub> with low affinity, but As(GS)<sub>3</sub> does not replace ArsD as an intracellular metallochaperone for high affinity As(III) binding.

To see the effect of glutathione on the cooperation of ArsD and ArsA, the change of apparent affinity of ArsA for As(III) by ArsD was determined in the absence and presence of 5 mM glutathione. 3 μM ArsD increases apparent affinity of ArsA to about 34 μM in the absence of glutathione and 5 μM in the presence of glutathione (Figure 2-9A). To study in more detail, the change of apparent affinity of ArsA for As(III) by different concentrations of ArsD was determined. 0.3 μM ArsA was used in the assay. In the absence of glutathione, when ArsD concentration was increased from 0.3 μM to 3

$\mu\text{M}$ , the apparent affinity was increased from 0.6 mM to a plateau of 30  $\mu\text{M}$ . In the presence of 5mM glutathione, when ArsD concentration was increased from 0.3 $\mu\text{M}$  to 3 $\mu\text{M}$ , the apparent affinity was increased from 0.6 mM to a plateau of 5  $\mu\text{M}$ , six fold less comparing in the absence of glutathione (Figure 2-9B). From another aspect, in the presence of glutathione, less ArsD is required to stimulate ArsA ATPase activity to the same extent. To exclude the possibility that the effect of glutathione is due to prevention of ArsA and ArsD from oxidation, 5mM TCEP was added in the buffer and it show almost no effect on the cooperation of ArsA and ArsD (Figure 2-9B). These results suggests that glutathione increases the binding rate of As(III) to ArsD, therefore increasing the transferring rate of As(III) from ArsD to ArsA and stimulating ArsA ATPase activity at low concentration of As(III) when As(III) binding is the rate-limiting step in ArsA ATP hydrolysis cycle.

### **2.3.5 ArsD transfers As(III) directly to ArsA**

From the results of yeast two-hybrid analysis, it is clear that ArsD and ArsA physically interact (Lin et al., 2006). How is As(III) transferred during this interaction? One possibility is that the metalloid dissociates from ArsD and re-associates with ArsA. A second possibility is that there is direct transfer from the thiols of ArsD to the thiols of ArsA in a step-wise fashion (Lin et al., 2007a), similar to the mechanism of copper transfer from the yeast Atx1p chaperone to the Ccc2p copper efflux pump (Pufahl et al., 1997).

Metabolic trapping is often applied to examine for channeling (Anderson, 1999; Kwok et al., 2006). To differentiate between channeling and a dissociation/re-association mechanism, the As(III) chelator DMSA was added to the reaction. DMSA

has an apparent affinity of approximately 20  $\mu\text{M}$  for As(III) (Spuches et al., 2005), which is between the ArsD and ArsA affinities. Direct transfer of As(III) from ArsD to ArsA would be expected to be insensitive to DMSA. In contrast, if As(III) dissociates from ArsD before binding to ArsA, an excess of DMSA should prevent transfer. Using the stimulation of ArsA ATPase by the ArsD-As(III) complex, the effect of DMSA was examined (Figure 2-10). DMSA did not affect the basal activity of ArsA, but the As(III)-stimulated rate of ArsA activity was inhibited by DMSA. In that experiment ArsA + As(III) was titrated with DMSA, and the stimulated ATPase activity returned to basal level at higher concentrations of DMSA. When ArsD was preincubated with As(III) and then added to ArsA, the rate of ATP hydrolysis was stimulated, reflecting the chaperone activity of ArsD. Titration of that mixture with DMSA resulted in an initial decrease in activity as free As(III) was chelated, but the activity plateaued at a level corresponding to the activated rate. Since ArsD has higher affinity for As(III) than DMSA, it is able to retain and transfer metalloid even at higher concentrations of DMSA. These results are consistent with direct transfer of As(III) from ArsD to ArsA.

### **2.3.6 Transfer of As(III) from ArsD to ArsA requires catalysis**

We have previously shown that ArsD transfers Sb(III) to ArsA in the presence of MgATP (Lin et al., 2007a). Here transfer of As(III) from ArsD to ArsA was compared under catalytic and noncatalytic conditions. Purified MBP-ArsD109 was bound to an amylose column. Sufficient As(III) was added to the column to saturate ArsD, following which free As(III) was washed off. Next either ArsA or BSA pre-incubated with nucleotides was passed through the column. When ArsA pre-incubated with MgATP was passed through the column at room temperature, conditions under which ArsA

hydrolyzes ATP, nearly all of the As(III) eluted in the ArsA-containing fractions, with almost none in the MBP-ArsD109-containing fractions (Figure 2-11A and B). In contrast, when BSA preincubated with MgATP was passed through the column, almost none of the As(III) eluted in the BSA-containing fractions, but eluted in the MBP-ArsD109-containing fractions (Figure 2-11C).

When MgADP was used instead of MgATP, As(III) eluted with MBP-ArsD109 and not with ArsA (Figure 2-11D). Similarly, the MgATP- $\gamma$ -S, a nonhydrolyzable nucleotide, did not promote transfer (Figure 2-11E). When the reaction with MgATP and column elution were at 4<sup>0</sup> C, where ArsA hydrolyzes ATP very slowly, almost no As(III) eluted with ArsA but remained bound to MBP-ArsD109 (Figure 2-11F). These data demonstrate that ATP hydrolysis is required for As(III) transfer from ArsD to ArsA.

## 2.4 Discussion

*In vivo* results quite clearly demonstrate that ArsD is an As(III)/Sb(III) chaperone that transfers metalloid to the ArsA ATPase (Lin et al., 2006; Lin et al., 2007a), but the molecular details of the process are lacking. In this study the questions of the nature of the metalloid binding site in ArsD and requirements for the transfer reaction were addressed.

From genetic analysis and conservation of residues in homologues, it seemed likely that the metalloid binding site in ArsD involved the three conserved cysteines, residues 12, 13 and 18. Here the EXAFS data with wild type ArsD unambiguously demonstrate that the binding site is a three-coordinate sulfur-containing site, similar in nature but not sequence to the ArsA As(III) binding site (Bhattacharjee et al., 1995) and the three convergently evolved sites of three different ArsR repressors (Ordóñez et al.,

2008; Qin et al., 2007; Shi et al., 1996). This suggests that a common type of As(III) binding site in proteins is composed of three cysteine residues, with similar As-S bond distances of 2.24 Å and probably similar geometries.

While EXAFS is useful for determining the environment surrounding the bound metalloid, a more complete analysis requires quantitative measurements of As(III) binding. Previous assays using gel filtration yield stoichiometries, but it is difficult to extract more detailed information from analysis conducted after the reaction is complete. Changes in intrinsic protein fluorescence can provide real-time information about ligand binding or catalysis. Full length ArsD has three vicinal cysteines pairs, Cys12-Cys13, Cys112-Cys113 and Cys119-Cys120, and two tryptophan residues, Trp35 and Trp97. Trp97 fluorescence reports binding of Sb(III) or As(III) to the vicinal Cys112-Cys113 pair (Li et al., 2001; Li et al., 2002). However, only the N-terminal Cys12-Cys13 pair is involved in chaperone activity; the C-terminal pairs are dispensable and not present in the constructs used for this study. For that reason, the two endogenous tryptophan residues were altered by site-directed mutagenesis, and new tryptophan residues introduced singly at positions 15 and 17, near the Cys12-Cys13-Cys18 As(III) binding site. Fluorescence of either single tryptophan derivative was blue-shifted approximately 14 nm compared with free tryptophan. The fluorescence was red-shifted and decreased by denaturation with guanidine. These results indicate that the two tryptophan residues are in a less aqueous environment compared with free tryptophan. These two tryptophans are located between the three cysteines that form the As(III) binding site. Both single tryptophan derivatives of ArsD exhibited substantial quenching of protein fluorescence upon addition of either As(III) or Sb(III), consistent with the region of ArsD

containing the metalloid binding site undergoing a conformational change when the site is filled.

However, the rate of quenching with As(III) was slower than might be expected for a simple binding reaction. If *in vivo* binding to ArsD was slower than the transfer to ArsA, then free arsenite might accumulate in the cytosol, negating the value of a chaperone. As(III) likely forms a  $\text{As}(\text{GS})_3$  complex with cytosolic GSH, the major reduced thiol in *E. coli*, where it can accumulate to concentrations as high as 10 mM (Apontoweil and Berends, 1975; Fahey and Sundquist, 1991). However, ArsA accepts metalloid from  $\text{As}(\text{GS})_3$  no faster than it binds free As(III), so, even though GSH might serve as an As(III) buffer, it does not aid in detoxification via the ArsAB pump. In contrast, ArsD accepts metalloid from  $\text{As}(\text{GS})_3$  faster than can be determined with our instrumentation. These considerations lead us to propose that the physiological donor to ArsD is  $\text{As}(\text{GS})_3$  (Figure 2-12). As arsenite enters *E. coli* cells via the aquaglyceroporin GlpF as  $\text{As}(\text{OH})_3$ , the high concentration of GSH would by mass action rapidly drive exchange of hydroxyls for thiols.

The next series of steps is proposed to involve the step-wise transfer of As(III) from ArsD thiolates to ArsA thiolates. The lack of effect of the As(III) chelator DMSA on the transfer reaction indicates that transfer is direct channeling from one protein to the other, rather than dissociation from ArsD and re-association with ArsA. The transfer reaction itself apparently requires ArsA to be undergoing catalysis. As(III) is not transferred from ArsD to ArsA in the presence of MgADP or MgATP- $\gamma$ -S, but only in the presence of MgATP, and then only at a temperature at which hydrolysis occurs. During the catalytic cycle ArsA undergoes a series of conformational changes in which the A1

and A2 halves are open relative to each other to a tightly closed conformation in which the product MgADP is trapped (Zhou et al., 2000, 2001). In our model, ArsD would interact with one of the transitional conformations, with transfer of As(III) integral to formation of the closed conformation. Further details of the transfer reaction will require structural information about ArsD and the ArsD-ArsA complex.

## CHAPTER 3

### Correlation between ArsD dimerization and metallochaperone function

#### 3.1 Introduction

*In vivo* results demonstrate that ArsD is an As(III)/Sb(III) chaperone that transfers metalloid to the ArsA ATPase (Lin et al., 2006). ArsD and ArsA interact with each other by yeast two-hybrid analysis. ArsD transfers As(III) to ArsA in the presence of  $Mg^{2+}$  and ATP. Channeling of arsenic from ArsD to ArsA protected As(III) from chelation by the chelator dimercaptosuccinic acid (DMSA). ArsA (Zhou et al., 2000) and ArsD (Ye et al., 2010). Structures have been solved by crystallization. But the details of interaction between ArsD and ArsA are still unknown. Non-tagged wild-type ArsD has been shown to be a homodimer by Sephacryl S-200 chromatography (Chen and Rosen, 1997). ArsD is also a dimer in the crystal structure. In this section, the question, whether ArsD dimerization is required for its function is studied.

The residues in dimerization interface observed in the ArsD crystal structure were mutated by site-directed mutagenesis. The dimerization status of the mutants was analyzed by gel-filtration chromatography. The activity of the mutants was also examined.

In addition, we did random mutagenesis of the *arsD* gene by error-prone PCR induced with  $Mn^{2+}$  (Cadwell and Joyce, 1992). Then ArsD mutants that lose interaction with wild-type ArsD was selected by reverse yeast two-hybrid analysis. The yeast two-hybrid system is a genetic system engineered to study protein-protein interactions (Fields and Song, 1989). Yeast two-hybrid analysis takes advantage of the properties of yeast transcriptional factor such as GAL4. GAL4 is a transcriptional activator required



for expression of genes encoding enzymes for utilizing galactose. It consists of two separate and essential domains. One is the N-terminal DNA binding domain (BD). The other is the C-terminal activation domain (AD). The BD binds to a small DNA element (UAS, upstream activation sequence), usually in the promoter region of the activated genes. The AD recruits the transcriptase to initiate transcription. By expressing a bait protein fused with BD and prey protein fused with AD separately from different plasmids, a functional GAL4 transcriptional activator can be reconstituted through their interaction. A reporter gene was engineered in the yeast chromosome as a marker for selection. When the two proteins interact, the reporter gene will be expressed. Usually the yeast two-hybrid system uses a nutritional synthetic gene such as *his3*, a histidine synthesis gene, as reporter gene. So only when two proteins interact with each other can the yeast cells grow on medium lacking histidine. New systems are also constructed using a toxic gene such as *ura3* as a reporter gene. *ura3* encodes orotidine 5-phosphate decarboxylase. It can metabolize 5-FOA (5-fluoroorotic acid) to 5-fluorouridine, an analog of uridine, inhibiting cell growth. Therefore it can be used to select for the mutants with weaker interaction or no interaction by growing the yeast cells on the plate with 5-FOA.

## 3.2 Materials and Methods

### 3.2.1 Strains, plasmids and media

*E. coli* cells were grown in Luria-Bertani (LB) medium (Sambrook et al., 1989) at 37°C. Ampicillin (100 µg/ml) or kanamycin (40 µg/ml) was added as required. *E. coli* strain JM109 [*recA1 supE44 endA1 hsdR17 gyrA96 relA1 thiΔ(lac-proAB)* F' (*traD36 proAB<sup>+</sup> lacI<sup>q</sup> lacZΔM15*)] was used for molecular cloning. *E. coli* strain BL21(DE3) [F-

*ompT hsdS<sub>B</sub>* ( $r_{B-m_B^-}$ ) *gal dcm* (DE3 [*lacI lacUV5-T7 gene1 ind1 Sam7 nin5*]) was used for protein expression and purification. ArsA with a C-terminal 6-histidine tag was expressed from plasmid pAlter-dAhB (Li and Rosen, 2000). N-terminal MBP-fused ArsD<sub>1-109</sub> (henceforth designated MBP-ArsD109) was expressed from plasmid pMAL-ArsD109 (Lin et al., 2007a). ArsD<sub>1-109</sub> with an N-terminal six-histidine tag (henceforth designated as wild type His6-ArsD109) was expressed from plasmid pET28a-ArsD109. Site-directed mutagenesis was done on plasmid pET28a-ArsD109 to get the mutant ArsD109<sub>S68A/R87A/R96A</sub>. Plasmid pGBT9 and pACT2 were used as *S. cerevisiae*/*E. coli* shuttle vectors for yeast two-hybrid assay (Lin et al., 2007b). *S. cerevisiae* strain AH109 (*MAT $\alpha$* , *trp1-901*, *leu2-3, 112*, *ura3-52*, *his3-200*, *gal4 $\Delta$* , *gal80 $\Delta$* , *LYS2::GAL1<sub>UAS</sub>-GAL1<sub>TATA</sub>-HIS3*, *GAL2<sub>UAS</sub>-GAL2<sub>TATA</sub>-ADE2*, *URA3::MEL1<sub>UAS</sub>-MEL1<sub>TATA</sub>-lacZ*) (Clontech, Mountain View, CA) and MAV203 (*MAT $\alpha$* ; *leu2-3,112*; *trp1-901*; *his3 $\Delta$ 200*; *ade2-101*; *cyh2<sup>R</sup>*; *can1<sup>R</sup>*; *gal4 $\Delta$* ; *gal80 $\Delta$* ; *GAL1::lacZ*; *HIS3<sub>UASGAL1</sub>::HIS3@LYS2*; *SPAL10::URA*) (Invitrogen, Carlsbad, CA) were used for yeast two-hybrid assay. Yeast cells were grown in complete yeast extract-peptone-dextrose (YPD) or minimal synthetic dextrose (SD) media with the appropriate supplements at 30°C (Adams et al., 1998). Growth in liquid culture was estimated from the absorbance at 600 nm. The strains and plasmids are listed in Table 3-1.

### 3.2.2 DNA manipulation and mutagenesis

Plasmid extraction, DNA restriction endonuclease analysis, ligation and other general molecular biological procedures were performed as described (Sambrook et al., 1989). Transformation of *E. coli* cells was carried out using a BIO-RAD MicroPluser (BIO-RAD, Hercules, CA). Transformation of Yeast cells was performed using Fast

Yeast Transformation™ kit from G-Biosciences (Maryland Heights, MO). DNA purification kits were obtained from QIAGEN (Valencia, CA). Either a Qiaprep Spin Miniprep kit or a Qiaquick gel extraction kit (QIAGEN) was used to prepare plasmid DNA for restriction enzyme digestion, sequencing, and recovering DNA fragments from agarose gels. Zymoprep II™ Yeast Plasmid Miniprep (Zymo Research, Orange, CA) was used to extract plasmid from yeast cells. The sequence of new plasmid constructs was confirmed by DNA sequencing of the entire gene. Site-directed mutagenesis was performed using Quick-change Site-Directed Mutagenesis kit (Stratagene, La Jolla, CA) and confirmed by sequencing. DNA sequencing was performed using a CEQ2000 DNA sequencer (Beckman Coulter, Brea, CA). The primers used are listed in Table 3-2.

### 3.2.3 Protein expression and purification

Cells bearing the indicated plasmids were grown in LB medium overnight at 37°C and then diluted 50-fold into 1 L of the same medium. Proteins were expressed by induction with 0.3 mM isopropyl-β-D-thiogalactopyranoside at  $A_{600}$  of 0.6-0.8 for 3 hrs. MBP-ArsD109 was purified from *E. coli* strain BL21(DE3) bearing plasmid pMAL-ArsD109 as described (Lin et al., 2006). ArsA with a six histidine tag at the C-terminus was purified from cells of strain BL21(DE3) expressing pAlter-1-dAhB plasmid, as described (Zhou and Rosen, 1997). ArsD and its derivatives with a six histidine tag at the N-terminus were purified similarly. Purified proteins were stored at -80°C until use, and their concentrations were determined according to the method of Bradford (Bradford, 1976) or from the absorption at 280 nm (Gill and von Hippel, 1989).

### 3.2.4 Gel-filtration chromatography

A 1.5cm diameter column filled with 165ml home-packed Superdex-75 (GE

Healthcare) gel-filtration column was used to analyze His6-ArsD109 truncation and ArsD109 derivatives on a Bio-rad Biological LP chromatography system. 1.5mg ovalbumin, 1.5mg carbonic anhydrase and 1.5mg ribonuclease were used as internal standard. 2mg His6-ArsD109 or His6-ArsD109 mutants and protein standards in 1ml buffer were loaded onto the column pre-equilibrated with column buffer (50mM MOPS, 200mM NaCl, 5mM 2-mercaptoethanol and 2mM DTT, pH 7.5). A 1.5cm diameter column filled with 165ml home-packed Sephacryl-200 (GE Healthcare) gel-filtration column was used to analyze MBP-ArsD109 on a Bio-rad Biological LP chromatography system. 1.5mg aldolase, 1.5mg conalbumin, and 1.5mg ovalbumine were used as internal standard. 2.4mg MBP-ArsD109 and protein standards in 1ml buffer were loaded onto the column pre-equilibrated with same column buffer as above. Then the column was washed with 200ml of column buffer. Elutions were collected as 1.5ml each fraction. Fractions were analyzed by 16% SDS-PAGE for His6-ArsD109 and 12% SDS-PAGE for MBP-ArsD109. Standard proteins are from Gel Filtration LMW Calibration Kit and Gel Filtration HMW Calibration Kit (GE Healthcare).

### **3.2.5 ATPase activity assays**

ATPase activity was estimated using a couple assay (Vogel and Steinhart, 1976), as described (Hsu and Rosen, 1989). ArsA was added at a final concentration of 0.3  $\mu$ M into an assay mixture containing 5 mM ATP, 1.25 mM phosphoenolpyruvate, 0.25 mM NADH, 10 units of pyruvate kinase and lactate dehydrogenase with or without the indicated concentrations of potassium antimonyl tartrate or sodium arsenite, in the buffer containing 50 mM MOPS-KOH, pH 7.5, 0.25 mM EDTA. ArsD was added at the indicated concentrations. The mixture was pre-warmed to 37°C, and the reaction was

initiated by addition of 2.5 mM MgCl<sub>2</sub> and measured at 340 nm. The linear steady state rate of ATP hydrolysis was used to calculate specific activity. The reaction volume was 0.2 ml each in 96-well microplates, and the reactions were monitored by microplate reader SPECTRA max 340PC (Molecular Devices).

### 3.2.6 Generation of a random mutated library of PCR fragments

Random mutagenesis of *ArsD* was performed using ep-PCR (Cadwell and Joyce, 1992) by employing biased nucleotide composition of the PCR buffer, high concentration of Mg<sup>2+</sup> and addition of Mn<sup>2+</sup>. The ep-PCR reaction mixture (50 µl) contained 20 mM Tris-HCl (pH 8.4), 50 mM KCl, 7 mM MgCl<sub>2</sub>, 0.2 mM each of dATP and dGTP, 1 mM each of dCTP and dTTP, 25 pmol each of the oligonucleotide primers, 80 ng of template DNA, 2.5 U of Taq DNA polymerase (Invitrogen). pGBT9-D plasmid DNA was used as template. Primer pGBT9-s (TAA AGA TGC CGT CAC AGA TAG ATT G) and pGBT9-a (ACC TGA CCT ACA GGA AAG AGT TAC T) were used as primer, and 0.5 mM Mn<sup>2+</sup> was added. PCR condition was 1× 96 °C for 3 min, 30× 94 ° for 30 s, 1×55 °C for 30 s, 1×72 °C for 100s, and, finally, 1× 72 °C for 10 min. The ep PCR product was analyzed by agarose gel, extracted from gel and quantified by absorption at 260nm.

### 3.2.7 Yeast two-hybrid analysis

Two yeast stains, AH109 (Fields and Song, 1989) and MAV203 (Vidal et al., 1996), were used. Both are GAL4-based yeast two-hybrid system. Yeast cells are co-transformed with *ars* gene-fused pGBT9-X (BD-X) and pACT2-Y (AD-Y) plasmids. pGBT9 was modified to pGBT9-k by inserting kanamycin resistant gene for easier selection of the mutants. Primers pET28a-3600-AatII (CTA TGA CGT CCA ACC CGG

TAA GAC ACG ACT TAT C) and pET28a-5300-AatII (CTA TGA CGT CCG CCC GCT CCT TTC GCT TTC TTC C) were used to amplify kanamycin resistant gene from pET28a by PCR. Then the PCR product was analyzed by agarose gel, extracted from gel and digested by AatII. pGBT9 was also digested with AatII. Then digested PCR fragment and vector are ligated and transformed into JM109. The cells were plated on the LB plate with kanamycin to select for the vector, pGBT9-k, which shows kanamycin resistance. For unknown reason, pGBT9-k loses ampicillin resistance.

MAV203 was firstly used to select for *ArsD* mutants that lose the capability of dimerization with wild-type *ArsD*. The ep-PCR fragment was mixed with pGBT9-k vector linearized by *EcoRI* and *BamHI*, and co-transformed with pACT2-D into MAV203 and selected on the SD-L-W plate supplemented with 0.2% 5-FOA (5-Fluoroorotic Acid) (Fermentas, Burlington, Ontario). The PCR fragment will be ligated into the vector *in vivo* through homology recombination (Hua et al., 1997). The colonies were pooled and colony-PCR was done with primer pGBT-s and pGBT9-a. PCR product was purified by agarose gel-extraction, mixed with pGBT9-k vector linearized by *EcoRI* and *BamHI*, and co-transformed with pACT2-A into AH109 and selected on the SD-L-W-H plates lacking histidine. To determine protein-protein interaction by growth of series of dilutions, the transformed cells were cultured overnight in SD medium at 30°C and then washed, suspended and adjusted to an absorbance of 1 at  $A_{600nm}$  in 20 mM Tris-HCl pH 7.5. Portions of the cell suspensions (1  $\mu$ l) were inoculated in serial 10-fold dilutions on SD agar plates lacking histidine or with 3-AT at indicated concentration. The plates were incubated at 30°C for 3 days.

### 3.2.8 Sequencing of *ArsD* mutant genes in yeast colonies

Each yeast colony was grown in corresponding liquid SD medium. The plasmids were isolated from yeast by Zymoprep II™ Yeast Plasmid Miniprep Kit (Zymo Research Cop. Orange, CA), transformed to *E. coli* JM109 and grown on LB plate with kanamycin. Then the plasmids were extracted from *E. coli* JM109 and sequenced with the GAL4-BD sequencing primer (GAG TAG TAA CAA AGG TCA A).

### 3.3 Results

#### 3.3.1 Dimerization equilibria of MBP-ArsD109 and His6-ArsD109

Non-tagged wild-type ArsD has been shown to be a homodimer by Sephacryl S-200 chromatography (Chen and Rosen, 1997). In my studies, both N-terminal MBP (maltose binding protein) tagged ArsD and N-terminal six-histidine-tagged ArsD were used. Both MBP-ArsD109 and His6-ArsD109 could stimulate ArsA ATPase activity. ArsA exhibits apparent affinity for As(III) of approximately 0.5 mM. Both MBP-ArsD109 and His6-ArsD109 increased ArsA the apparent affinity for As(III) to around 10  $\mu$ M (Figure 3-1). However, these two different ArsD derivatives showed different dimerization equilibria by gel-filtration chromatography. The apparent molecule weight of MBP-ArsD109 monomer is 56 kDa. It elutes out between standard conalbumin (75 kDa) and ovalbumin (43 kDa) and is more likely a monomer (Figure 3-2A). The molecule weight of His6-ArsD109 is predicted to be 16 kDa for a monomer and 32 kDa for a dimer. It elutes out before standard carbonic anhydrase (29 kDa) and so is more likely a dimer (Figure 3-2B). Since dimerization is concentration dependent, both MBP-ArsD109 and His6-ArsD109 could be in equilibrium between monomer and dimer. This leads to the question whether ArsD interacts with ArsA as a dimer or a monomer. It is also possible that both dimer and monomer are able to interact with ArsA.

### 3.3.2 Mutations at the putative dimerization interface shift ArsD to a monomer

We attempted to make monomeric ArsD by mutating residues located at the major dimerization interface observed in the crystal structure to test whether it is still active. Whether the crystallographic ArsD dimer represents the solution dimer is not known, but the observed dimer has an extensive interface between two subunits mainly contributed by the 4<sup>th</sup>  $\beta$ -sheet and 3<sup>rd</sup> and 4<sup>th</sup>  $\alpha$ -helix. In the crystallographic dimer, a total surface area of 1,338  $\text{\AA}^2$  is buried between the two ArsD monomers. This represents 11.5% of the total solvent-accessible surface. The dimer is mainly held together by hydrogen bonds. Notably, there are at least 10 hydrogen bonds, and the donors from one monomer and the acceptor from the other are less than 3.2  $\text{\AA}$  apart. The hydrogen bond and salt bridge was shown in Figure 3-3. The amide and carbonyl groups of Ala85 from one monomer make hydrogen bonds to the carbonyl and amide of Ala85 from the other monomer, respectively. The hydroxyl of the Ser68 side chain from one monomer is hydrogen bonded to the carbonyl of Val83 from the other monomer. The carbonyl of Gly86 from one monomer makes hydrogen bonds to the side chain amides of Arg96 from the other monomer. The carbonyl of Gly86 from one monomer also makes hydrogen bonds to the side chain amides of Arg87 from the other monomer. Arg96 and Glu71 form salt-bridge.

The side chains of Ser68, Arg87 and Arg96 are predicted to contribute hydrogen bonds and a salt bridge. A triple mutant was made by mutating these three residues to alanines. Eight hydrogen bonds should be eliminated if no new bonds are formed. This triple mutant His6-ArsD109<sub>S68A/R87A/R96A</sub> is predicted to have molecular weight of 16 kDa for a monomer and 32 kDa for a dimer, similar to the wild-type His6-ArsD109. In gel-



filtration chromatography, this mutant elutes after carbonic anhydrase (29 KDa) (Figure 3-4A) and so is most likely in an equilibrium between dimer and monomer, compared with wild-type His6-ArsD109, which elutes before carbonic anhydrase (Figure 3-2B). Thus the dimerization equilibrium of this mutant is shifted toward the monomer. This suggests that Ser68, Arg87 and Arg96 are involved in dimerization in the solution, and that the dimer interface in the crystal structure is similar to that in solution.

We further mutated four other residues, Glu81, Thr82, Val83 and Met84 to alanine residues, creating His6-ArsD109<sub>S68A/R87A/R96A/E81A/T82A/V83A/M84A</sub>. These seven mutations totally changed the 4<sup>th</sup>  $\beta$ -sheet, which is predicted to be involved in dimerization. In gel-filtration chromatography, this mutant elutes between carbonic anhydrase (29 kDa) and ribonuclease (13 kDa), suggesting that it is in equilibrium between monomer and dimer (Figure 3-4B). However, it does not totally correspond to a monomer size, making interpretation difficult.

The mutant ArsD109<sub>S68A/R87A/R96A/E81A/T82A/V83A/M84A</sub> stimulated ArsA ATPase activity as well as the wild type. Both of wild type His6-ArsD109 and this mutant increased the apparent affinity of ArsA for As(III) to around 10  $\mu$ M (Figure 3-4C), suggesting that dimerization may be not required for the ArsD metallochaperone function. However, since the mutants are in monomer-dimer equilibrium, this conclusion is not firm.

### 3.3.3 Generating an ArsD mutant with weaker dimerization

Since we were unable to change ArsD entirely to a monomeric form by site-directed mutagenesis, we use yeast random mutagenesis coupled with the yeast two-hybrid system to select for ArsD mutants that show weaker dimerization. Yeast strain

MAV203 has *ura3* reporter gene that encodes an enzyme metabolizing 5-FOA (5-fluoroorotic acid) to 5-fluorouridine, an analog of uridine, inhibiting cell growth. Therefore MAV203 can be used to select for mutants with weaker interaction or no interaction as a result of ability to grow on plates with 5-FOA (Vidal et al., 1996). ArsD have been shown to dimerize by GAL4 yeast two-hybrid analysis with yeast strain AH109 (Lin et al., 2007b). We confirmed that ArsD also dimerizes in MAV203 and determined that MAV203 co-transformed with pACT2-D (encoding wild type AD-ArsD) and pGBT9-D (encoding wild type BD-ArsD) cannot grow on SD-L-W plates with 0.2 % 5-FOA. So we used 0.2 % 5-FOA to select for ArsD mutants that cannot interact with wild type ArsD or interacts more weakly.

Using a pair of primers homologous to regions on pGBT9-D (encoding BD-ArsD) flanking the inserted *arsD* gene, error-prone PCR was performed on ArsD as described under 'Materials and Methods'. The purified PCR product was mixed with pGBT9-k vector linearized by *EcoRI* and *BamHI*, and co-transformed with pACT2-D (encoding wild type AD-ArsD) into MAV203 and selected on SD-L-W plates with 0.2 % 5-FOA. 240 colonies could grow on 5-FOA plates, 8% of the 3000 clones that grew on plates without 5-FOA. Presumably these colonies might contain not only ArsD mutants interacting more weakly with wild type ArsD, but also truncated ArsD mutants, non folding ArsD mutants, or even empty pGBT9 vector. Since ArsD interacts with ArsA in yeast strain AH109 (Lin et al., 2007b), we further screened the mutants for their ability to still interact with ArsA. If they retained the ability to interact with ArsA, they should fold normally. We pooled the resulting 240 colonies and used the same primer, homologous to regions on pGBT9-D flanking the inserted *arsD* gene for colony PCR. Then the purified PCR

products were mixed with vector plasmid pGBT9-k linearized by *EcoRI* and *BamHI*. The mixture was co-transformed with pACT2-A (encoding AD-ArsA) into AH109, and colonies were selected on SD-L-W-H plates. 55 colonies grew on SD-L-W-H plates, 0.8% compared with 6500 colonies on the SD-L-W plates. 24 colonies were picked and sequenced. Finally, we isolated two ArsD mutants that showed no interaction with wild type ArsD but retained interaction with ArsA (Figure 3-5A). These two mutants are ArsD<sub>L36H, I43F, G86E</sub> and ArsD<sub>G86E</sub>.

Only the G86E mutation was found in both mutants. Gly86 sits in the dimerization interface (Figure 3-3C), suggesting this mutant might be a monomer. His6-ArsD109<sub>G86E</sub> was constructed by site-directed mutagenesis. The protein was expressed, purified and analyzed by gel-filtration chromatography. His6-ArsD109<sub>G86E</sub> eluted between carbonic anhydrase (29 KDa) and ribonuclease (13 KDa), suggesting an equilibrium between monomer and dimer (Figure 3-5B). Compared with wild-type His6-ArsD109, which elutes before carbonic anhydrase (Figure 3-2B), mutant His6-ArsD109<sub>G86E</sub> was shifted toward monomer, consistent with yeast two-hybrid analysis.

The ability of mutant ArsD109<sub>G86E</sub> to stimulate ArsA ATPase activity was examined. His6-ArsD109<sub>G86E</sub> increased the apparent affinity of ArsA for As(III) to around 10  $\mu$ M (Figure 3-6), again suggesting dimerization may be not required for the ArsD metallochaperone function.

### 3.4 Discussion

*In vivo* results demonstrate that ArsD is an As(III)/Sb(III) chaperone that transfers metalloid to the ArsA ATPase (Lin et al., 2006; Lin et al., 2007a), but the molecular details of the process are lacking. Structural information about ArsD and the ArsD-ArsA

complex is needed to understand the details. ArsD has been shown to be a dimer in crystal structure. In this study the correlation between ArsD dimerization and metallochaperone function was studied.

Non-tagged wild-type *E. coli* R773 ArsD has been shown to be a homodimer by Sephacryl S-200 chromatography (Chen and Rosen, 1997). ArsD is also a dimer in the crystal structure (Ye et al., 2010). ArsD constructs with either an N-terminal maltose binding protein (MBP) tag or an N-terminal His6 tag were used in this study. They were both active but behaved differently in gel-filtration chromatography. The monomer-dimer equilibrium of MBP-ArsD109 is toward monomer, while the equilibrium of His6-ArsD109 is toward dimer. These results could mean that either monomer or dimer of ArsD interact with ArsA, so further analysis was required.

The crystallographic dimerization interface of ArsD involves a series of hydrogen bonds and one salt bridge, with the side chains of Ser68, Arg87 and Arg96 participating. As a consequence of mutating these residues to alanines, there was a shift in the equilibrium toward the monomer direction, but each mutant was still active in terms of metallochaperone activity. Using the yeast two-hybrid assay to select and screen mutants with reduced interaction with wild-type ArsD but retaining interaction with ArsA, the mutation G86E was found to decrease ArsD dimerization. Gly86 is located in the dimerization interface in the crystal structure. Gel-filtration chromatography confirmed that the equilibrium of His6-ArsD109<sub>G86E</sub> is shifted toward monomer direction, and this mutant retains ability to stimulate ArsA ATPase activity. All these results suggest that the dimerization region observed in the crystal structure also exists in solution, and that dimerization is not strictly required for ArsD metallochaperone function.

Recently the crystal structure of another ArsD homolog from *Bacteroides vulgatus* ATCC 8482 was deposited in the Protein Data Base (pdb: 3KTB; Kim, Y., Tesar, C., Feldmann, B., Joachimiak, A., Midwest Center for Structural Genomics (MCSG), unpublished). *E. coli* R773 ArsD is clearly a dimer (Figure 3-7A). However, *Bacteroides vulgatus* ATCC 8482 ArsD has four molecules in the crystallographic unit (Figure 3-7C). In all four molecules, Cys13 and Cys18 form intra-subunit disulfide bonds. Each two of the subunits form an inter-subunit disulfide bond with Cys12 from each subunit. Then two dimers form a tetramer noncovalently. 3KTB and R773 ArsDs can be superimposed with an RMSD of 1.0 Å (Figure 3-7B).

Although *Bacteroides vulgatus* ATCC 8482 ArsD is a tetramer in crystal structure, it is not known the aggregation status in the solution. But the structure definitely suggests different subunit contact positions. The cysteine residues position of *Bacteroides vulgatus* ATCC 8482 ArsD is very consistent with our previous result of cysteine crosslinking by dibromobimane that Cys12, Cys13 and Cys18 from one subunit are close to the cysteine residues from another subunit (Lin et al., 2007a). So it is also possible R773 ArsD may have more than one site of contact between subunits, one at the interface shown in R773 ArsD crystal structure and another one is close to the cysteines. This may be one reason that no mutant is totally monomeric ArsD.

Very recently a new ArsD mutant, P52L, which exhibits increased affinity for wild type ArsD was isolated using random mutagenesis and a modified yeast two-hybrid assay (unpublished data). In the standard assay cells of histidine-requiring yeast are screened for interaction between proteins by the ability to grow in the absence of histidine. 3-Aminotriazole (3-AT) is a HIS3 competitive inhibitor that prevents growth.

The two proteins fused to AD and BD should interact stronger to support the yeast cell growth on the plates with 3-AT. Yeast cells co-transformed with BD-ArsD P52L (mutant ArsD fused to BD) and AD-ArsD (wild-type ArsD fused to AD) grow in the presence of 60 mM 3-AT (Figure 3-8). Interestingly, the yeast two-hybrid results suggest that P52L loses interaction with ArsA (Figure 3-8). This may indicate that there is another dimerization interface that involves Pro52 (Figure 3-9A and B). The crystal structure suggests that a hydrophobic patch may be involved in interaction between subunits in neighboring asymmetric units, including Leu48, Phe52, Met53, Phe55, Val56, Val61, Ile66 and Ala70, which may form an extensive hydrophobic interface (Figure 3-9C and D). Residues Leu48, Pro52, Met53 and Val56 are close to an adjacent subunit, contributing to this crystallographic dimerization interface. Although the side chains of residues Phe55, Val61 and Ile66 point inward, they are less than 5Å from corresponding residues in the adjacent subunit, close enough to form an intra-subunit hydrophobic core. They may be important for maintaining the angles between the  $\alpha 2$  and  $\alpha 3$  helices and may contribute to dimerization as well (Figure 3-9E). This hypothesis can explain why mutations in the previous dimerization interface do not result in strict monomer. This idea will be tested by future students in the lab.

In addition, ultra-centrifugation will be used to analyze the aggregation status of ArsD in the solution and to obtain the associating constant of ArsD. In summary, it is still unclear whether ArsD is a monomer or dimer when it interacts with ArsA.

## CHAPTER 4

### Mapping ArsA-ArsD interaction interface by genetic analysis

#### 4.1 Introduction

ArsD is an As(III)/Sb(III) chaperone that transfers metalloid to the ArsA ATPase (Lin et al., 2006). ArsD transfers As(III) to ArsA in the presence of  $Mg^{2+}$  and ATP. Correspondingly, ArsD can be crosslinked with ArsA in the presence of  $Mg^{2+}$  and ATP, by the homofunctional cysteine crosslinker dibromobimane. ArsA structure has been solved by crystallization (Zhou et al., 2000). Cys113, Cys172 and Cys422 are close to each other and involved in metal binding (Ruan et al., 2006, 2008). ArsD structure has been recently solved (Ye et al., 2010). Though the metal binding site is missing in the structure, biochemical results suggest that Cys12, Cys13 and Cys18 form a three-sulfur coordinated metal binding site important for transferring As(III) to ArsA (Lin et al., 2007a). According to this, we proposed a model for the metal transfer similar as the model shown in Figure 2-12 (Lin et al., 2007a), that ArsA and ArsD interact at their metal binding sites, then As(III) is transferred through ligand-exchange between cysteine residues of ArsA and ArsD. Consistent with this model, As(III) is protected from sequestration by As(III) chelator, DMSA, during transfer from ArsD to ArsA, suggests that ArsA-ArsD interaction forms a channel for As(III) transferring from MBS of ArsD to MBS of ArsA. However, a detail of interaction between ArsD and ArsA is still unknown.

Copper chaperone has been found from prokaryotic cells to eukaryotic cells. They are most well studied metallochaperone protein. The study of interaction between copper chaperone proteins and their targets are summarized in Table 4-1. So far, no co-crystallization of the wild-type chaperone proteins and their targets has been successful.

Through gel-filtration, Cu(I)-CopZ transfer Cu(I) to CopY. But these two protein do not come off the gel-filtration column as a complex (Cobine et al., 1999). Similar to this, ArsD transfers As(III) to ArsA but they do not form stable complex. The interaction between HAH1, and the second or the fifth soluble domains of ATP7A (MNK2 and MNK5, respectively), was investigated in solution using heteronuclear NMR. No stable adduct is formed between either of the MNK domains and HAH1 (Banci et al., 2005). NMR titration shows the formation of an adduct by Cu(I)-HAH1 with WLN4 that is in fast exchange on the NMR time scale with the isolated protein species as confirmed by  $^{15}\text{N}$  relaxation data. A similar interaction is also observed between Cu(I)-HAH1 and WLN2; however, the relative amount of the adduct in the protein mixture is lower. In both cases the interaction interface can not be mapped by NMR (Achila et al., 2006). All these results suggest that the interaction between copper chaperone proteins and their targets is weak and transient. Maybe this is a common nature for all metallochaperone proteins since their roles are to escort the metal to the target proteins but not stick to their target proteins. Unless we can stop the transfer process, the complex will not be stable. One example is the complex structure of yeast copper chaperone yCCS and its partner protein, superoxide dismutase (SOD1). His48, one of the ligand for copper was mutated to Phe in SOD1; in this mutant transfer could not be completed. yCCS and this mutant SOD1 form stable complex (Lamb et al., 2000) and can be co-crystallized (Lamb et al., 2001).

Another complex structure was characterized by combination of NMR and *in silico* modeling. The study was conducted with Atx1 and the first MBD of Ccc2. By following the  $^{15}\text{N}$  and  $^1\text{H}$  chemical shifts, a new species was detected. This species is in



fast exchange with the parent species on the NMR time scale. Nuclear relaxation data are consistent with the formation of an adduct (Arnesano et al., 2001). Based on NMR chemical shift mapping information, a structure model of the transient complex was proposed through *in silico* docking. The model shows that the interaction is mainly of an electrostatic nature with hydrogen bonds stabilizing the complex (Arnesano et al., 2004).

Crystallization and NMR are two major tools to get the details of structural information. Dr. Abdul Ajees Abdul Salam in our laboratory is trying to get the crystal structure of ArsA-ArsD complex, but with no success so far. Dr. Jun Ye and I tried NMR study on ArsD in the hope of mapping interaction interface by following the  $^{15}\text{N}$  and  $^1\text{H}$  chemical shifts. However, the inhomogeneous nature of ArsD aggregation state at high concentration such as 1 mM required for NMR study has delayed complete assignment.

Yeast two-hybrid has been used to show interaction between Atx1 and the N-terminal MBD of Ccc2 (Pufahl et al., 1997), between Atx1 and copper amine oxidase Cao1 (Peter et al., 2008), between HAH1 and the 2<sup>nd</sup> or 4<sup>th</sup> MBD of ATP7B (van Dongen et al., 2004), and also between HAH1 and 2<sup>nd</sup>-6<sup>th</sup> MBD of ATP7A (Larin et al., 1999).

The yeast two-hybrid system is a genetic system engineered to study protein-protein interaction (Fields and Song, 1989). It has been widely used to build protein-protein interaction networks (Bruckner et al., 2009). Yeast two-hybrid analysis takes advantage of the properties of yeast transcriptional factor such as GAL4. GAL4 is a transcriptional activator required for expression of genes encoding enzymes for utilizing galactose. It consists of two separate and essential domains. One is the N-terminal

DNA binding domain (BD). The other is the C-terminal activation domain (AD). DNA binding domain (BD) binds to a small DNA element (UAS, upstream activation sequence), usually in the promoter region of the activated genes. The activation domain (AD) recruits the transcriptase to initiate the transcription. By expressing bait protein fused with BD and prey protein fused with AD separately from different plasmids, only when bait protein and prey protein interact with each other, a functional GAL4 transcriptional activator can be reconstituted. Usually a reporter gene was engineered in the yeast chromosome as a marker for selection. When two proteins interact, the reporter gene will be expressed. Normal yeast two-hybrid analysis uses nutrition synthetic genes such as *his3*, a histidine synthesis gene, as a reporter. So only when two proteins interact with each other, can the yeast cells grow on media lacking histidine. New systems have also been devised using a toxic gene such as *ura3* as a reporter gene. *ura3* encodes orotidine 5-phosphate decarboxylase. It can metabolize 5-FOA (5-fluoroorotic acid) to 5-fluorouridine, an analog of uridine, inhibiting cell growth. Therefore it can be used to select for the mutants with weaker interaction or no interaction by growing the yeast cells on the plate with 5-FOA. This is also called reverse yeast two-hybrid analysis (Vidal et al., 1996). Mutations interfering with interaction can give information about the protein-protein interaction interface. The normal yeast two-hybrid analysis has been used to select for the mutants retaining the interaction. The absence of interference of these mutation points was used to map the protein-protein interaction interface (Dhayalan et al., 2008).

Using a yeast two-hybrid system based on the GAL4 transcriptional factor, ArsD and ArsA were shown to interact with each other (Lin et al., 2006). Plasmid pACT2 was

used to express ArsD or ArsA fused with GAL4 activation domain (GAL4-AD). Plasmid pGBT9 was used to express ArsD or ArsA fused with GAL4 DNA binding domain (GAL4-BD). Yeast strain AH109 with *his3* as reporter gene was used to show ArsD-ArsA interaction. *his3* encodes imidazole glycerol-phosphate dehydratase, catalyzing the sixth step in histidine biosynthesis. ArsD-ArsA interaction is indicated by cell growth on the plate lacking histidine.

Histidine synthesis by HIS3 enzyme is competitively inhibited by 3-AT (3-amino-1,2,4-triazole) (Klopotowski and Wiater, 1965). If 3-AT was added to the medium, the yeast cells need to synthesize more HIS3 to grow normally. 3-AT has been used in the yeast three-hybrid system to select RNA with higher affinity to the protein (Cassiday and Maher, 2003; Hook et al., 2005).

We did random mutagenesis by error-prone PCR induced with  $Mn^{2+}$  on both ArsA and ArsD (Cadwell and Joyce, 1992). Then we selected for mutants that lose interaction using reverse yeast two-hybrid analysis. 3-AT was used with the yeast two-hybrid strain AH109 using *his3* as a report gene to select for mutants showing stronger interaction. In addition, we also did site-directed mutagenesis on lysine residues of ArsD and obtained mutants losing function. All these mutants will give us information about ArsA-ArsD interaction interface.

## 4.2 Materials and Methods

### 4.2.1 Reagents

3-AT (3-amino-1,2,4-triazole) was purchased from MP Biomedicals (Solon, OH). 5-FOA (5-Fluoroorotic Acid) was purchased from Fermentas (Burlington, Ontario). Yeast minimal SD base, amino acid Drop-out supplements, -Leu/-Trp and -Leu/-Trp/-His

were purchased from Clontech (Mountain view, CA). Sulfo-NHS Acetate (Sulfosuccinimidyl Acetate) was purchased from Thermo Scientific (Rockford, IL). Unless otherwise mentioned, all other chemicals were obtained from Sigma.

#### 4.2.2 Strains, plasmids and media

*E. coli* strain JM109 [*rcA1 supE44 endA1 hsdR17 gyrA96 relA1 thiΔ(lac-proAB) F'* (*traD36 proAB<sup>+</sup> lacI<sup>q</sup> lacZΔM15*)] was used for molecular cloning. *E. coli* strain BL21(DE3) [*hsdS gal(Δclts857 ind1 Sam7 nin5 lacUV5-T7 gene1)*] was used for protein expression and purification. ArsA with C-terminal His6 tag was cloned in the expression vector pAlter-1 as pAlter-dAhB (Li and Rosen, 2000). Six histidines tagged ArsD<sub>1-109</sub> truncation was cloned in the expression vector pET28a as pET28a-ArsD109 (Chapter 2). *E. coli* cells were grown in Luria-Bertani (LB) medium (Sambrook et al., 1989) at 37°C. Ampicillin (100 μg/ml), kanamycin (40 μg/ml) and 0.3 mM isopropyl-β-D-thiogalactopyranoside were added as required. Plasmids pGBT9 and pACT2 were used as *S. cerevisiae/E. coli* shuttle vectors for yeast two-hybrid assay (Lin et al., 2007b). *S. cerevisiae* strains AH109 (*MAT<sub>a</sub>, trp1-901, leu2-3, 112, ura3-52, his3-200, gal4Δ, gal80Δ, LYS2::GAL1<sub>UAS</sub>-GAL1<sub>TATA</sub>-HIS3, GAL2<sub>UAS</sub>-GAL2<sub>TATA</sub>-ADE2, URA3::MEL1<sub>UAS</sub>-MEL1<sub>TATA</sub>-lacZ*) (Clontech, Mountain View, CA) and MAV203 (*MAT<sub>α</sub>; leu2-3,112; trp1-901; his3Δ200; ade2-101; cyh2<sup>R</sup>; can1<sup>R</sup>; gal4Δ; gal80Δ; GAL1::lacZ; HIS3<sub>UAS</sub>GAL1::HIS3@LYS2; SPAL10::URA*) (Invitrogen, Carlsbad, CA) were used for yeast two-hybrid assay. Yeast cells were grown in complete yeast extract-peptone-dextrose (YPD) or minimal synthetic dextrose (SD) media with the appropriate supplements at 30°C (Adams et al., 1998). Growth in liquid culture was estimated from the absorbance at 600 nm. The strains and plasmids are listed in Table 4-2.

### 4.2.3 DNA manipulation and mutagenesis

Plasmid extraction, DNA restriction endonuclease analysis, ligation and other general molecular biological procedures were performed as described (Sambrook et al., 1989). Transformation of *E. coli* cells was carried out using a BIO-RAD MicroPluser (BIO-RAD, Hercules, CA). Transformation of Yeast cells was performed using Fast Yeast Transformation™ kit from G-Biosciences (Maryland Heights, MO). DNA purification kits were obtained from QIAGEN (Valencia, CA). Either a Qiaprep Spin Miniprep kit or a Qiaquick gel extraction kit (QIAGEN) was used to prepare plasmid DNA for restriction enzyme digestion, sequencing, and recovering DNA fragments from agarose gels. Zymoprep II™ Yeast Plasmid Miniprep (Zymo Research, Orange, CA) was used to extract plasmid from yeast cells. The sequence of new plasmid constructs was confirmed by DNA sequencing of the entire gene. Site-directed mutagenesis was performed using Quick-change Site-Directed Mutagenesis kit (Stratagene, La Jolla, CA) and confirmed by sequencing. DNA sequencing was performed using a CEQ2000 DNA sequencer (Beckman Coulter, Brea, CA). The primers used are listed in Table 4-3.

### 4.2.4 Generation of a random mutated library of PCR fragments

Random mutagenesis of *ArsA* or *ArsD* was performed using ep-PCR (Cadwell and Joyce, 1992) by employing biased nucleotide composition of the PCR buffer, high concentration of  $Mg^{2+}$  and addition of  $Mn^{2+}$ . The ep-PCR reaction mixture (50  $\mu$ l) contained 20 mM Tris-HCl (pH 8.4), 50 mM KCl, 7 mM  $MgCl_2$ , 0.2 mM each of dATP and dGTP, 1 mM each of dCTP and dTTP, 25 pmol each of the oligonucleotide primers, 80 ng of template DNA, 2.5 U of Taq DNA polymerase (Invitrogen).

For *ArsA*, pACT2-A plasmid DNA was used as template, and pACT2-s (CTA TTC GAT GAT GAA GAT ACC CCA CCA AAC CC) and pACT2-a (AGG TTA CAT GGC CAA GAT TGA AAC TTA GAG GAG) were used as primer, 0.1mM Mn<sup>2+</sup> was added. PCR condition was 1× 96 °C for 3 min, 30× 94 ° for 30 s, 1× 55 °C for 30 s, 1× 72 °C for 4 min, and, finally, 1× 72 °C for 10 min. For *ArsD*, pGBT9-D plasmid DNA was used as template, and pGBT9-s (TAA AGA TGC CGT CAC AGA TAG ATT G) and pGBT9-a (ACC TGA CCT ACA GGA AAG AGT TAC T) were used as primer. 0.5mM Mn<sup>2+</sup> was added. PCR condition was similar to the condition for *ArsA*, only extension time at 72°C is changed to 100 s. The ep PCR product was analyzed by agarose gel, extracted from gel and quantified by absorption at 260nm.

#### 4.2.5 Yeast two-hybrid analysis

Two yeast stains, AH109 (Fields and Song, 1989) and MAV203 (Vidal et al., 1996), were used. Both are GAL4-based yeast two-hybrid system. AH109 was used to analyze protein-protein interaction or select the mutants that retaining capability of interaction or showing stronger interaction in the presence of 3-AT (3-amino-1,2,4-triazole) (Sigma-Aldrich, St. Louis, MO). MAV203 was used to select for the mutants that lose the capability of interaction through counter-selection in the presence of 5-FOA (5-Fluoroorotic Acid) (Fermentas, Burlington, Ontario). Yeast cells are co-transformed with *ars* gene-fused pGBT9-X (BD-X) and pACT2-Y (AD-Y) plasmids. To determine protein-protein interaction by growth of series of dilutions, the transformed cells were cultured overnight in SD medium at 30°C and then washed, suspended and adjusted to an absorbance of 1 at A<sub>600nm</sub> in 20 mM Tris-HCl pH 7.5. Portions of the cell suspensions

(1 µl) were inoculated in serial 10-fold dilutions on SD agar plates lacking histidine or with 3-AT at indicated concentration. The plates were incubated at 30°C for 3 days.

pGBT9 was modified to pGBT9-k as in Chapter 2. To select for *ArsD* mutants, the ep-PCR fragment was mixed with pGBT9-k vector linearized by *EcoRI* and *BamHI*, and co-transformed with pACT2-A or pACT2-D into yeast-strains and selected on the indicated plates. The PCR fragment will be ligated into the vector *in vivo* through homology recombination (Hua et al., 1997). To select for *ArsA* mutants, the ep-PCR fragment was mixed with pACT2 vector linearized by *EcoRI* *EcoRI* and *BamHI*, and co-transformed with pGBT9-k-D into yeast-strains and selected on the indicated plates.

#### 4.2.6 Sequencing of *ArsD* and *ArsA* mutant genes in yeast colonies

Each yeast colony was grown in corresponding liquid SD medium. The plasmids were isolated from yeast by Zymoprep II™ Yeast Plasmid Miniprep Kit (Zymo Research Cop. Orange, CA), transformed to *E. coli* JM109 and grown on LB plate with ampicillin for *ArsA* and kanamycin for *ArsD*. Then the plasmids were extracted from *E. coli* JM109 and sequenced as the following. For *ArsD*, mutant genes on pGBT9-k vector were sequenced with the GAL4-BD sequencing primer (GAG TAG TAA CAA AGG TCA A). For *ArsA*, mutant genes on pACT2 vector were sequenced with five sets of primers (GAL4-AD sequencing primer: AAT ACC ACT ACA ATG GAT; *ArsA*-100-s: GTC CTG CCT GAT GAC GTT GTT TCC A; *ArsA*-220-s: GTC GCC CGG ACT CAT CTG GAA CTT G; *ArsA*-420-s: AAG AGG ACT TAC GCT CAC CTT GCA C; *ArsA*-480-a: CGT GAC CAG TAA CAC TTT AGT GCG).

#### 4.2.7 Protein expression and purification

Cells bearing the indicated plasmids were grown in LB medium overnight at 37°C

and then diluted 50-fold into 1 L of the same medium. Proteins were expressed by induction with 0.3 mM isopropyl- $\beta$ -D-thiogalactopyranoside at  $A_{600}$  of 0.6-0.8 for 3 hrs. ArsA with a six histidine tag at the C-terminus was purified from cells of strain BL21(DE3) expressing pAlter-1-dAhB plasmid, as described (Zhou and Rosen, 1997). Cells were harvested by centrifugation and washed once with a buffer containing 50 mM MOPS, pH 7.5, 0.5 M NaCl, 30 mM Imidazole and 10 mM 2-mercaptoethanol (Buffer A). The cells were suspended in 5 ml of Buffer A per gram of wet cells and lysed by a single passage through a French press at 20,000 psi. Diisopropyl fluorophosphate (DIFP) (Sigma) was added at 2.5  $\mu$ l/g wet cells immediately following French press. Unbroken cells and membranes were removed by centrifugation at 150,000 x g for 1 hr at 4°C. The supernatant was loaded to 10 ml Probond Ni-column (Invitrogen) pre-equilibrated with Buffer A. Unbound proteins were washed by 60 ml of buffer A, and ArsA was eluted with imidazole gradient generated by Buffer A and Buffer B (50 mM MOPS, pH 7.5, 0.5 M NaCl, 300 mM Imidazole and 10 mM 2-mercaptoethanol), followed by addition of 0.25 mM EDTA and 5 mM DTT to each fraction. ArsA containing fractions were identified by sodium dodecyl sulfate polyacrylamide gel electrophoresis (SDS-PAGE), pooled, concentrated by Amicon Ultra-15 Centrifugal Filter Unit with Ultracel-10 membrane (Millipore), mixed with 10% glycerol, aliquoted and stored at -80°C until used. ArsD and its derivatives with a six histidine tag at the N-terminus were purified similarly. Purified proteins were stored at -80°C until use, and their concentrations were determined according to the method of Bradford (Bradford, 1976) or from the absorption at 280 nm (Gill and von Hippel, 1989).

#### 4.2.8 ATPase activity assays



ATPase activity was estimated using a couple assay (Vogel and Steinhart, 1976), as described (Hsu and Rosen, 1989). ArsA was added at a final concentration of 0.3  $\mu\text{M}$  into an assay mixture containing 5 mM ATP, 1.25 mM phosphoenolpyruvate, 0.25 mM NADH, 10 units of pyruvate kinase and lactate dehydrogenase with or without the indicated concentrations of sodium arsenite, in the buffer containing 50 mM MOPS-KOH, pH 7.5, 0.25 mM EDTA. ArsD was added at the indicated concentrations. The mixture was pre-warmed to 37°C, and the reaction was initiated by addition of 2.5 mM  $\text{MgCl}_2$  and measured at 340 nm. The linear steady state rate of ATP hydrolysis was used to calculate specific activity. The reaction volume was 0.2 ml each in 96-well microplates, and the reactions were monitored by microplate reader SPECTRA max 340PC (Molecular Devices).

#### 4.2.9 Acetylation of lysine by Sulfo-NHS acetate

The Buffer of purified ArsD or ArsD derivatives was exchanged with a buffer containing 50 mM MOPS-KOH, 200mM NaCl, pH 7.8, 0.25 mM EDTA, 5mM TCEP and 5mM DTT. Dissolve Sulfo-NHS acetate in pure water to 100mM. Dilute protein to 1 mM concentration. Add Sulfo-NHS acetate at 10 fold concentration of free amine in the protein solution. It is like mixing 1 ml of 1 M protein solution with 0.7 ml of 100 mM Sulfo-NHS acetate for ArsD109 or 0.3 ml of 100 mM Sulfo-NHS acetate for ArsD109<sub>K2/104A-K37/62R</sub> and ArsD109<sub>K2/104A-K60/90A</sub>. Mixture was incubated for 60 min at room temperature. 200 ul of 0.5 M Tris pH 6.8 was added to quench the reaction for 20 min. Then protein was diluted with 10ml buffer of 50 mM MOPS-KOH, pH 7.5, 200 mM NaCl, 0.25 mM EDTA, 5 mM TCEP and 5 mM DTT and concentrated to 1ml with Amicon Ultra-15 Centrifugal Filter Unit. Repeat dilution with buffer and concentrating for

three more times to totally change protein buffer. Finally protein was concentrated, mixed with 10% glycerol, aliquoted and stored at -80°C until used.

#### 4.2.10 Metalloid binding assay

The buffer of purified ArsD was exchanged with a buffer containing 50 mM MOPS-KOH, pH 7.5, 0.25 mM EDTA (ATPase assay buffer), using a Bio-Gel P-6 Micro Bio-Spin column (Bio-Rad, Hercules, CA). Purified protein (100 µM) was incubated at 4°C with 300 µM potassium antimonyl tartrate. After 1 h, each sample was passed through a Bio-Gel P-6 column pre-exchanged with the ATPase assay buffer. ArsA protein concentration in the flow through was quantified from the absorption at 280 nm (Gill and von Hippel, 1989) or according to the method of Bradford (Bradford, 1976). Flow through were diluted with 2% HNO<sub>3</sub>, and the quantity of metalloid was measured by inductively coupled mass spectrometry (ICP-MS) with a PerkinElmer ELAN 9000. Antimony standard solutions in the range of 1-20 ppb in 2% HNO<sub>3</sub> were obtained from Ultra Scientific, Inc. (North Kingstown, RI). From the ratio of antimony concentration and protein concentration in the flow through, the binding molar ratio is calculated.

### 4.3 Results

#### 4.3.1 ArsD mutants showing stronger interaction with ArsA

AH109 uses *his3* as the reporter gene. *his3* will be transcribed when two proteins interact with each other. Histidine synthesis by HIS3 enzyme is competitively inhibited by 3-AT (3-amino-1,2,4-triazole) (Klopotoski and Wiater, 1965). If 3-AT was added to the medium, the yeast cells need to synthesize more HIS3 to grow normally. Here 3-AT was used in yeast two-hybrid analysis to qualitatively distinguish interaction strength between two proteins and select for stronger interaction mutants. Using a pair of primer

homologous to regions on pGBT9-D flanking the inserted *arsD* gene, error-prone PCR was done on *ArsD* in the presence of  $Mn^{2+}$ . The purified ep-PCR product was mixed with pGBT9-k vector linearized by *EcoRI* and *BamHI*, co-transformed with pACT2-D into AH109 and selected on SD-L-W-H plates with 10 mM 3-AT. The PCR fragment was ligated into the vector *in vivo* through homology recombination (Hua et al., 1997). Around 30 colonies grew on SD-L-W-H plates with 10 mM 3-AT. We sequenced the *ArsD* gene in each colony. Some contained a single mutation, while others contained multiple mutations. Some mutations occurred only once, but mutations such as S14R, T20I, Q24L, D28V and Q34R were found in many mutants. These mutations were reintroduced by site-directed mutagenesis as single mutation and tested to see whether they increased the strength of interaction with *ArsA*, as shown in Figure 4-1 (only mutants with stronger interaction are shown).

*ArsDs* with any of nine mutations at eight positions, including two at Asp 28, D28V and D28V, exhibit stronger interaction with *ArsA* (Figure 4-1). AH109 yeast cells co-transformed with pGBT9-k-D (encoding the GAL4 DNA binding domain fused with wild-type *ArsD*, BD-*ArsD*) and pACT2-A (encoding the GAL4 activation domain fused with wild-type *ArsA*, AD-*ArsA*) do not grow on SD-L-W-H plates with 10 mM 3-AT, while AH109 yeast cell co-transformed with pGBT9-k-D<sub>S14R</sub> (encoding BD-*ArsD*<sub>S14R</sub>) and pACT2-A grows normally on plates with 30mM 3-AT, and the mutation has no effect on dimerization with wild-type *ArsD* when co-transformed with pACT2-D (encoding wild-type AD-*ArsD*) (Figure 4-1, right panel). *ArsD* mutants, T20I, Q24L, D28V, D28T, T31A, Q34R and V61A behave similarly as the S14R mutant. Mutant Q38R only slightly increases the strength of interaction with *ArsA*, as shown that cells grow on plates

containing 10 mM 3-AT but not on plates containing 30 mM 3-AT. Ser 14 and Thr 20 are in the loop containing the metal binding site formed by three cysteine residues Cys12, Cys13 and Cys18. Four residues, Gln24, Asp28, Thr31 and Gln34, are located on the same face of the first  $\alpha$ -helix (Figure 4-7A). Q38R shows a slight effect on the interaction with ArsA and is located just following the above four residues on the same  $\alpha$ -helix. These results suggest that a strip formed by these 5 residues on this  $\alpha$ -helix may be involved in direct contact of ArsD with ArsA.

#### 4.3.2 Lys37 and Lys62 are involved in interaction with ArsA

One unsuccessful approach had been to attempt to crosslink the ArsD dimer using amine-specific homofunctional crosslinker. As part of that, we made series of ArsD lysine mutants to reduce nonspecific crosslinking. ArsD has 6 lysine residues, Lys2, Lys 37, Lys60, Lys62, Lys90 and Lys104. One of the mutants, ArsD109<sub>K2/104A-K37/62A</sub>, was not able to stimulate ArsA ATPase activity (Figure 4-2A), suggesting that one or more of those four lysine residues might be involved in ArsD metallochaperone function, shown as increasing the apparent affinity of ArsA for As(III) in this assay. To identify which lysine residue(s) is (are) involved, we examined more ArsD mutants carrying fewer lysine mutations. ArsD109<sub>K2/104A</sub> stimulates ArsA ATPase activity as well as the parental ArsD109. ArsD109 increases ArsA apparent affinity for As(III) from 535  $\mu$ M to 15  $\mu$ M, and ArsD<sub>K2/104A</sub> increases to 8  $\mu$ M. However, ArsD109<sub>K37A</sub> and ArsD109<sub>K62A</sub> individually only increase ArsA apparent affinity for As(III) to 126  $\mu$ M and 289  $\mu$ M respectively, suggesting that Lys37 and Lys62 together, but not Lys2 and Lys104, may play roles during arsenic transfer from ArsD to ArsA. Thus, it appears that

the two mutations at Lys37 and Lys62 are synergistic in their effect on ArsD metallochaperone function.

We further examined lysine residues Lys60 and Lys90 to see whether they are involved in the arsenic transfer. By mutating both of them to alanine, ArsD109<sub>K2/104A-K60/90A</sub> increases ArsA apparent affinity for As(III) to 21  $\mu\text{M}$  (Figure 4-2B), almost same as wild-type ArsD109, indicating that neither Lys60 nor Lys90 are required for arsenic transfer from ArsD to ArsA.

To examine the requirement for a positive charge, Lys37 and Lys62 were changed to arginine. ArsD109<sub>K2/104A-K37/62R</sub> increases the apparent affinity of ArsA for As(III) to 15  $\mu\text{M}$ , similar to ArsD109 (Figure 4-2B). Compared with ArsD109<sub>K2/104A-K37/62A</sub>, which loses ability to stimulate ArsA ATPase activity, arginine mutant ArsD109<sub>K2/104A-K37/62R</sub> is still active, suggesting that a positive charge may be required for ArsD metallochaperone function. This was further supported by chemical modification of lysine residues with Sulfo-NHS acetate (sulfosuccinimidyl acetate), which acetylates amine group and neutralizes the positive charge. ArsD109 increases the apparent affinity of ArsA for As(III) from 521  $\mu\text{M}$  to 12  $\mu\text{M}$  before acetylation, and 204  $\mu\text{M}$  after acetylation, consistent with the involvement of lysine residues in metallochaperone activity. Acetylation decreases wild-type activity dramatically although not completely, which might be due to partial acetylation (Figure 4-3). Mutant ArsD109<sub>K2/104A-K60/90A</sub>, with only lysine residues Lys37 and Lys62 remaining, increases the apparent affinity of ArsA for As(III) to 26  $\mu\text{M}$  before acetylation, and 283  $\mu\text{M}$  after acetylation. This suggests that acetylation of Lys37 and Lys62 causes loss of ArsD metallochaperone function. Mutant ArsD109<sub>K2/104A-K37/62R</sub>, with only lysine residues Lys60 and Lys90 left, increases ArsA

apparent affinity for As(III) to 12  $\mu\text{M}$  before acetylation, and 7  $\mu\text{M}$  after acetylation. This is consistent with the result above that Lys 60 and Lys 90 are not required for stimulating ArsA ATPase activity. It also indicates that acetylation has no effect on other non-lysine residues. It is not surprised that acetylation has no effect on ArsD109<sub>K2/104A-K37/62R</sub>, in which Lys37 and Lys62 were mutated to arginine, since acetylation by Sulfo-NHS does not change the positive charge of arginine residues. All of these results suggest that Lys37 and Lys62 are involved for the ArsD metallochaperone function and that a positive charge at these positions is important.

The antimony binding capability of the mutant ArsD109<sub>K2/104A-K37/62A</sub> was measured by gel-filtration and ICP-MS quantification. As expected, the parental ArsD109 binds approximately one Sb(III) per monomer (Lin et al., 2007a). ArsD109<sub>C12/13S-C18A</sub>, with no metalloid binding site, binds only a background level of Sb(III) (Lin et al., 2007a). ArsD109<sub>K2/104A-K37/62A</sub> binds Sb(III) as well as ArsD109, about one Sb(III) per monomer (Figure 4-4A). Interaction between ArsD lysine mutants and ArsA was investigated using yeast two-hybrid analysis. All of the mutants interact with wild-type ArsD, suggesting these mutants fold and dimerize (Figure 4-4B). This is also supported by the fact that these mutants can be overexpressed in *E. coli* and purified from the cytosolic soluble fraction. ArsD<sub>K2/104A-K37/62A</sub> does not interact with ArsA, while ArsD<sub>K2/104A-K37/62R</sub> and ArsD<sub>K2/104A-K60/90A</sub> interacts with ArsA as well as wild-type ArsD. This is consistent with above results that ArsD109<sub>K2/104A-K37/62A</sub> does not stimulate ArsA ATPase activity, but ArsD109<sub>K2/104A-K37/62R</sub> and ArsD109<sub>K2/104A-K60/90A</sub> do stimulate. K37A and K62A mutations were separated, and their individual effects on ArsA interaction was examined by yeast two-hybrid analysis. ArsD109<sub>K2/104A-K37A</sub> interacts with ArsA

poorly compared with wild-type ArsD, while ArsD109<sub>K2/104A-K62A</sub> interacts with ArsA almost same as wild-type, indicating that Lys37 may be more important than Lys62 in terms of interaction with ArsA.

All these results suggest that mutating Lys37 and Lys62 to alanine does not affect metal binding ability of ArsD but causes loss of interaction with ArsA, leading to inability of transfer As(III) to ArsA and to stimulate ArsA ATPase activity. In the crystal structure, Lys37 is in the same first  $\alpha$ -helix as residues Gln24, Asp28, Thr31, Gln34 and Gln38 (Fig. 4-7A). This is consistent with our hypothesis that this helix is involved in interaction with ArsA. On the other hand Lys62 is adjacent to Val61, located in the third  $\alpha$ -helix, which is on the other side of the ArsD structure compared with the first  $\alpha$ -helix (Figure 4-7A). The above results show that a V61A mutant interacts more strongly with ArsA, suggesting that the third  $\alpha$ -helix, in which Val61 and Lys62 are located, may be another point of interaction with ArsA.

#### **4.3.3 ArsD mutants showing weaker interaction with ArsA**

Yeast strain MAV203 has the reporter gene *ura3*, which encodes an enzyme that metabolizes 5-FOA (5-fluoroorotic acid) to 5-fluorouridine, a toxic analogue of uridine that inhibits cell growth. Therefore MAV203 can be used to select for mutants with weaker or no interaction by selecting for growth on plates with 5-FOA (Vidal et al., 1996). ArsA and ArsD have been shown to interact with each other in GAL4 yeast two-hybrid system AH109 (Lin et al., 2007b). We confirmed that ArsA and ArsD also interact with each other in strain MAV203 and determined that MAV203 co-transformed with pACT2-A (encoding AD-ArsA) and pGBT9-D (encoding wild-type BD-ArsD) cannot grow on SD-

L-W plates with 0.2 % 5-FOA. So we use 0.2 % 5-FOA to select for ArsD mutants that cannot interact with ArsA or interact more weakly.

Using a pair of primer homologous to regions on pGBT9-D (encoding BD-ArsD) flanking the inserted *arsD* gene, error-prone PCR was done as described under 'Materials and Methods'. The purified PCR product was mixed with pGBT9-k vector linearized by *EcoRI* and *BamHI*, and co-transformed with pACT2-A (encoding AD-ArsA) into MAV203 and selected on SD-L-W plates with 0.2 % 5-FOA. 70 colonies were isolated from 5-FOA plates, 7% of the 1000 clones on plates without 5-FOA. Of these mutants, some will be ArsD mutants that interact more weakly with ArsA, but others may be prematurely chain terminating ArsD mutants, unfolded ArsD mutants, or even empty pGBT9 vector. Since ArsD forms a dimer in yeast two-hybrid AH109 (Lin et al., 2007b), we further screened for those mutants that could still dimerize with wild-type ArsD, with the assumption that these should fold normally. We pooled all 70 colonies, and used the same primer, homologous to regions on pGBT9-D flanking the inserted *arsD* gene, for colony PCR. The purified PCR products were mixed with plasmid pGBT9-k that had been linearized with *EcoRI* and *BamHI*, co-transformed with plasmid pACT2-D (encoding AD-ArsD) into AH109 and selected on SD-L-W-H plates. 300 colonies grew on SD-L-W-H plates, 7% of the 4000 colonies that grew on SD-L-W plates. 30 colonies were purified and sequenced. Finally we isolated 5 ArsD mutants showing weaker or no interaction with ArsA but still dimerizing with wild-type ArsD (Figure 4-5A). These mutants are ArsD<sub>V17A</sub>, ArsD<sub>V22A</sub>, ArsD<sub>V27D</sub>, ArsD<sub>Q51H</sub>, and ArsD<sub>F55L</sub>. Residues Val17 and Val22 are in the loop containing the metalloid binding site (Cys12, Cys13 and Cys18). Val27 is in the first  $\alpha$ -helix, in which residues Gln24, Asp28, Thr31,



Gln34, Lys37 and Gln38 have been shown above to be important for the interaction with ArsA (Figure 4-7A). This supports our hypothesis that this first  $\alpha$ -helix is involved in the interaction with ArsA.

#### 4.3.4 ArsA mutants restoring interaction with ArsD mutants

To select for mutants that restored the ability of ArsD mutants to interact with ArsA, we used random mutagenesis of ArsA in plasmid pACT2-A. Using a pair of primer homologous to regions on pACT2 flanking the multiple cloning sites, error-prone PCR was done on ArsA, as described under 'Materials and Methods'. The purified PCR product was mixed with the plasmid pACT2 linearized with *EcoRI* and *BamHI*, co-transformed with ArsD mutants in the plasmid pGBT9-k into strain AH109 and selected on SD-L-W-H plates. Five ArsA mutants, *ArsA*<sub>P9L,L74H,D121G,F123L,E425A</sub>, *ArsA*<sub>D121E</sub>, *ArsA*<sub>G111C,E400V,L530H,Q557L</sub>, *ArsA*<sub>L179R,H219L</sub>, and *ArsA*<sub>A29S,R88G,D121N,V215A,T401A</sub>, restored interaction with *ArsD*<sub>V22A</sub> but also retained ability of interaction with wild-type *ArsD* (Figure 4-5B). Three ArsA mutants, *ArsA*<sub>D121E</sub>, *ArsA*<sub>E425K,L564H</sub>, and *ArsA*<sub>D417N</sub>, restored interaction with *ArsD*<sub>F55L</sub> (Figure 4-5C). Six ArsA mutants, *ArsA*<sub>L152R,F162L,D513Y,S560C</sub>, *ArsA*<sub>D121E,L207P</sub>, *ArsA*<sub>I65T,Q84L,D121E,H453L</sub>, *ArsA*<sub>V101A,R151H,S570T</sub>, *ArsA*<sub>T149A,I150H,E438D</sub>, and *ArsA*<sub>D121G,E405V,E415V,H558R</sub>, restored interaction with *ArsD*<sub>Q51H</sub> (Figure 4-5D). All of the ArsA mutants retained the ability to interact with wild-type *ArsD*, and one mutant *ArsA*<sub>D121E</sub>, restored interaction with both *ArsD*<sub>V22A</sub> and *ArsD*<sub>F55L</sub>. This suggests that the compensation of mutation on ArsA is not specific for the particular mutation in *ArsD* but increase interactions from another site in *ArsD*, since an extensive interaction interface was identified on *ArsD*.

#### 4.3.5 ArsA mutants showing stronger interaction with ArsD

Using a pair of primer homologous to regions on pACT2 flanking the multiple cloning sites, error-prone PCR was done on *ArsA*. The purified PCR product was mixed with vector pACT2 linearized by *EcoRI* and *BamHI*, co-transformed with pGBT9-D into AH109 and selected on SD-L-W-H plates with 20 mM 3-AT. Six *ArsA* mutants show stronger interaction with wild-type *ArsD* (Figure 4-6). AH109 yeast cells co-transformed with pACT2-A or other *ArsA* mutants and pGBT9-k-D (encoding wild-type *ArsD*) were spotted on SD-L-W-H plates with different concentrations of 3-AT. Cells with wild-type *ArsA* cannot grow on plates with 10 mM 3-AT. *ArsA*<sub>I117M,E425G</sub> and *ArsA*<sub>H368L,E425K</sub> confer resistance to 60 mM 3-AT, and both have Glu425 mutation. *ArsA*<sub>F120L,L193S</sub> and *ArsA*<sub>F54L,F120L,H219R,E254V,F443L,K475R,A533T</sub> confer resistance to 120 mM 3-AT, and both have mutations at Phe120. *ArsA*<sub>D121E</sub> and *ArsA*<sub>D121N</sub> confer resistance to 30 mM 3-AT, and both have mutation at Asp121 position. These results suggest that *ArsA* residues Glu425, Phe120 and Asp121 may be involved in interaction with *ArsD*.

Another Asp121 mutant, *ArsA*<sub>D121G,E405V,E415V,H558R</sub>, which was isolated as complementing mutation Q51H in *ArsD*, also confers resistance to 60 mM 3-AT. *ArsA*<sub>P9L,L74H,D121G,F123L,E425A</sub> was isolated by ability to complement mutation V22A in *ArsD*. This multiple mutant contains changes at Asp121 and Glu425 and confers resistance to 90 mM 3-AT (Figure 4-6).

#### 4.4 Discussion

*ArsD* transfers As(III) to *ArsA* in the presence of  $Mg^{2+}$  and ATP (Lin et al., 2006). *In vitro* experiments suggest that *ArsD* and *ArsA* interact through their metal binding sites. *ArsA* and *ArsD* crystal structures have been solved individually, but the details of their interactions are still unknown. In this study, yeast forward and reverse two-hybrid

selections were used to isolate mutants with stronger or weaker interactions, providing information about the physical interface between ArsA and ArsD. Totally 16 mutations in ArsD were identified to affect ArsA-ArsD interaction (Table 4-4).

Using 3-AT and strain AH109 with *his3* as report gene, nine ArsD mutants were found to increase the strength of interaction with ArsA. They include ArsD<sub>S14R</sub>, ArsD<sub>T20I</sub>, ArsD<sub>Q24L</sub>, ArsD<sub>D28V</sub>, ArsD<sub>D28T</sub>, ArsD<sub>T31A</sub>, ArsD<sub>Q34R</sub>, ArsD<sub>Q38R</sub> and ArsD<sub>V61A</sub>. Using reverse yeast two-hybrid selection, five ArsD mutants were isolated that show loss of or weaker interaction with ArsA. These mutants still dimerize with wild-type ArsD, indicating that the mutations do not cause protein misfolding. These five mutants are ArsD<sub>V17A</sub>, ArsD<sub>V22A</sub>, ArsD<sub>V27D</sub>, ArsD<sub>Q51H</sub> and ArsD<sub>F55L</sub>.

Through site-directed mutagenesis, Lys37 and Lys62 were found to be significant for ArsD metallochaperone function. If mutated Lys37 or Lys62 to alanine individually, the resulting ArsD proteins partially lose the ability to stimulate ArsA ATPase activity. If mutated to alanine together, the resulting protein was unable to stimulate ArsA, suggesting a synergistic effect of these two lysines. However, if mutated to arginines, the resulting protein is still active, indicating that a requirement for positively charged residues. The effect of acetylation of lysine residues with Sulfo-NHS acetate further supported the requirement for positive charge. When both Lys37 and Lys62 were mutated to alanines, the resulting protein retains the ability to bind antimony but loses interaction with ArsA in yeast two-hybrid analysis.

In total, 16 mutations of 15 amino residues show either stronger or weaker interactions with ArsA. They are at amino acid residues, Ser14, Val17, Thr20, Val22, Gln24, Val27, Asp28, Thr31, Gln34, Lys37, Gln38, Gln51, Phe55, Val61 and Lys62

(Table 4-4). These residues were mapped on the structure of ArsD (Figure 4-7). The ArsD monomer has a thioredoxin fold of four  $\beta$ -strands flanked by four  $\alpha$ -helices. Residues 12 to 22 are mostly disordered in this structure. To show all the mutations, an ArsD structural model with residues 12 to 22 inserted was constructed by homology modeling (Ye et al., 2010). ArsD helices  $\alpha$ 1 and  $\alpha$ 4 are on one side of the  $\beta$ -strands;  $\alpha$ 2 and  $\alpha$ 3 are on the other side.  $\alpha$ 2 is almost perpendicular to  $\alpha$ 3, with only one residue between them.  $\beta$ 1 is between  $\beta$ 2 and  $\beta$ 3, parallel to  $\beta$ 2 and anti-parallel to  $\beta$ 3.  $\beta$ 3 and  $\beta$ 4 form a  $\beta$ -hairpin. Residues 70 to 72 form a short  $3_{10}$  helix.

Four residues, Ser14, Val17, Thr20 and Val22, are in the same loop as Cys12-Cys13-Cys18. This is consistent with our model that the region near metal binding site is involved in direct contact with ArsA. Seven residues, Gln24, Val27, Asp28, Thr31, Gln34, Lys37 and Gln38, are in helix  $\alpha$ 1 just following the loop containing the metal binding site. They are aligned on one side of the helix and solvent exposed, suggesting that this surface is directly involved in interaction, or, alternatively, that the helix helps to position the metalloid binding loop in correct orientation to interact with ArsA. Another four residues Gln51, Phe55, Val61 and Lys62, are on helices  $\alpha$ 2 and  $\alpha$ 3. This region could also be involved in interaction with ArsA or, again, may also serve to position the loop for interaction with ArsA.

Metallated ArsD interacts with and transfers As(III) to ArsA during catalysis, when the ATPase cycles between open to closed conformations (Lin et al., 2007a; Ruan et al., 2006). The x-ray crystal structure of ArsA has been solved in the closed form (Zhou et al., 2000, 2001). A yeast homologue termed Arr4p or Get3 (Auld et al., 2006) is involved in targeting tail-anchored proteins in the endoplasmic reticulum (Bozkurt et al.,

2009). Recently crystal structures of Get3 were solved in the open (nucleotide free) and closed (ADP-AlF<sub>4</sub><sup>-</sup>) conformations (Mateja et al., 2009). ArsA has two homologous halves, A1 and A2, each with a nucleotide binding domain (NBD) connected by a short linker, while Get3 is a dimer of two identical monomers, each homologous to either A1 or A2. In the open Get3 conformation there is a large conformational change, and the two monomers are separated by approximately 37° rotation of one subunit towards the other relative to their orientation in the closed form, which is more compact. The ADP-AlF<sub>4</sub><sup>-</sup> closed ArsA structure can be superimposed with Get3 closed structure with an RMSD of 3.4 Å for 420 Cα atoms (Figure 4-9A). ArsA NBD1 (residue 1-297) and NBD2 (298-583) can be superimposed with the two monomers in the Get3 open structure, with RMSD of 2.3 Å and 3.0 Å, respectively (Figure 4-9B). An open model of the ArsA structure based on the open Get3 structure was generated for analysis of ArsA-ArsD interactions and docking studies (Figure 4-9C) (Ye et al., 2010).

The open ArsA and metallated ArsD models were docked by using the fully automated, web-based program ClusPro Version 2.0 with balanced coefficients and default parameters (Ye et al., 2010). The ClusPro docking server yielded several top-scoring solutions. One of the solutions with relative good score was consistent with biochemical analysis indicating that the three cysteines of ArsD and the three cysteines of ArsA must be in proximity for transfer (Figure 4-10). According to this model, most likely ArsA and ArsD interact with each other at multiple points. It is consistent with yeast two-hybrid results that the loop containing Cys12-Cys13-Cys18 metal binding site and helix α1 are directly involved in protein contact.

Six ArsA mutants,  $ArsA_{I117M,E425G}$ ,  $ArsA_{H368L,E425K}$ ,  $ArsA_{F120L,L193S}$ ,  $ArsA_{F54L,F120L,H219R,E254V,F443L,K475R,A533T}$ ,  $ArsA_{D121E}$  and  $ArsA_{D121N}$ , show stronger interaction with wild-type ArsD. Mutations at Glu425, Phe120 and Asp121 occurred twice in different mutants, and they are spatially closing to ArsA MBS (metalloid binding site) (Figure 4-8). These mutations might change the local conformation of the MBS to increase the strength of interaction with ArsD, or they are possibly located in the interaction interface. Whichever it is, that all these mutations are located close to the ArsA MBS supports the model that ArsA and ArsD interacts at their metal binding sites.

ArsA mutants were isolated that restore interaction with  $ArsD_{V22A}$ ,  $ArsD_{Q51H}$  or  $ArsD_{F55L}$ . One common feature of all ArsA complementary mutants is that they all have one mutation spatially closing to the ArsA MBS, while most other mutations are scattered around all over the protein. The mutations near the MBS could slightly change the local conformation of MBS and restore the interaction with ArsD mutants. Among all 14 ArsA mutants, seven contain mutations at Asp121, and two have mutations at Glu425. These two positions were shown to increase the interaction strength when they are mutated. These results suggest that restoration of interaction with ArsD mutants is not site-specific, but more likely ArsD and ArsA have multi-point contact sites, considering the extensive interaction interface on ArsD was identified. The loss of interaction at one point can be compensated by stronger interaction at another site.

Currently, the effect of mutation F120L, D121E, D121G, E425K and E425A on ArsA and on ArsA-ArsD interaction is being studied. By changing these residues to other residues, more mutants will be constructed and studied. These ArsA mutants could be useful for co-crystallization with ArsD since they show stronger interaction with

ArsD. Probably these mutants could lock ArsA to the open conformation therefore interacting with ArsD better. All ArsD mutants showing stronger interaction with ArsA in yeast two-hybrid analysis will also be tried to co-crystallize with ArsA.

In addition, methods quantitatively measuring ArsA-ArsD interaction will be very helpful to understand not only the effect of the mutations but also the basic mechanism of arsenic transfer. Some preliminary work using SPR (surface plasmon resonance) has been done. By immobilizing ArsD on the chip and flowing ArsA solution through the surface, ArsA-ArsD interaction could be watched. The result until now looks promising but stricter negative control is needed. ArsD<sub>109<sub>K2/104A-K37/62A</sub></sub> could be a good negative control. This mutant has been shown not to stimulate ArsA ATPase activity and not to interact with ArsA in yeast two-hybrid analysis. Single molecule fluorescence resonance energy transfer could also be used to study ArsA-ArsD interaction. It has been successfully used to study transient interaction between copper chaperone HAH1 and Wilson disease protein (Benitez et al., 2008). This method has advantage not only to study ArsA-ArsD interaction in simulated pre-hydrolysis state, intermediate or post-hydrolysis state but also to watch interaction change between single ArsA-ArsD molecule pair during ATP hydrolysis.

Table 2-1

## Strains and plasmids used in CHAPTER 2

Strains/Plasmids	Genotype/description	Reference
<u>Strains</u>		
JM109	<i>endA1, recA1, gyrA96, thi, hsdR17</i> (rk-, mk+), <i>relA1, supE44, λ-</i> , $\Delta$ ( <i>lac-proAB</i> ), [F', <i>traD36, proAB, lacI<sup>q</sup>Z</i> $\Delta$ M15]	(Sambrook et al., 1989)
BL21(DE3)	[F- <i>ompT hsdS<sub>B</sub></i> ( $\Gamma_B$ -m <sub>B</sub> -) <i>gal dcm</i> (DE3 [ <i>lac lacUV5-T7 gene1 ind1 Sam7 nin5</i> ])	(Sambrook et al., 1989)
<u>Plasmids</u>		
pAlter-dAhB	Six histidine codons added to the 3'-end of <i>arsA</i> gene (Ap <sup>r</sup> )	(Li and Rosen, 2000)
pMAL-ArsD109	<i>arsD<sub>1-109</sub></i> truncation was fused to the C-terminal of MBP (Ap <sup>r</sup> )	(Lin et al., 2007a)
pET28a	For expression of his-tagged protein controlled by T7 promoter (Kana <sup>r</sup> )	Novagen
pET28a-ArsD109	<i>arsD<sub>1-109</sub></i> truncation was inserted into pET28a through <i>EcoRI</i> and <i>Sall</i> sites (Kana <sup>r</sup> )	This study
pET28a-ArsD109 W35/97Y	Trp35 and Trp97 were mutated to Tyr by site directed mutagenesis on pET28a-ArsD109 (Kana <sup>r</sup> )	This study
pET28a-ArsD109 T15W	Thr15 was mutated to Trp by site directed mutagenesis on pET28a-ArsD109 W35/97Y (Kana <sup>r</sup> )	This study
pET28a-ArsD109 V17W	Val17 was mutated to Trp by site directed mutagenesis on pET28a-ArsD109 W35/97Y (Kana <sup>r</sup> )	This study
pET28a-ArsD109 C12G	Cys12 was mutated to Gly by site directed mutagenesis on pET28a-ArsD109 (Kana <sup>r</sup> )	This study



Table 2-1

## Strains and plasmids used in CHAPTER 2 (continued)

Strains/Plasmids	Genotype/description	Reference
<u>Plasmids</u>		
pET28a-ArsD109 C13G	Cys13 was mutated to Gly by site directed mutagenesis on pET28a-ArsD109 (Kana <sup>r</sup> )	This study
pET28a-ArsD109 C18G	Cys18 was mutated to Gly by site directed mutagenesis on pET28a-ArsD109 (Kana <sup>r</sup> )	This study
pET28a-ArsD109 C12G,T15W	Cys12 was mutated to Gly by site directed mutagenesis on pET28a-ArsD109 <sub>T15W</sub> (Kana <sup>r</sup> )	This study
pET28a-ArsD109 C13G,T15W	Cys13 was mutated to Gly by site directed mutagenesis on pET28a-ArsD109 <sub>T15W</sub> (Kana <sup>r</sup> )	This study
pET28a-ArsD109 C18G,T15W	Cys18 was mutated to Gly by site directed mutagenesis on pET28a-ArsD109 <sub>T15W</sub> (Kana <sup>r</sup> )	This study

Table 2-2

## Oligonucleotide primers used in CHAPTER 2

Primer	Sequence (5'–3')	Target / Direction
T7 promoter sequencing primer	TAATACGACTCACTATAGGG	pET28a forward sequencing primer
T7 terminator sequencing primer	GCTAGTTATTGCTCAGCGG	pET28a reverse sequencing primer
ArsD-T15W-s	GCGATGTGTTGCAGCTGGGGC GTCTGCGGTACAG	Mutate ArsD Thr15 to Trp, sense
ArsD-T15W-a	CTGTACCGCAGACGCCCCAGC TGCAACACATCGC	Mutate ArsD Thr15 to Trp, antisense
ArsD-V17W-s	GTGTTGCAGCACCGGCTGGTG CGGTACAGATGTTG	Mutate ArsD Val17 to Trp, sense
ArsD-V17W-a	CAACATCTGTACCGCACCCAGCC GGTGCTGCAACAC	Mutate ArsD Val17 to Trp, antisense
ArsD-C12G-s	GGTATTTGACCCGGCGATGGGT TGCAGCACCGGCGTC	Mutate ArsD Cys12 to Gly, sense
ArsD-C12G-a	GACGCCGGTGCTGCAACCCAT CGCCGGGTCAAATACC	Mutate ArsD Cys12 to Gly, antisense
ArsD-C13G-s	GTATTTGACCCGGCGATGTGTG GCAGCACCGGCGTCTGC	Mutate ArsD Cys13 to Gly, sense
ArsD-C13G-a	GCAGACGCCGGTGCTGCCACA CATCGCCGGGTCAAATAC	Mutate ArsD Cys13 to Gly, antisense
ArsD-C18G-s	GTTGCAGCACCGGCGTCCGGCG GTACAGATGTTGATC	Mutate ArsD Cys18 to Gly, sense
ArsD-C18G-a	GATCAACATCTGTACCGCCGAC GCCGGTGCTGCAAC	Mutate ArsD Cys18 to Gly, antisense
ArsD-12G15W-s	GGTATTTGACCCGGCGATGGGT TGCAGCTGGGGCGTC	Mutate ArsD Cys12 to Gly and Thr15 to Trp, sense
ArsD-12G15W-a	GACGCCCCAGCTGCAACCCAT CGCCGGGTCAAATACC	Mutate ArsD Cys12 to Gly and Thr15 to Trp, antisense

Table 2-2

## Oligonucleotide primers used in CHAPTER 2 (continued)

Primer	Sequence (5'–3')	Target / Direction
ArsD-13G15W-s	GTATTTGACCCGGCGATGTGTG GCAGCTGGGGCGTCTGC	Mutate ArsD Cys13 to Gly and Thr15 to Trp, sense
ArsD-13G15W-a	GCAGACGCCCCAGCTGCCACA CATCGCCGGGTCAAATAC	Mutate ArsD Cys13 to Gly and Thr15 to Trp, antisense
ArsD-18G15W-s	GTTGCAGCTGGGGCGTCGGCG GTACAGATGTTGATC	Mutate ArsD Cys18 to Gly and Thr15 to Trp, sense
ArsD-18G15W-a	GATCAACATCTGTACCGCCGAC GCCCCAGCTGCAAC	Mutate ArsD Cys18 to Gly and Thr15 to Trp, antisense

Table 2-3

Summary of the best-fit parameters from the Arsd<sub>1-109</sub>-As EXAFS fitting analysis<sup>a</sup>.  
Fits in bold are the best fit for each sample.

Sample	Ligand Environment <sup>b</sup>				Ligand Environment <sup>b</sup>				F' <sup>g</sup>
	Atom <sup>c</sup>	R(Å) <sup>d</sup>	C.N. <sup>e</sup>	Å <sup>2f</sup>	Atom <sup>c</sup>	R(Å) <sup>d</sup>	C.N. <sup>e</sup>	Å <sup>2f</sup>	
ArsD <sub>1-109,C18G</sub>	<b>O/N</b>	<b>1.79</b>	<b>3.0</b>	<b>5.53</b>					<b>0.58</b>
	S	2.5	1	12.6					4.6
	O/N	1.79	2.0	3.2	O/N	2.28	1.0	16.5	0.96
	O/N	1.79	2.0	3.2	S	2.48	0.5	10.2	0.93
ArsD <sub>1-109,C13G</sub>	O/N	1.79	2.0	3.0					0.79
	S	1.97	1	3.02					1.98
	<b>O/N</b>	<b>1.79</b>	<b>2.5</b>	<b>4.37</b>	<b>O/N</b>	<b>2.13</b>	<b>1.0</b>	<b>3.63</b>	<b>0.67</b>
	O/N	1.79	2.0	4.8	S	1.96	1.0	8.8	0.66
ArsD <sub>1-109,C12G</sub>	O/N	1.79	2.0	4.50					1.6
	S	2.5	1	20.4					4.1
	<b>O/N</b>	<b>1.79</b>	<b>2.0</b>	<b>4.86</b>	<b>O/N</b>	<b>2.16</b>	<b>1.5</b>	<b>4.16</b>	<b>1.58</b>
	O/N	1.79	2.0	4.87	S	2.41	1.0	24.3	1.56
ArsD <sub>1-109</sub>	O/N	2.08	3	0.9					3.86
	S	2.24	3	2.4					0.89
	O/N	2.01	2	-4.1	O/N	2.13	1	-7.8	6.01
	<b>O/N</b>	<b>2.06</b>	<b>0.5</b>	<b>4.4</b>	<b>S</b>	<b>2.24</b>	<b>3</b>	<b>2.6</b>	<b>0.84</b>

<sup>a</sup> Data were fit over a  $k$  range of 1 to 13 Å<sup>-1</sup>.

<sup>b</sup> Independent metal-ligand scattering environment

<sup>c</sup> Scattering atoms: O (oxygen), N (nitrogen), S (sulfur) and C (carbon), Cu (Copper)

<sup>d</sup> Average metal-ligand bond length from three independent samples

<sup>e</sup> Average metal-ligand coordination number from three independent samples

<sup>f</sup> Average Debye-Waller factor in Å<sup>2</sup> x 10<sup>3</sup> from three independent samples

<sup>g</sup> Number of degrees of freedom weighted mean square deviation between data and fit.

Table 3-1

## Strains and plasmids used in CHAPTER 3

Strains/Plasmids	Genotype/description	Reference
<u><i>E. coli</i> strains</u>		
JM109	<i>endA1, recA1, gyrA96, thi, hsdR17</i> (rk-, mk+), <i>relA1, supE44, λ</i> -, $\Delta$ ( <i>lac-proAB</i> ), [F', <i>traD36, proAB, lacI<sup>q</sup>Z</i> $\Delta$ M15]	(Sambrook et al., 1989)
BL21(DE3)	[F- <i>ompT hsdS<sub>B</sub></i> ( $\Gamma_B$ -m <sub>B</sub> <sup>-</sup> ) <i>gal dcm</i> (DE3 [ <i>lacI lacUV5-T7 gene1 ind1 Sam7 nin5</i> ])	(Sambrook et al., 1989)
<u><i>S. cerevisiae</i> strains</u>		
AH109	<i>MATa, trp1-901, leu2-3, 112, ura3-52, his3-200, gal4<math>\Delta</math>, gal80<math>\Delta</math>, LYS2::GAL1<sub>UAS</sub>-GAL1<sub>TATA</sub>-HIS3, GAL2<sub>UAS</sub>-GAL2<sub>TATA</sub>-ADE2, URA3::MEL1<sub>UAS</sub>-MEL1<sub>TATA</sub>-lacZ</i>	Clontech
MAV203	<i>MAT<math>\alpha</math>; leu2-3, 112; trp1-901; his3<math>\Delta</math>200; ade2-101; cyh2<sup>R</sup>; can1<sup>R</sup>; gal4<math>\Delta</math>; gal80<math>\Delta</math>; GAL1::lacZ; HIS3<sub>UASGAL1</sub>::HIS3@LYS2; SPAL10::URA3.</i>	Invitrogen
<u>Plasmids</u>		
pGBT9	GAL4 <sub>(1-147)</sub> DNA-binding domain, <i>TRP1</i> (Ap <sup>r</sup> )	Clontech
pACT2	GAL4 <sub>(768-881)</sub> activation domain, <i>LEU2</i> (Ap <sup>r</sup> )	Clontech
pACT2-A	<i>arsA</i> gene cloned in pACT2 (Ap <sup>r</sup> )	(Lin et al., 2006)
pACT2-D	<i>arsD</i> gene cloned in pACT2 (Ap <sup>r</sup> )	(Lin et al., 2006)
pGBT9-D	<i>arsD</i> gene cloned in pGBT9 (Ap <sup>r</sup> )	(Lin et al., 2006)
pGBT9-k	Kanamycin resistance gene is amplified from pET28a and inserted into pGBT9 at AatII site (Kana <sup>r</sup> )	This study
pGBT9-k-D	Kanamycin resistance gene is amplified from pET28a and inserted into pGBT9-D at AatII site (Kana <sup>r</sup> )	This study
pGBT9-k-D <sub>G86E</sub>	Selected by yeast two-hybrid (Kana <sup>r</sup> )	This study

Table 3-1

## Strains and plasmids used in CHAPTER 3 (continued)

Strains/Plasmids	Genotype/description	Reference
<u>Plasmids</u>		
pAlter-dAhB	Six histidine codons added to the 3'-end of <i>arsA</i> gene (Ap <sup>r</sup> )	(Li and Rosen, 2000)
pET28a	For expression of his-tagged protein controlled by T7 promoter (Kana <sup>r</sup> )	Novagen
pET28a-ArsD109	<i>arsD</i> <sub>1-109</sub> truncation was inserted into pET28a through <i>EcoRI</i> and <i>SaII</i> sites (Kana <sup>r</sup> )	Chapter 2
pET28a-ArsD109 G86E	Gly86 was mutated to Glu by site directed mutagenesis on pET28a-ArsD109 (Kana <sup>r</sup> )	This study
pET28a-ArsD109 S68A/R87A/R96A	Ser68, Arg87 and Arg96 were mutated to Ala by site directed mutagenesis on pET28a-ArsD109 (Kana <sup>r</sup> )	This study
pET28a-ArsD109 S68A/R87A/R96A/E81A/T82A/V83A/M84A	Ser68, Arg87, Arg96, Glu81, Thr82, Val83 and Met84 were mutated to Ala by site directed mutagenesis on pET28a-ArsD109 (Kana <sup>r</sup> )	This study
pMAL-ArsD109	<i>arsD</i> <sub>1-109</sub> truncation was fused to the C-terminal of MBP (Ap <sup>r</sup> )	(Lin et al., 2007a)

Table 3-2

## Oligonucleotide primers used in CHAPTER 3

Primer	Sequence (5'–3')	Target / Direction
GAL4-BD sequencing primer	GAGTAGTAACAAAGGTCAA	pGBT9 Forward sequencing primer
T7 promoter sequencing primer	TAATACGACTCACTATAGGG	pET28a forward sequencing primer
T7 terminator sequencing primer	GCTAGTTATTGCTCAGCGG	pET28a reverse sequencing primer
pET28a-3600-AatII	CTATGACGTCCAACCCGGTAA GACACGACTTATC	Sense primer for amplifying kanamycin resistance gene from pET28a
pET28a-5300-AatII	CTATGACGTCCGCCCGCTCCT TTCGCTTTCTTCC	Antisense primer for amplifying kanamycin resistance gene from pET28a
pGBT9-s	TAAAGATGCCGTCACAGATAGA TTG	Sense primer for ep-PCR of ArsD on pGBT9-k-D
pGBT9-a	ACCTGACCTACAGGAAAGAGTT ACT	Antisense primer for ep-PCR of ArsD on pGBT9-k-D
D109-XhoI	CAGCTCGAGTTAAGGCGCTAA TCCCACCTTTATCCAG	Using with pGBT9-s to amplify ArsD mutant gene from pGBT-k-D <sub>x</sub> vector to put into pET28 vector between <i>EcoRI</i> and <i>XhoI</i>
ArsD-S68A-s	GTTTATTGAAGCTGCCGGGGC AGAAGGTC	Mutate ArsD Ser68 to Ala, sense
ArsD-S68A-a	GACCTTCTGCCCGGCAGCTT CAATAAAC	Mutate ArsD Ser68 to Ala, antisense
ArsD-R87A-s	GAAACAGTGATGGCCGGGGCT TACCCGAAACGCGC	Mutate ArsD Arg87 to Ala, sense
ArsD-R87A-a	GCGCGTTTTCGGGTAAGCCCCG GCCATCACTGTTTC	Mutate ArsD Arg87 to Ala, antisense

**Table 3-2****Oligonucleotide primers used in CHAPTER 3 (continued)**

<b>Primer</b>	<b>Sequence (5'–3')</b>	<b>Target / Direction</b>
ArsD-R96A-s	CGCGCTGAGCTGGCTGCCTGG TTTGGCATTCCACTG	Mutate ArsD Arg96 to Ala, sense
ArsD-R96A-a	CAGTGGGAATGCCAAACCAGGC AGCCAGCTCAGCGCG	Mutate ArsD Arg96 to Ala, antisense
ArsD-81-84A-s	CATTGTTGTTACTGGATGGCGC AGCAGCGGCAGCCGGGGCTTA CCCGAAACG	Mutate ArsD residues from 81 to 84 to Ala, sense
ArsD-81-84A-a	CGTTTCGGGTAAGCCCCGGCT GCCGCTGCTGCGCCATCCAGT AACAACAATG	Mutate ArsD residues from 81 to 84 to Ala, antisense



**Table 4-1**

**Summary of study of interaction between copper-chaperone proteins and their targets**

Species	Chaperone	Target protein	Yeast-2-hybrid	In vitro binding	NMR
Enterococcus hirae	CopZ	CopY			
		CopA		SPR (Multhaup et al., 2001)	
Yeast	Atx1	Ccc2	(Pufahl et al., 1997)		Complex detected (Arnesano et al., 2001)
		CAOs	(Peter et al., 2008)		
human	HAH1	MNK	(Larin et al., 1999)	Co-IP (Hamza et al., 1999)	Complex Not-detected (Banci et al., 2005)
		WLN	(van Dongen et al., 2004)	Pull-down, Co-IP (Hamza et al., 1999)	Lower ratio of complex (Achila et al., 2006)

Table 4-2

## Strains and plasmids used in CHAPTER 4

Strains/Plasmids	Genotype/description	Reference
<u><i>E. coli</i> strains</u>		
JM109	<i>endA1, recA1, gyrA96, thi, hsdR17</i> (rk-, mk+), <i>relA1, supE44, λ</i> -, $\Delta$ ( <i>lac-proAB</i> ), [F', <i>traD36, proAB, lacI<sup>q</sup>Z</i> $\Delta$ M15]	(Sambrook et al., 1989)
BL21(DE3)	[F- <i>ompT hsdS<sub>B</sub></i> ( $\Gamma_B$ -m <sub>B</sub> <sup>-</sup> ) <i>gal dcm</i> (DE3 [ <i>lacI lacUV5-T7 gene1 ind1 Sam7 nin5</i> ])	(Sambrook et al., 1989)
<u><i>S. cerevisiae</i> strains</u>		
AH109	<i>MATa, trp1-901, leu2-3, 112, ura3-52, his3-200, gal4<math>\Delta</math>, gal80<math>\Delta</math>, LYS2::GAL1<sub>UAS</sub>-GAL1<sub>TATA</sub>-HIS3, GAL2<sub>UAS</sub>-GAL2<sub>TATA</sub>-ADE2, URA3::MEL1<sub>UAS</sub>-MEL1<sub>TATA</sub>-lacZ</i>	Clontech
MAV203	<i>MAT<math>\alpha</math>; leu2-3, 112; trp1-901; his3<math>\Delta</math>200; ade2-101; cyh2<sup>R</sup>; can1<sup>R</sup>; gal4<math>\Delta</math>; gal80<math>\Delta</math>; GAL1::lacZ; HIS3<sub>UASGAL1</sub>::HIS3@LYS2; SPAL10::URA3.</i>	Invitrogen
<u>Plasmids</u>		
pGBT9	GAL4 <sub>(1-147)</sub> DNA-binding domain, <i>TRP1</i> (Ap <sup>r</sup> )	Clontech
pACT2	GAL4 <sub>(768-881)</sub> activation domain, <i>LEU2</i> (Ap <sup>r</sup> )	Clontech
pACT2-A	<i>arsA</i> gene cloned in pACT2 (Ap <sup>r</sup> )	(Lin et al., 2006)
pACT2-D	<i>arsD</i> gene cloned in pACT2 (Ap <sup>r</sup> )	(Lin et al., 2006)
pGBT9-A	<i>arsA</i> gene cloned in pGBT9 (Ap <sup>r</sup> )	(Lin et al., 2006)
pGBT9-D	<i>arsD</i> gene cloned in pGBT9 (Ap <sup>r</sup> )	(Lin et al., 2006)
pGBT9-k	Kanamycin resistance gene is amplified from pET28a and inserted into pGBT9 at <i>AatII</i> site (Kana <sup>r</sup> )	Chapter 3
pGBT9-k-D	Kanamycin resistance gene is amplified from pET28a and inserted into pGBT9-D at <i>AatII</i> site (Kana <sup>r</sup> )	Chapter 3

Table 4-2

## Strains and plasmids used in CHAPTER 4 (continued)

Strains/Plasmids	Genotype/description	Reference
<u>Plasmids</u>		
pGBT9-k-D <sub>S14R</sub>	Ser14 was mutated to Arg by site directed mutagenesis on pGBT9-k-D (Kana <sup>r</sup> )	This study
pGBT9-k-D <sub>T20I</sub>	Thr20 was mutated to Ile by site directed mutagenesis on pGBT9-k-D (Kana <sup>r</sup> )	This study
pGBT9-k-D <sub>Q24L</sub>	Gln24 was mutated to Leu by site directed mutagenesis on pGBT9-k-D (Kana <sup>r</sup> )	This study
pGBT9-k-D <sub>D28V</sub>	Asp28 was mutated to Val by site directed mutagenesis on pGBT9-k-D (Kana <sup>r</sup> )	This study
pGBT9-k-D <sub>D28T</sub>	Asp28 was mutated to Thr by site directed mutagenesis on pGBT9-k-D (Kana <sup>r</sup> )	This study
pGBT9-k-D <sub>T31A</sub>	Thr31 was mutated to Ala by site directed mutagenesis on pGBT9-k-D (Kana <sup>r</sup> )	This study
pGBT9-k-D <sub>Q34R</sub>	Gln34 was mutated to Arg by site directed mutagenesis on pGBT9-k-D (Kana <sup>r</sup> )	This study
pGBT9-k-D <sub>Q38R</sub>	Gln38 was mutated to Arg by site directed mutagenesis on pGBT9-k-D (Kana <sup>r</sup> )	This study
pGBT9-k-D <sub>V61A</sub>	Val61 was mutated to Ala by site directed mutagenesis on pGBT9-k-D (Kana <sup>r</sup> )	This study
pGBT9-k-D <sub>F55L</sub>	Selected by yeast two-hybrid (Kana <sup>r</sup> )	This study
pGBT9-k-D <sub>Q51H</sub>	Selected by yeast two-hybrid (Kana <sup>r</sup> )	This study
pGBT9-k-D <sub>V22A</sub>	Val22 was mutated to Ala by site directed mutagenesis on pGBT9-k-D (Kana <sup>r</sup> )	This study
pGBT9-k-D <sub>V17A</sub>	Val17 was mutated to Ala by site directed mutagenesis on pGBT9-k-D (Kana <sup>r</sup> )	This study
pGBT9-k-D <sub>V27D</sub>	Selected by yeast two-hybrid (Kana <sup>r</sup> )	This study

Table 4-2

## Strains and plasmids used in CHAPTER 4 (continued)

Strains/Plasmids	Genotype/description	Reference
<u>Plasmids</u>		
pAlter-dAhB	Six histidine codons added to the 3'-end of <i>arsA</i> gene (Ap <sup>r</sup> )	(Li and Rosen, 2000)
pET28a	For expression of his-tagged protein controlled by T7 promoter (Kana <sup>r</sup> )	Novagen
pET28a-ArsD109	<i>arsD</i> <sub>1-109</sub> truncation was inserted into pET28a through <i>EcoRI</i> and <i>Sall</i> sites (Kana <sup>r</sup> )	Chapter 2
pET28a-ArsD109 K2/104A	Lys2 and Lys104 were mutated to Ala by site directed mutagenesis on pET28a-ArsD109 (Kana <sup>r</sup> )	This study
pET28a-ArsD109 K2/104A-K37/62A	Lys37 and Lys62 were mutated to Ala by site directed mutagenesis on pET28a-ArsD109 <sub>K2/104A</sub> (Kana <sup>r</sup> )	This study
pET28a-ArsD109 K2/104A-K37/62R	Lys37 and Lys62 were mutated to Arg by site directed mutagenesis on pET28a-ArsD109 <sub>K2/104A</sub> (Kana <sup>r</sup> )	This study
pET28a-ArsD109 K2/104A-K60/90A	Lys60 and Lys90 were mutated to Ala by site directed mutagenesis on pET28a-ArsD109 <sub>K60/90A</sub> (Kana <sup>r</sup> )	This study
pGBT9-k-D <sub>K2/104A-K37/62A</sub>	<i>arsD</i> <sub>K2/104A-K37/62A</sub> inserted into pGBT9-k (Kana <sup>r</sup> ) between <i>EcoRI</i> and <i>BamHI</i>	This study
pGBT9-k-D <sub>K2/104A-K37/62R</sub>	<i>arsD</i> <sub>K2/104A-K37/62R</sub> inserted into pGBT9-k (Kana <sup>r</sup> ) between <i>EcoRI</i> and <i>BamHI</i>	This study
pGBT9-k-D <sub>K2/104A-K60/90A</sub>	<i>arsD</i> <sub>K2/104A-K60/90A</sub> inserted into pGBT9-k (Kana <sup>r</sup> ) between <i>EcoRI</i> and <i>BamHI</i>	This study
pGBT9-k-D <sub>K2/104A-K37A</sub>	<i>arsD</i> <sub>K2/104A-K37A</sub> inserted into pGBT9-k (Kana <sup>r</sup> ) between <i>EcoRI</i> and <i>BamHI</i>	This study
pGBT9-k-D <sub>K2/104A-K62A</sub>	<i>arsD</i> <sub>K2/104A-K62A</sub> inserted into pGBT9-k (Kana <sup>r</sup> ) between <i>EcoRI</i> and <i>BamHI</i>	This study

**Table 4-3****Oligonucleotide primers used in CHAPTER 4**

<b>Primer</b>	<b>Sequence (5'–3')</b>	<b>Target / Direction</b>
GAL4-BD sequencing primer	GAGTAGTAACAAAGGTCAA	pGBT9 Forward sequencing primer
GAL4-AD sequencing primer	AATACCACTACAATGGAT	pACT2 Forward sequencing primer
ArsA-100-s	GTCCTGCCTGATGACGTTGTT CCA	ArsA forwarding sequencing primer from 100 <sup>th</sup> residue
ArsA-220-s	GTCGCCCGGACTCATCTGGAA CTTG	ArsA forwarding sequencing primer from 220 <sup>th</sup> residue
ArsA-420-s	AAGAGGACTTACGCTCACCTTG CAC	ArsA forwarding sequencing primer from 420 <sup>th</sup> residue
ArsA-480-a	CGTGACCAGTAACACTTTAGTG CG	ArsA reversing sequencing primer from 480 <sup>th</sup> residue
pET28a-3600-AatII	CTATGACGTCCAACCCGGTAA GACACGACTTATC	Sense primer for amplifying kanamycin resistance gene from pET28a
pET28a-5300-AatII	CTATGACGTCCGCCCGCTCCT TTCGCTTTCTTCC	Antisense primer for amplifying kanamycin resistance gene from pET28a
pGBT9-s	TAAAGATGCCGTCACAGATAGA TTG	Sense primer for ep-PCR of ArsD on pGBT9-k-D
pGBT9-a	ACCTGACCTACAGGAAAGAGTT ACT	Antisense primer for ep-PCR of ArsD on pGBT9-k-D
pACT2-s	CTATTCGATGATGAAGATACCC CACCAAACCC	Sense primer for ep-PCR of ArsA on pACT2-A
pACT2-a	AGGTTACATGGCCAAGATTGAA ACTTAGAGGAG	Antisense primer for ep-PCR of ArsA on pACT2-A

**Table 4-3****Oligonucleotide primers used in CHAPTER 4 (continued)**

<b>Primer</b>	<b>Sequence (5'–3')</b>	<b>Target / Direction</b>
ArsD-S14R-s	ACCCGGCGATGTGTTGCAGAAC CGGCGTCTGCGGTACAG	Mutate ArsD Ser14 to Arg, sense
ArsD-S14R-a	CTGTACCGCAGACGCCGGTTCT GCAACACATCGCCGGGT	Mutate ArsD Ser14 to Arg, antisense
ArsD-T20I-s	CACCGGCGTCTGCGGTATAGAT GTTGATCAGGCTCT	Mutate ArsD Thr20 to Ile, sense
ArsD-T20I-a	AGAGCCTGATCAACATCTATAC CGCAGACGCCGGTG	Mutate ArsD Thr20 to Ile, antisense
ArsD-Q24L-s	GCGGTACAGATGTTGATCTGGC TCTGGTTCGATTTTTC	Mutate ArsD Gln24 to Leu, sense
ArsD-Q24L-a	GAAAAATCGACCAGAGCCAGAT CAACATCTGTACCGC	Mutate ArsD Gln24 to Leu, antisense
ArsD-D28V-s	GTTGATCAGGCTCTGGTCGTTT TTTCTACAGATGTGCAAT	Mutate ArsD Asp28 to Val, sense
ArsD-D28V-a	ATTGCACATCTGTAGAAAAAAC GACCAGAGCCTGATCAAC	Mutate ArsD Asp28 to Val, antisense
ArsD-D28T-s	TGATCAGGCTCTGGTCACTTTT TCTACAGATGTGC	Mutate ArsD Asp28 to Thr, sense
ArsD-D28T-a	GCACATCTGTAGAAAAAGTGAC CAGAGCCTGATCA	Mutate ArsD Asp28 to Thr, antisense
ArsD-T31A-s	GGCTCTGGTCGATTTTTTCTGCA GATGTGCAATGGCTCAA	Mutate ArsD Thr31 to Ala, sense
ArsD-T31A-a	TTGAGCCATTGCACATCTGCAG AAAAATCGACCAGAGCC	Mutate ArsD Thr31 to Ala, antisense
ArsD-Q34R-s	CGATTTTTCTACAGATGTGCGA TGGCTCAAACAATGCGG	Mutate ArsD Gln34 to Arg, sense
ArsD-Q34R-a	CCGCATTGTTTGAGCCATCGCA CATCTGTAGAAAAATCG	Mutate ArsD Gln34 to Arg, antisense

**Table 4-3****Oligonucleotide primers used in CHAPTER 4 (continued)**

<b>Primer</b>	<b>Sequence (5'–3')</b>	<b>Target / Direction</b>
ArsD-Q38R-s	GATGTGCAATGGCTCAAACGAT GCGGTGTACAAATTGAG	Mutate ArsD Gln38 to Arg, sense
ArsD-Q38R-a	CTCAATTTGTACACCGCATCGT TTGAGCCATTGCACATC	Mutate ArsD Gln38 to Arg, antisense
ArsD-V61A-s	CTTTGTACAGAACGAGAAGGCC AAAGCGTTTATTGAAGCTT	Mutate ArsD Val61 to Ala, sense
ArsD-V61A-a	AAGCTTCAATAAACGCTTTGGC CTTCTCGTTCTGTACAAAG	Mutate ArsD Val61 to Ala, antisense
ArsD-K2A-s	ATCCGAATTCCCGGGGGCAAC GTTAATGGTATTTGA	Mutate ArsD Lys2 to Ala on pET28a-ArsD109, sense
ArsD-K2A-a	TCAAATACCATTAACGTTGCC CCGGGAATTCGGAT	Mutate ArsD Lys2 to Ala on pET28a-ArsD109, antisense
ArsD-K37A-s	ACAGATGTGCAATGGCTCGCAC AATGCGGTGTACAAAT	Mutate ArsD Lys37 to Ala, sense
ArsD-K37A-a	ATTTGTACACCGCATTGTGCGA GCCATTGCACATCTGT	Mutate ArsD Lys37 to Ala, antisense
ArsD-K62A-s	TACAGAACGAGAAGGTCGCAG CGTTTATTGAAGCTTC	Mutate ArsD Lys62 to Ala, sense
ArsD-K62A-a	GAAGCTTCAATAAACGCTGCGA CCTTCTCGTTCTGTA	Mutate ArsD Lys62 to Ala, antisense
ArsD-K104A-s	TTGGCATTCCACTGGATGCAGT GGGATTAGCGCCTT	Mutate ArsD Lys104 to Ala, sense
ArsD-K104A-a	AAGGCGCTAATCCCACTGCATC CAGTGGAATGCCAA	Mutate ArsD Lys104 to Ala, antisense
ArsD-K60A-s	AGCTTTGTACAGAACGAGGCGG TCAAAGCGTTTATTGA	Mutate ArsD Lys60 to Ala, sense
ArsD-K60A-a	TCAATAAACGCTTTGACCGCCT CGTTCTGTACAAAGCT	Mutate ArsD Lys60 to Ala, antisense

Table 4-3

## Oligonucleotide primers used in CHAPTER 4 (continued)

Primer	Sequence (5'–3')	Target / Direction
ArsD-K90A-s	ATGGCCGGGCGTTACCCGGCA CGCGCTGAGCTGGCTCGC	Mutate ArsD Lys90 to Ala, sense
ArsD-K90A-a	GCGAGCCAGCTCAGCGCGTGC CGGGTAACGCCCGGCCAT	Mutate ArsD Lys90 to Ala, antisense
ArsD-K37R-s	ACAGATGTGCAATGGCTCAGAC AATGCGGTGTACAAAT	Mutate ArsD Lys37 to Arg, sense
ArsD-K37R-a	ATTTGTACACCGCATTGTCTGA GCCATTGCACATCTGT	Mutate ArsD Lys37 to Arg, antisense
ArsD-K62R-s	TACAGAACGAGAAGGTCAGAGC GTTTATTGAAGCTTC	Mutate ArsD Lys62 to Arg, sense
ArsD-K62R-a	GAAGCTTCAATAAACGCTCTGA CCTTCTCGTTCTGTA	Mutate ArsD Lys62 to Arg, antisense
Ec-N-ArsD-K2A-s	TCCGGAATTCATGGCAACGTTA ATGGTATTTG	Sense primer for amplifying ArsD <sub>K2/104A</sub> mutants to put into pGBT9-k between <i>EcoRI</i> and <i>BamHI</i>
Bm-D109-K104A-a	CGCGGATCCTTAAGGCGCTAAT CCCCTGCATCCAG	Antisense primer for amplifying ArsD <sub>K2/104A</sub> mutants to put into pGBT9-k between <i>EcoRI</i> and <i>BamHI</i>
T7 promoter sequencing primer	TAATACGACTCACTATAGGG	pET28a forward sequencing primer
T7 terminator sequencing primer	GCTAGTTATTGCTCAGCGG	pET28a reverse sequencing primer



**Table 4-4****ArsD mutations increasing or decreasing ArsA-ArsD interaction**

<b>method</b>	<b>effect</b>	<b>mutations</b>
yeast two-hybrid	stronger interaction with ArsA	S14R, T20I, Q24L, D28T, D28V, T31A, Q34R, Q38R, V61A
yeast two-hybrid	weaker interaction with ArsA	V17A, V22A, V27D, Q51H, F55L
site-directed mutagenesis	weaker interaction with ArsA	K37A, K62A

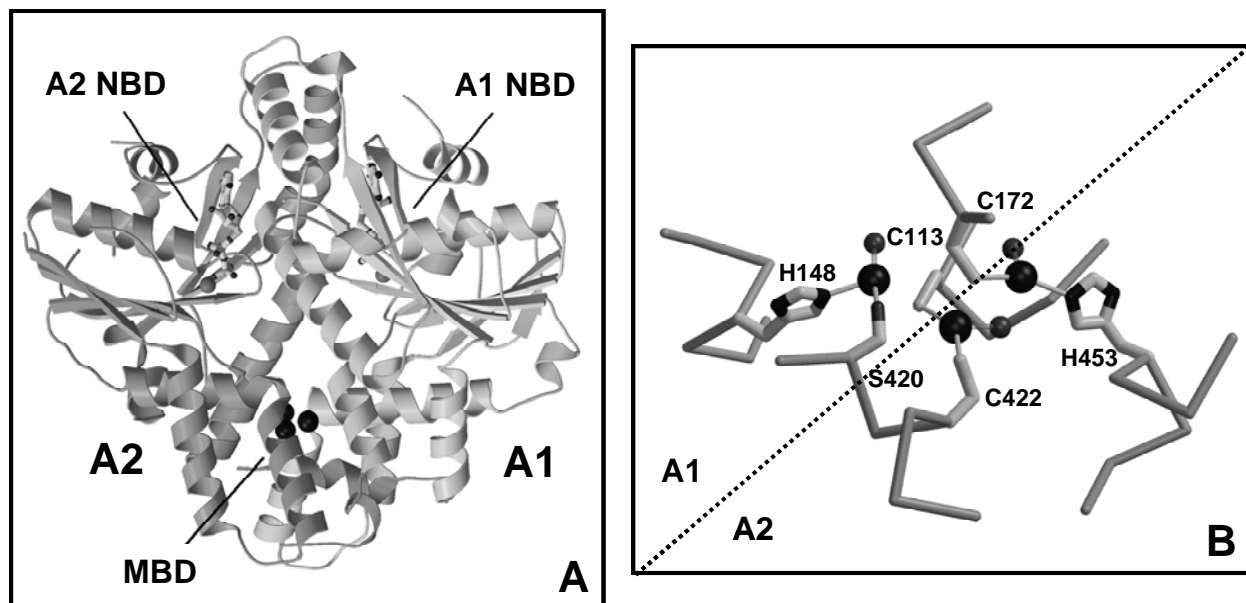


**Figure 1-1. Structure of R773 ArsA ATPase (Lin et al., 2007b).**

(A): The overall structure of ArsA is shown as a ribbon diagram.  $Mg^{2+}$ -ADP is bound to each of the two NBDs in the A1 and A2 halves of ArsA, while three Sb(III) are bound at the single MBD.

(B) The metalloid binding domain composed of three 3-coordinate As(III)/Sb(III) binding sites. Each site has two protein ligands, one from A1 and one from A2, plus a non-protein ligand that appears to be a chloride in the crystal structure but could be a hydroxyl in the native protein. The high affinity site is composed of Cys-113 from A1 and Cys-422 from A2. The other two sites are composed of His-148 from A1 and Ser-420 from A2 and Cys-172 from A1 and His-453 from A2. The two histidines come from the signal transduction domains ( $D_{142/447}TAPTGH_{148/453}$ ) that connect the two nucleotide binding domains, NBD1 and NBD2, to the MBD. Binding of metalloid acts like molecular glue to hold A1 and A2 in a conformation in which residues from both contribute to the formation of NBD1 and NBD2. Thus metalloid binding increases the affinity of NBD1 and NBD2 and activates catalysis.

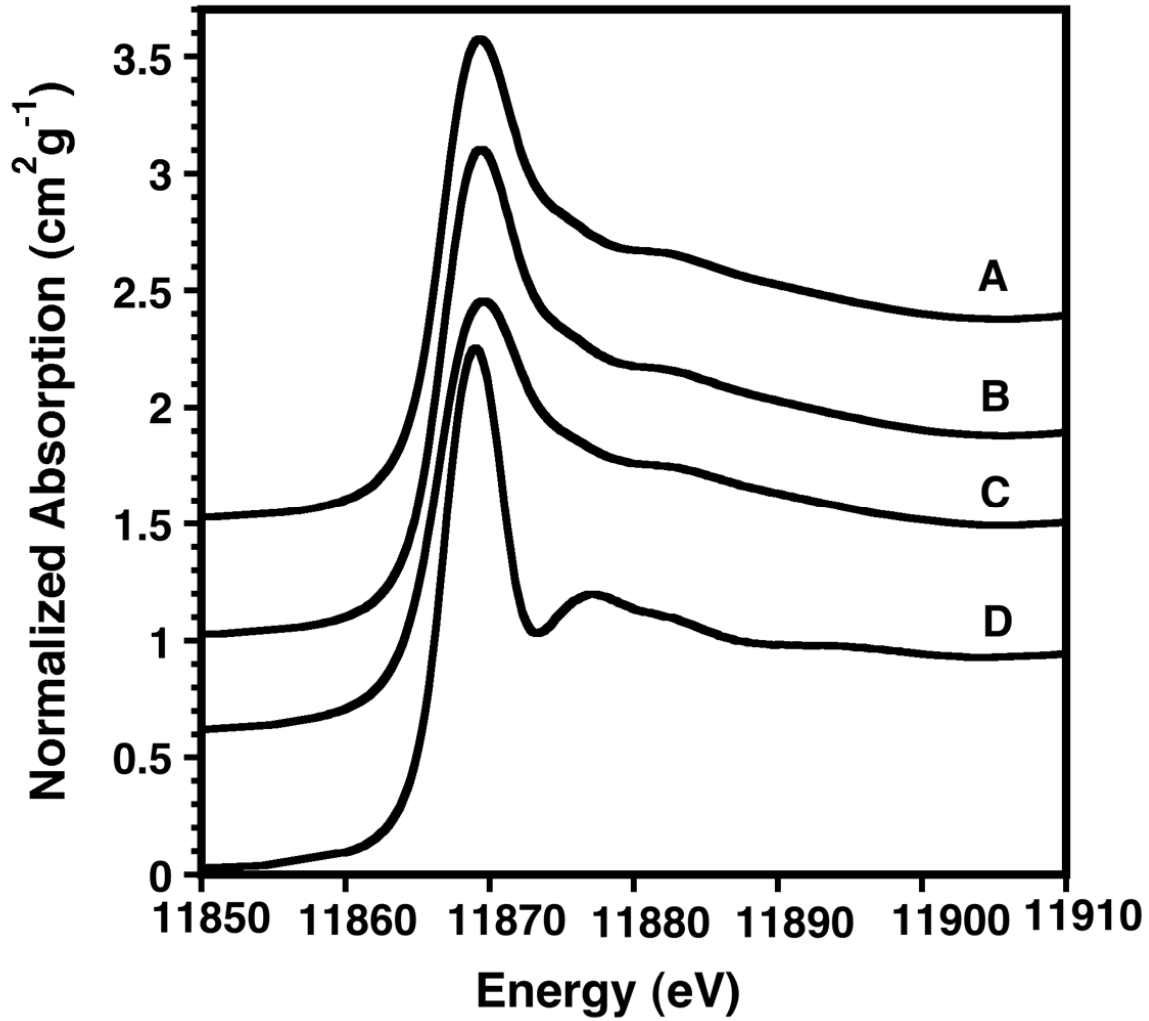


**Figure 2-1.** Normalized XANES spectra of ArsD and its derivatives.

Spectra from top to bottom include: C18G (A), C13G (B), C12G (C) and wild type ArsD109 (D). Spectra were offset for clarity.

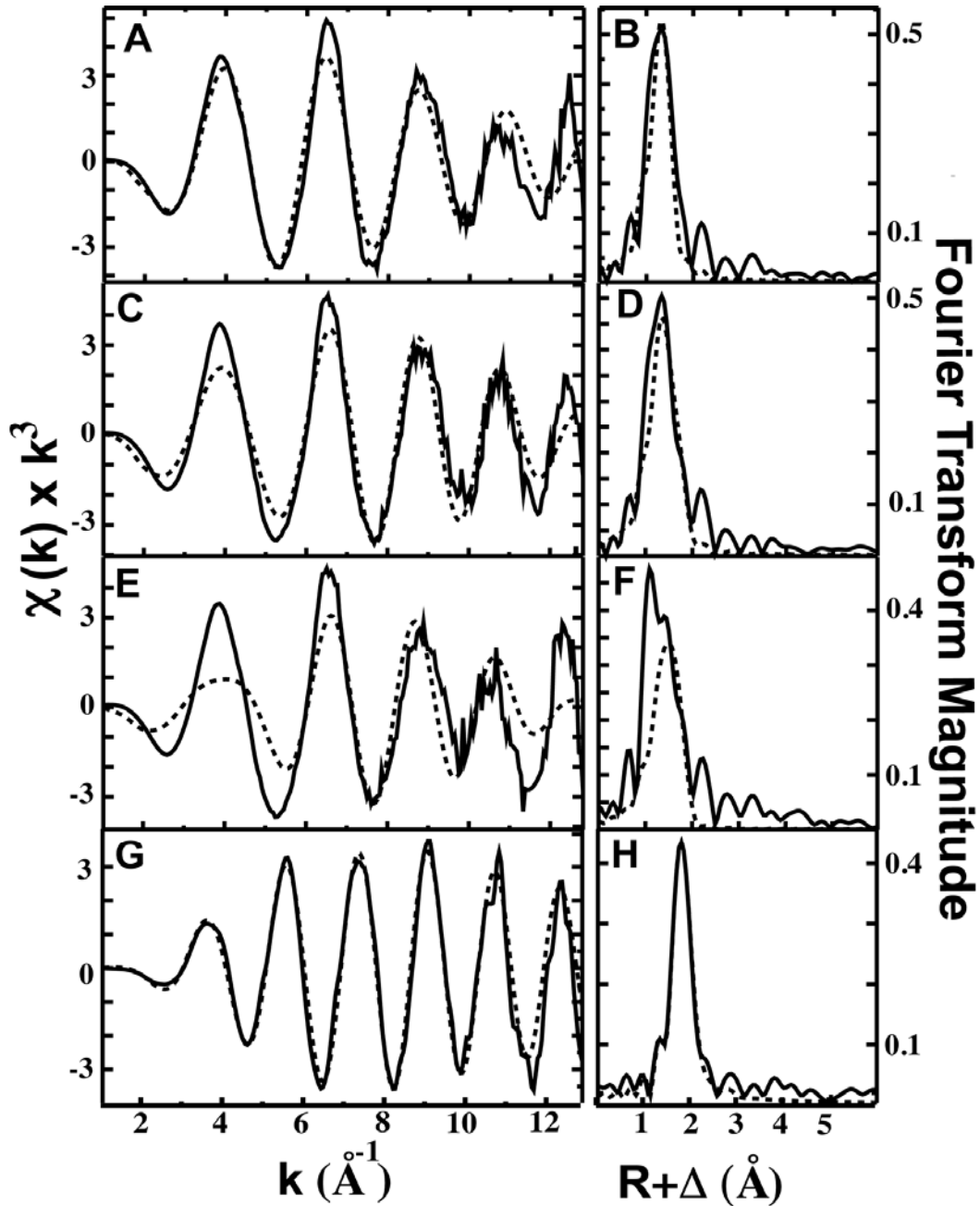


**Figure 2-2. Arsd EXAFS data and simulations.**

Raw EXAFS data and phase shifted Fourier Transforms of As bound to C18G (A, B), C13G (C, D), C12G (E, F) and wild type Arsd109 (G, H). Raw unfiltered data is given as solid lines, while the best-fit simulated data are shown as dotted lines.

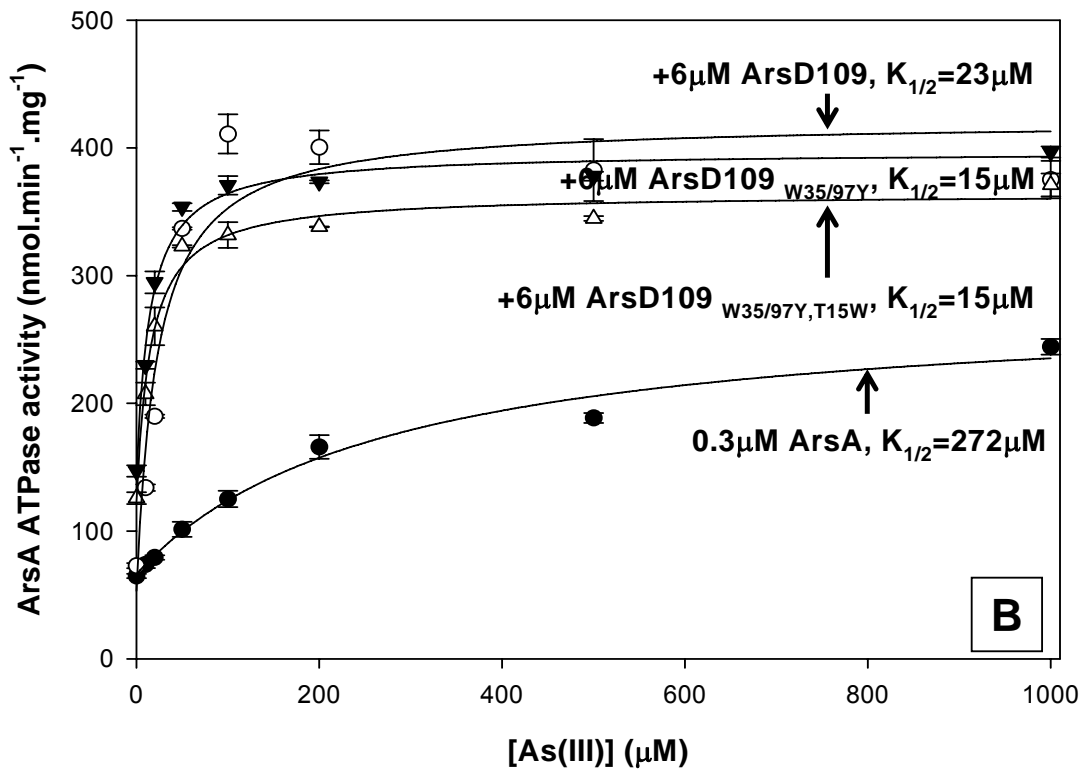
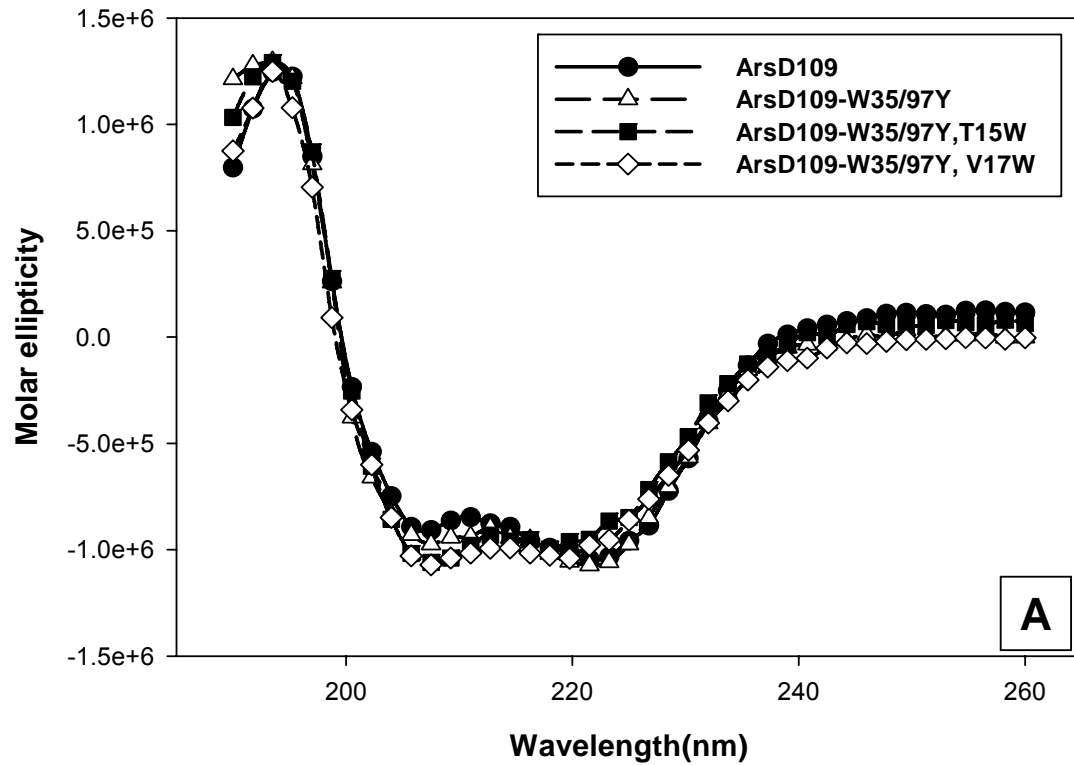


**Figure 2-3. ArsD109 tryptophan mutants fold normally and have same activity as wild type.**

**(A)** Circular CD spectra were collected with (●) 10  $\mu$ M ArsD109, ( $\Delta$ ) tryptophan-free ArsD109-W35Y/W97Y, (■) T15W and ( $\diamond$ ) V17W.

**(B)** ArsA ATPase activity was assayed at the indicated concentrations of sodium arsenite in the presence or absence of ArsD derivatives. ArsA ATPase activity was assayed as described under “Materials and Methods”. (●), no addition; (○), ArsD109; ( $\blacktriangledown$ ), tryptophan-free ArsD109-W35Y/W97Y;  $\Delta$ , T15W. The curves were fitted using SigmaPlot 9.0, with *error bars* represent standard deviation.

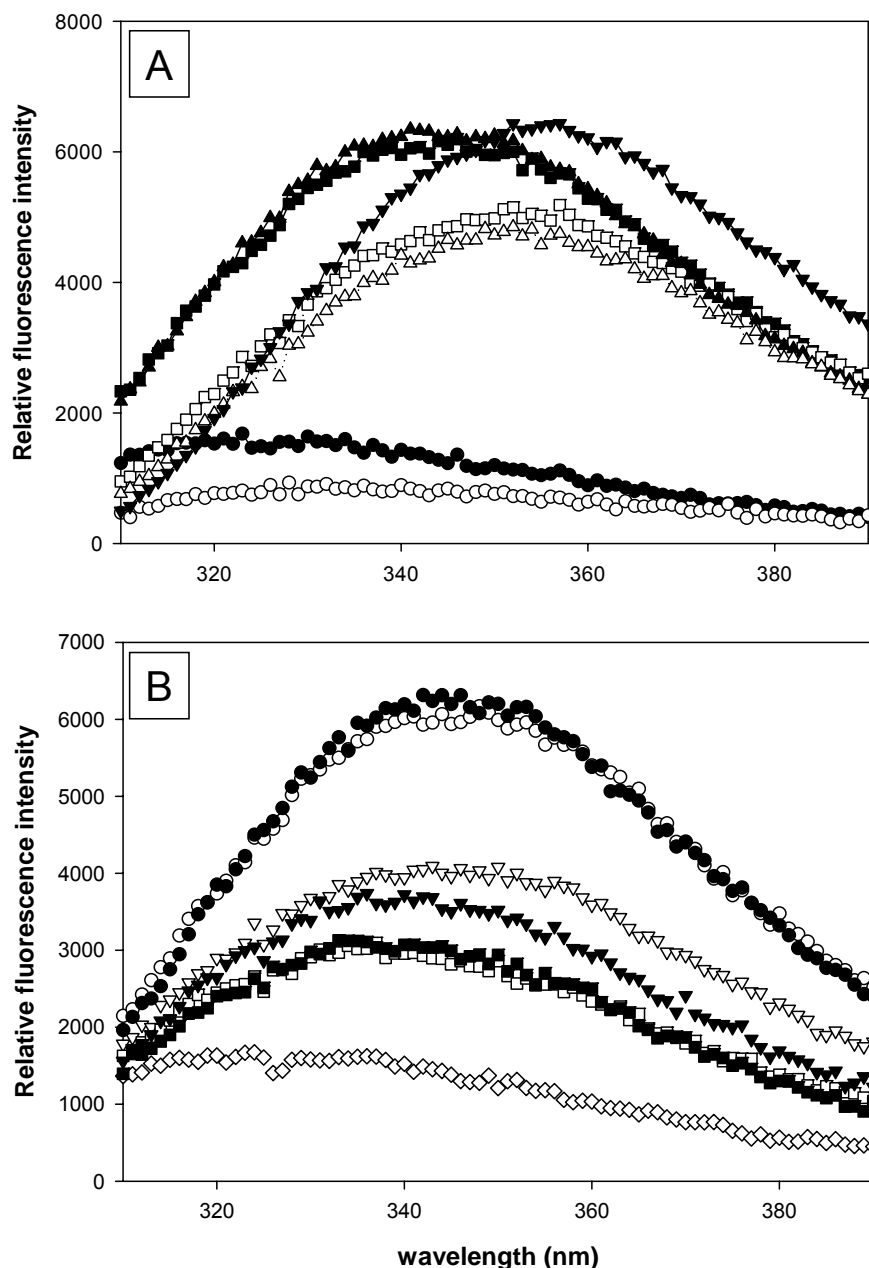


**Figure 2-4. Protein fluorescence of single tryptophan derivatives T15W and V17W reports metalloid binding.**

Emission scans were performed with excitation at 295 nm, as described under Materials and Methods.

**(A)** (▼), 1  $\mu$ M tryptophan; (●), tryptophan-free W35Y/97Y; (■), T15W; (▲), V17W; (○), W35Y/97Y + 6 M guanidinium-HCl; (□), T15W + 6 M guanidinium-HCl; (Δ), V17W + 6 M guanidinium-HCl.

**(B)** (○), T15W; (▽), T15W + 5 mM As(III); (□), T15W + 0.1 mM Sb(III); (●), V17W; (▼), V17W + 5 mM As(III); (■), V17W + 0.1 mM Sb(III); (◇), tryptophan-free W35Y/97Y.

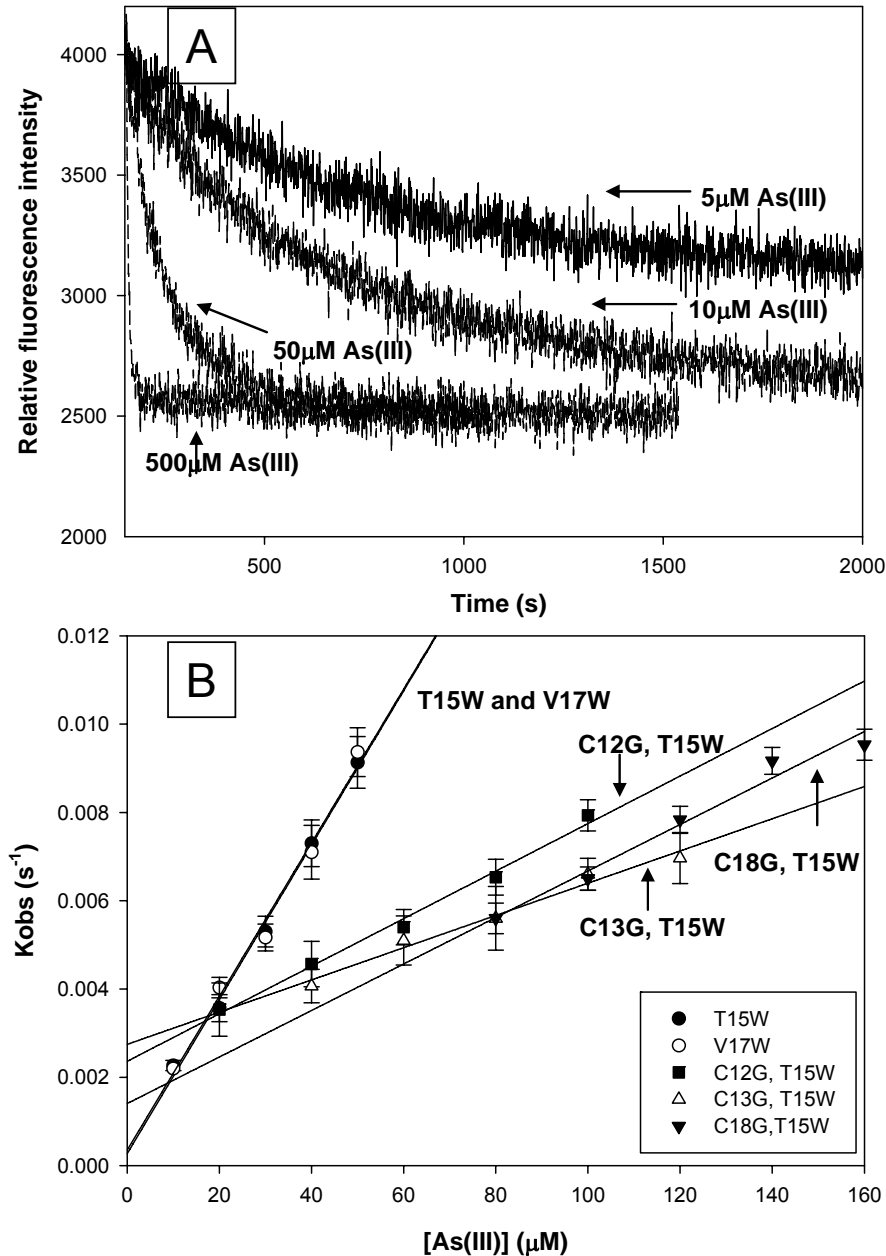


**Figure 2-5. Binding of As(III) by single tryptophan derivatives T15W and V17W and cysteine mutants.**

**(A)** Time course of 1 μM V17W fluorescence quenched by different concentration of As(III). The data were fitted using SigmaPlot 9.0 with function  $F = F_0 - F_m(1 - e^{-K_{obs}t})$ , in which  $K_{obs}$  is the binding rate used in Fig B.

**(B)** The rate of fluorescence quenching,  $K_{obs}$ , was determined as a function of arsenite concentration with excitation and emission wavelengths of 295 and 345 nm, respectively. (●), T15W; (○), V17W; (■), T15W/C12G; (△), T15W/C13G; (▼), T15W/C18G. The data were fitted using SigmaPlot 9.0, with error bars representing the standard deviation from three assays.



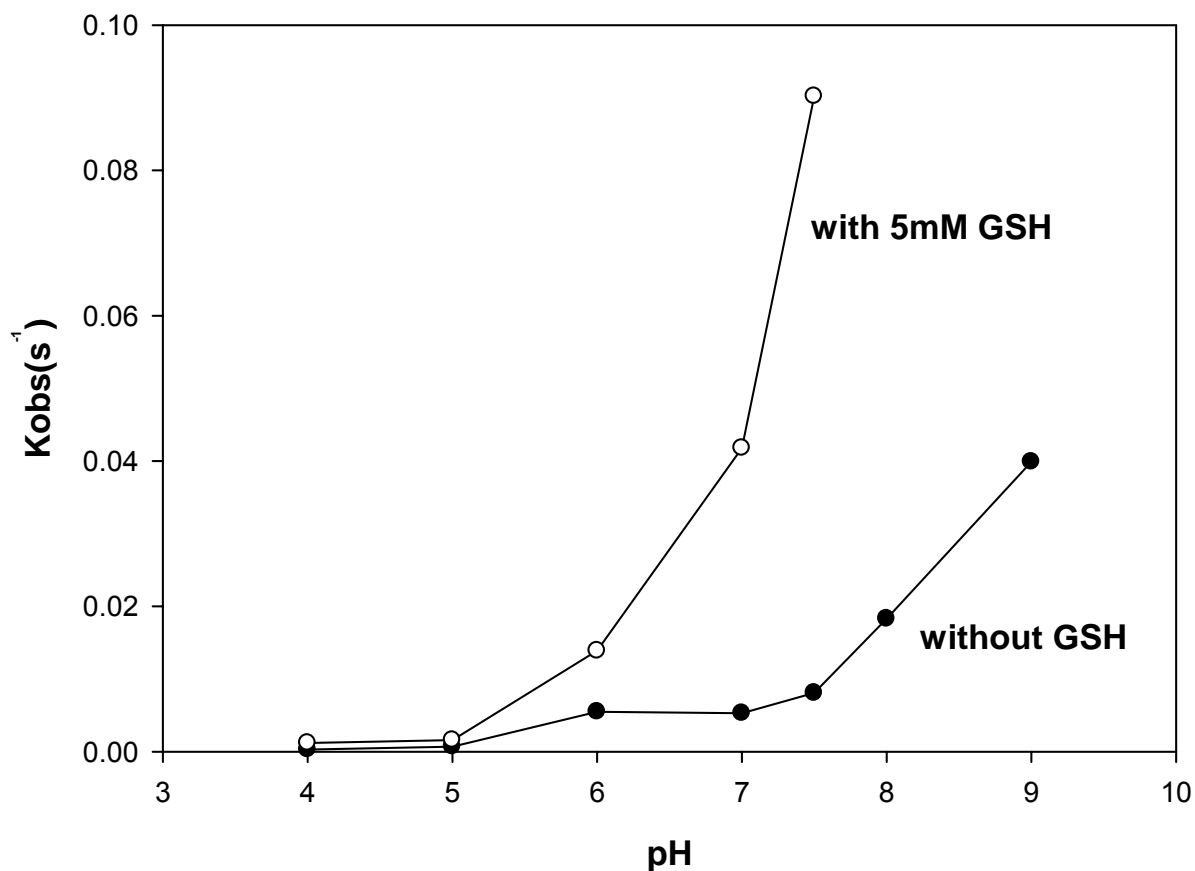


**Figure 2-6. GSH accelerates binding of As(III) binding by V17W.**

The rate of fluorescence quenching,  $K_{obs}$ , was determined as a function of pH in the presence (○) or absence (●) of 5 mM GSH.

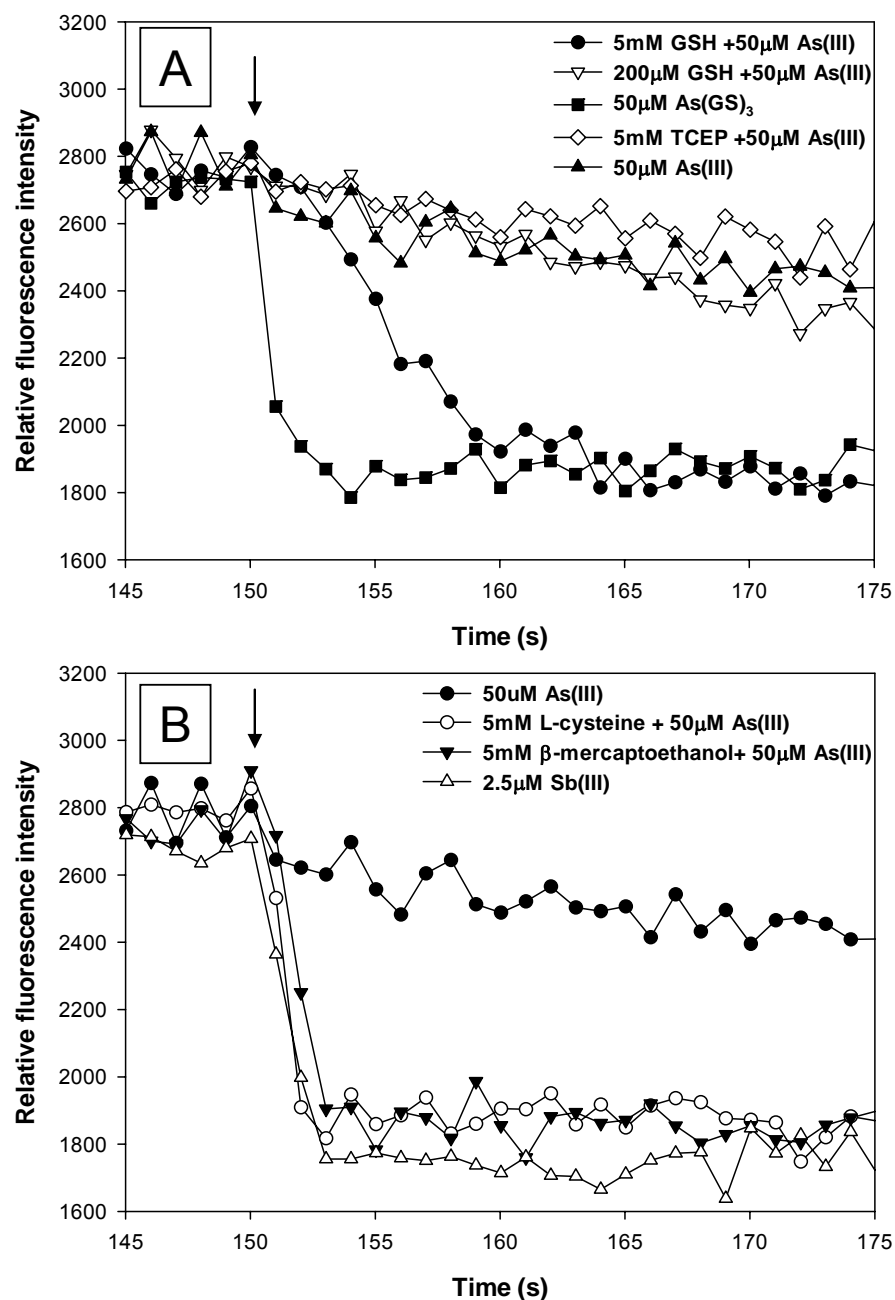


**Figure 2-7. As(GS)<sub>3</sub> is the metalloid donor to ArsD.**

Fluorescence of V17W was measured with excitation and emission wavelengths of 295 and 345 nm, respectively.

**(A)** At the arrow the following additions were made: (▲), 50 μM As(III); (▽), 0.2 mM GSH followed by 50 μM As(III); (◇), 5 mM TCEP followed by 50 μM As(III); (●), 5 mM GSH followed by 50 μM As(III); (■), 50 μM As(GS)<sub>3</sub>.

**(B)** At the arrow the following additions were made: (●), 50 μM As(III); (○), 5 mM L-cysteine followed by 50 μM As(III); (▼), 5 mM β-mercaptoethanol followed by 50 μM As(III); (△), 2.5 μM Sb(III).

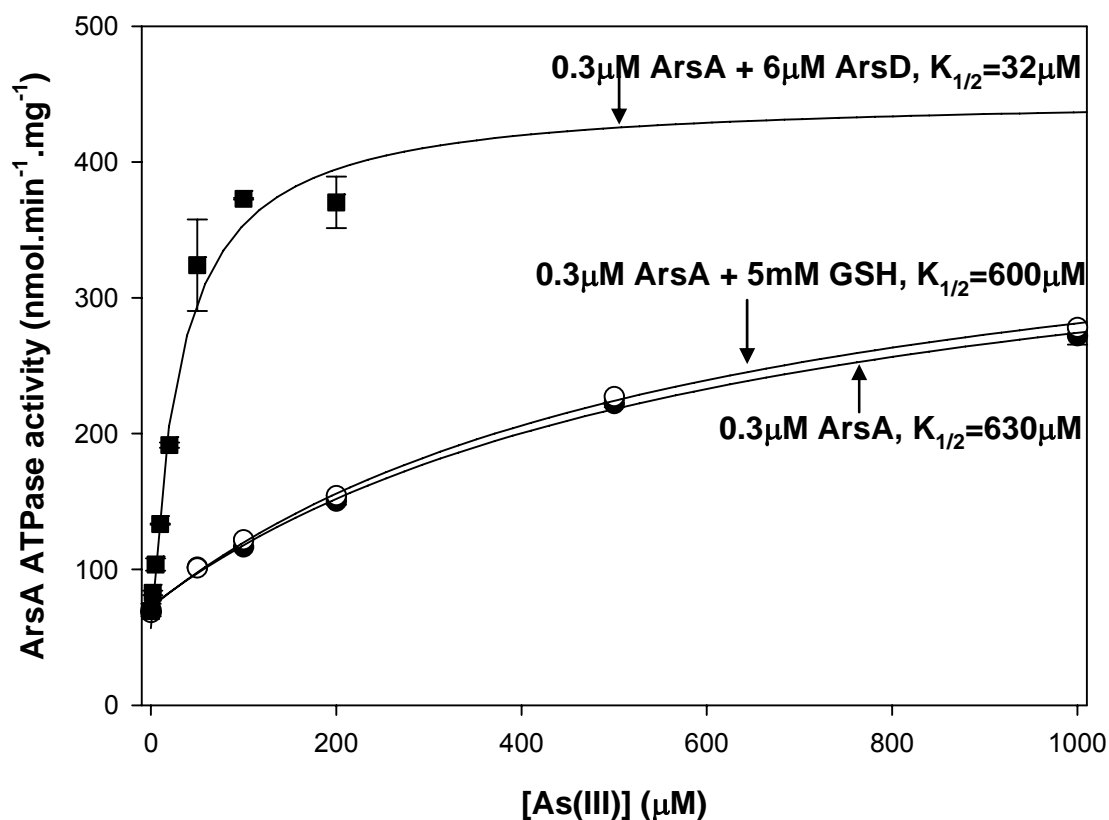


**Figure 2-8. As(GS)<sub>3</sub> does not activate ArsA.**

Activated ATPase activity of 0.3 μM ArsA was determined at the indicated concentrations of sodium arsenite, as described under Materials and Methods. (●), no addition; (○), 5 mM GSH; (■), 6 μM ArsD. The data were fitted using SigmaPlot 9.0, with error bars representing the standard deviation from three assays.

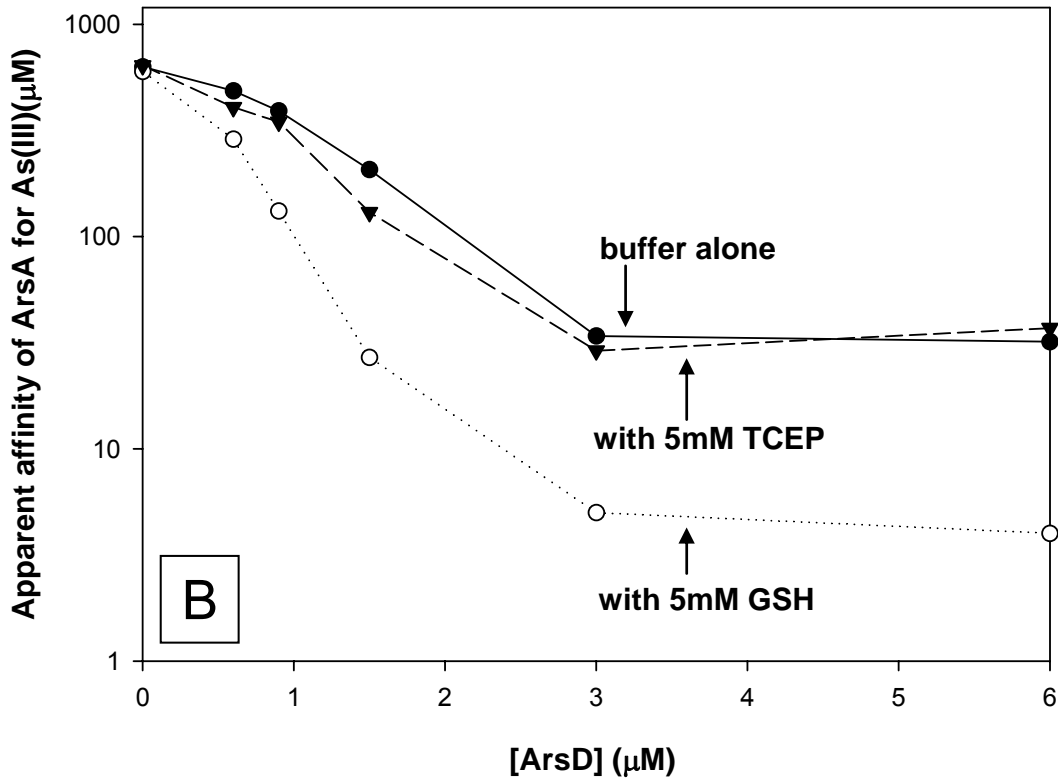
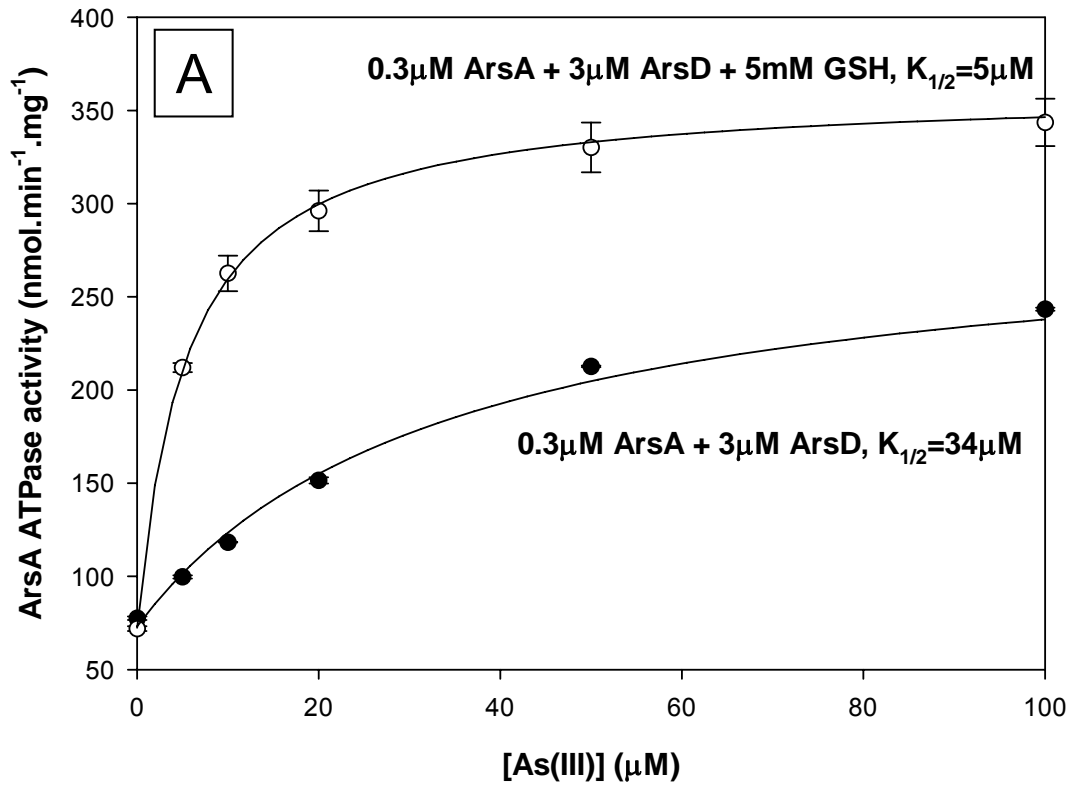


**Figure 2-9. GSH helps cooperation of ArsA and ArsD.**

**(A)** ATPase activity of 0.3  $\mu\text{M}$  ArsA was determined at the indicated concentrations of sodium arsenite in the presence of 3  $\mu\text{M}$  ArsD in buffer with or without 5mM GSH. ArsA ATPase activity was assayed as described under "Materials and Methods". ( $\bullet$ ), no addition; ( $\circ$ ), 5 mM GSH. The curves were fitted using SigmaPlot 9.0, with *error bars* representing standard deviation from three assays.

**(B)** The apparent affinity of ArsA for As(III), in ArsA ATPase activity assay, was determined at different concentrations of ArsD in different buffers. The enhancement of apparent affinity of ArsA for As(III) by ArsD was measured in buffers supplemented with or without TCEP and GSH. ( $\bullet$ ), buffer alone; ( $\blacktriangledown$ ), buffer supplemented with 5mM TCEP; ( $\circ$ ), buffer supplemented with 5mM glutathione.

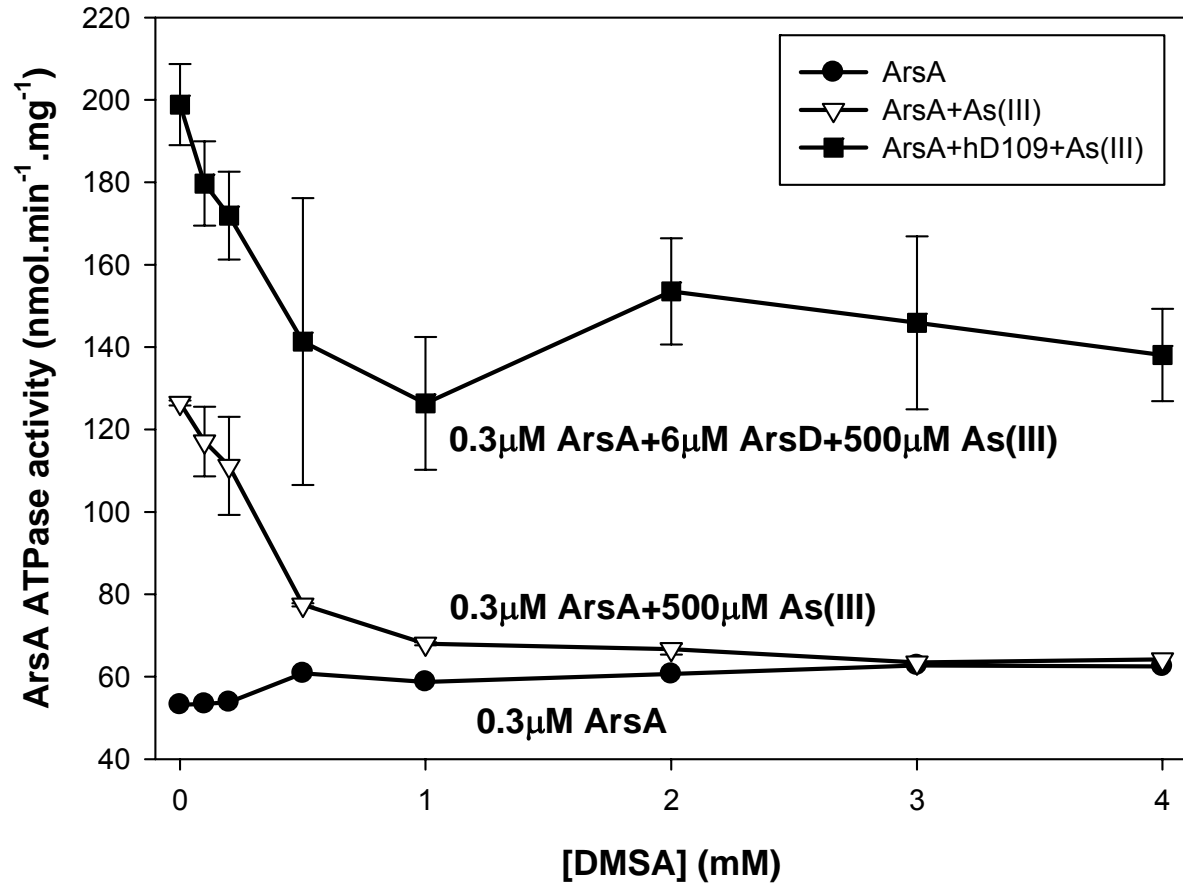


**Figure 2-10. ArsD channels As(III) to ArsA.**

The effect of the As(III) chelator DMSA on metalloid transfer from ArsD to ArsA was estimated from the activation of ATPase activity of 0.3 μM ArsA, as described under Materials and Methods. ATP hydrolysis was measured in the presence of the indicated concentrations of DMSA with (●) ArsA alone, (▽) ArsA + 0.5 mM sodium arsenite or (■) ArsA + 0.5 mM sodium arsenite plus 6 μM ArsD. The error bars represent the standard deviation from three assays.

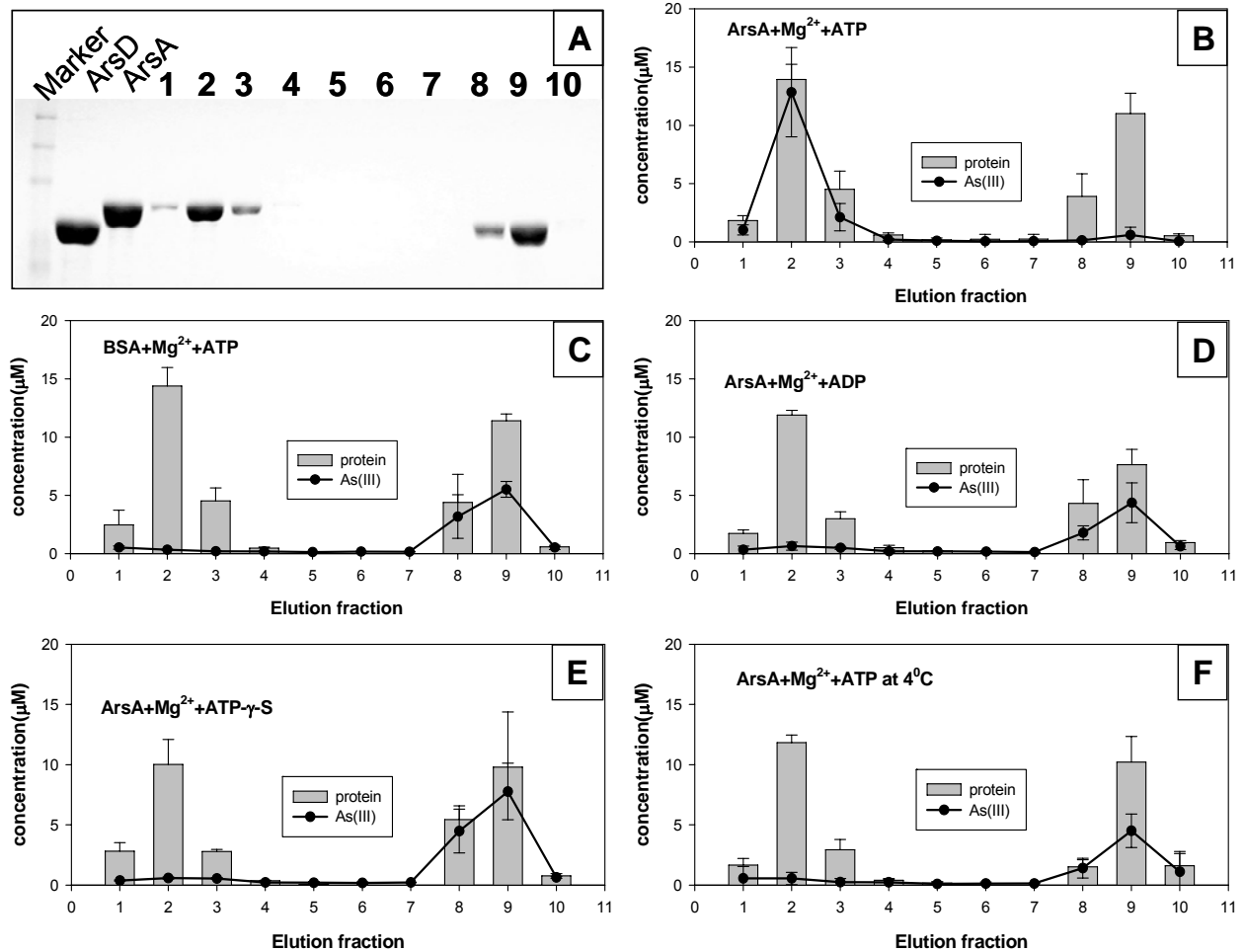


**Figure 2-11. Metalloid transfer from ArsD occurs during ArsA catalysis.**

As(III) transfer assays were performed as described under Materials and Methods. MBP-ArsD was bound to an amylose resin, following the column was charged with sodium arsenite to saturate ArsD. Next purified ArsA or BSA were applied to the columns with the indicated nucleotides (5 mM) at room temperature unless otherwise noted. Experiments were done at room temperature, except experiment in F was done at 4°C. (A), 10 fractions were collected and analyzed by SDS PAGE. Nearly all of the BSA or ArsA eluted in fraction 2, and fraction 9 contained nearly all of the MBP-ArsD. Nucleotides: (B), ArsA + MgATP; (C), BSA + MgATP, (D), ArsA + MgADP; (E), ArsA + MgATP- $\gamma$ -S; (F), ArsA + MgATP at 4°C. The concentration of protein (open bar) and As(III) (●) was quantified in each fraction. The error bars represent the standard deviation from three assays.

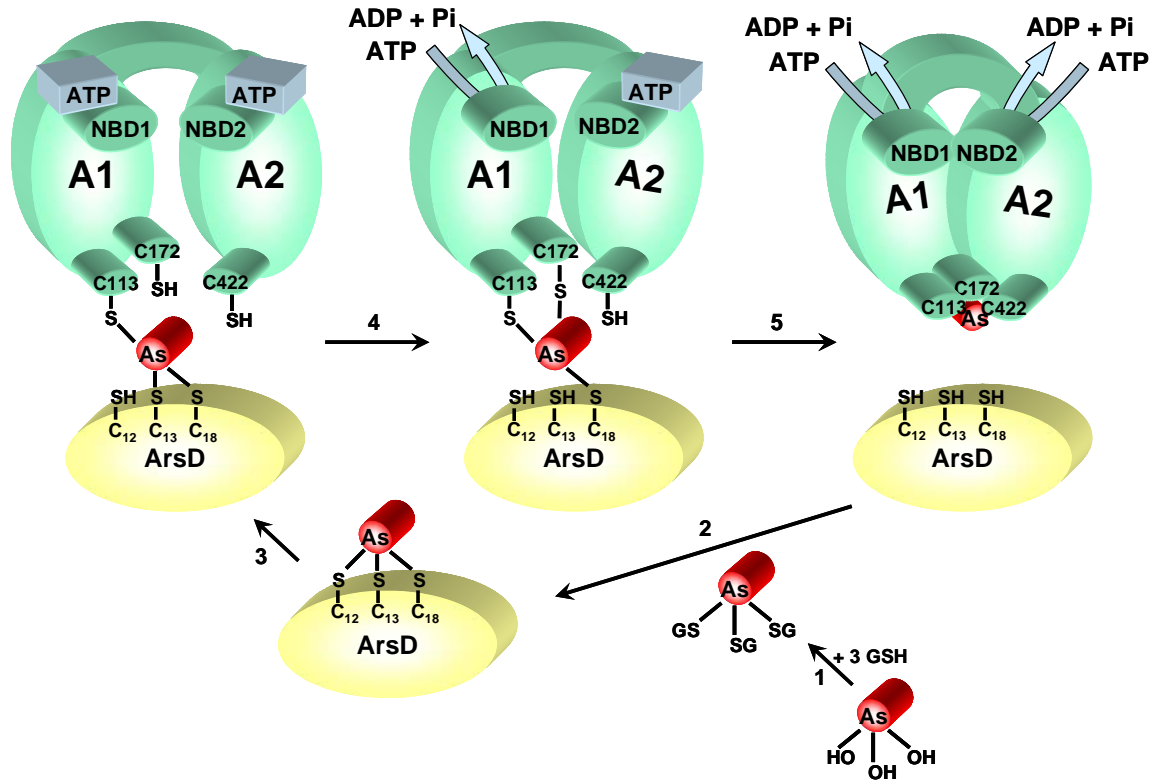


**Figure 2-12. Model of transfer from  $\text{As}(\text{GS})_3$  to  $\text{ArsD}$  to  $\text{ArsA}$ .**

In the first step  $\text{As}(\text{OH})_3$  forms  $\text{As}(\text{GS})_3$  with intracellular  $\text{GSH}$ . In the next step  $\text{ArsD}$  extracts  $\text{As}(\text{III})$  from  $\text{As}(\text{GS})_3$  by thiol exchange with residues  $\text{Cys}_{12}$ ,  $\text{Cys}_{13}$  and  $\text{Cys}_{18}$ . In a step-wise series of thiol exchanges (with an unknown order), the bound  $\text{As}(\text{III})$  is transferred to the thiolates  $\text{Cys}_{113}$ ,  $\text{Cys}_{172}$  and  $\text{Cys}_{422}$  of  $\text{ArsA}$  when the two nucleotide binding domains,  $\text{NBD1}$  and  $\text{NBD2}$ , hydrolyze  $\text{ATP}$ . Binding of  $\text{As}(\text{III})$  and  $\text{ATP}$  induces a series of conformational changes in  $\text{ArsA}$  resulting in activation of catalysis, with final extrusion of the metalloid out of the cells.



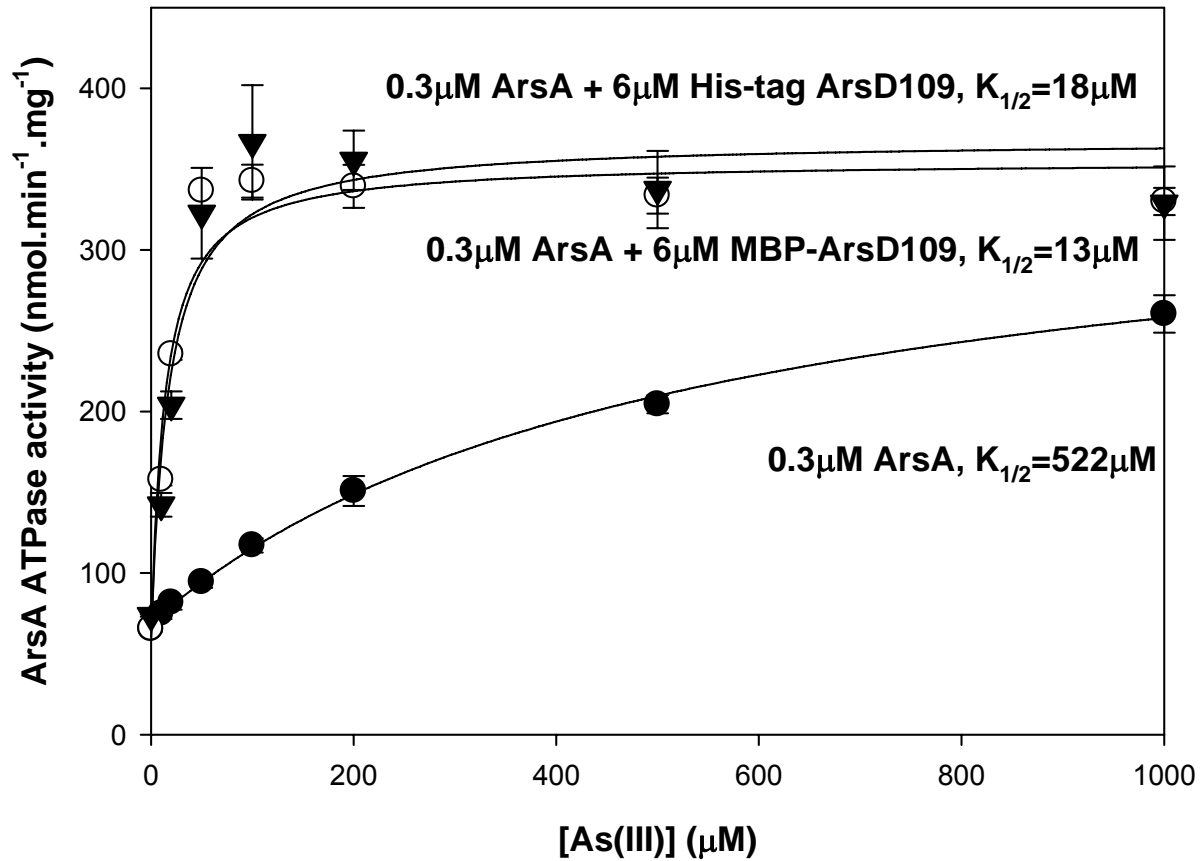


**Figure 3-1. MBP-ArsD109 and His6-ArsD109 both stimulate ArsA ATPase activity.**

ArsA ATPase activity was assayed at the indicated concentrations of sodium arsenite in the presence or absence of ArsD derivatives. ArsA ATPase activity was assayed as described under "Materials and Methods". (●), no addition; (○), MBP-ArsD109; (▼), His6-ArsD109. The curves were fitted using SigmaPlot 9.0, with *error bars* representing standard deviation from three assays.

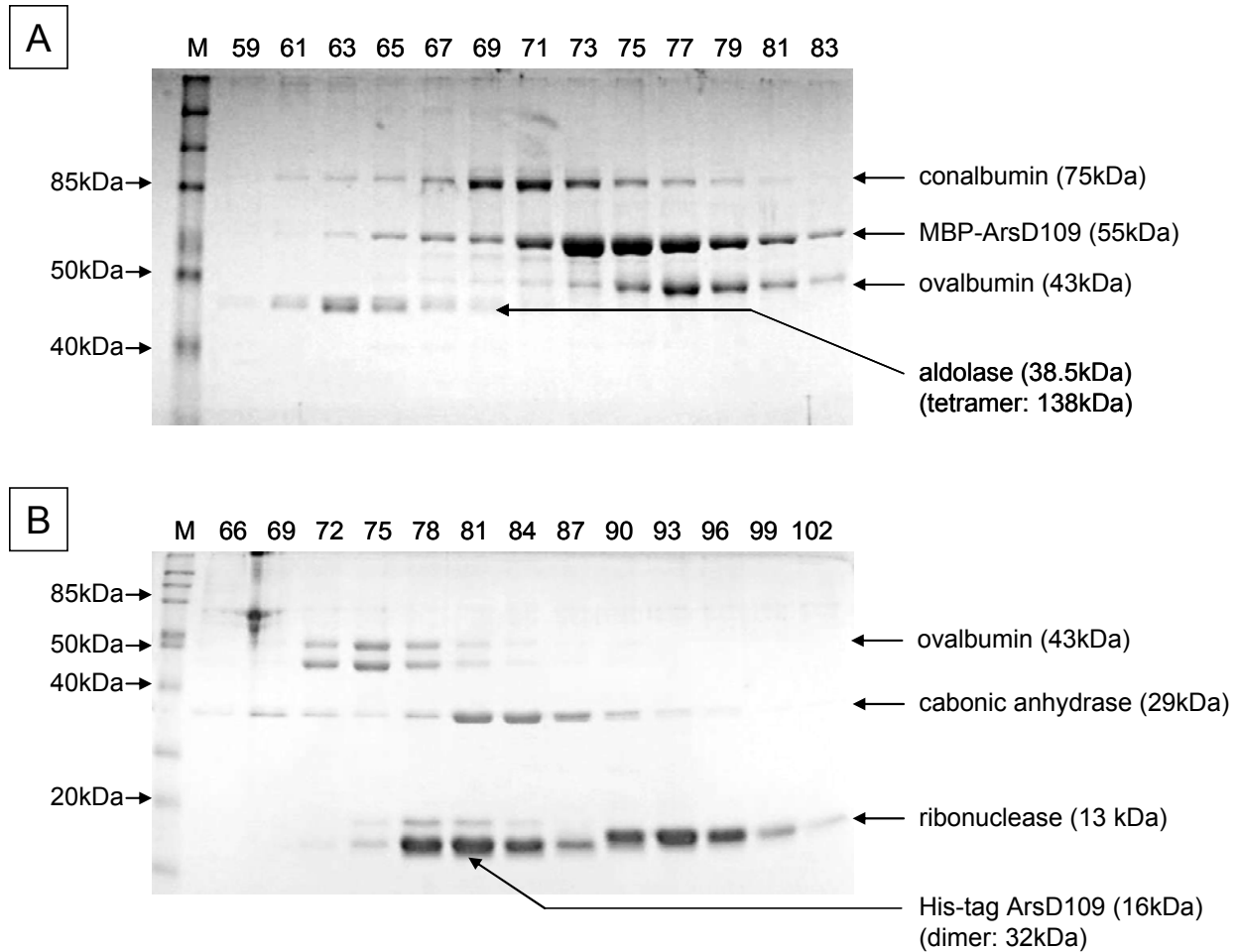


**Figure 3-2. Dimerization equilibrium states of MBP-ArsD109 and His6-ArsD109.**

**(A)** 2.4 mg of MBP-ArsD109 in 1 ml of buffer was loaded to a 1.5 cm diameter column filled with 165 ml Sephacryl-200 gel-filtration column on a Bio-rad Biological LP chromatography system as described under "Materials and Methods". 1.5 mg aldolase, 1.5 mg conalbumin, and 1.5 mg albumine were used as internal standards. The column was washed with 200 ml of column buffer. Elutions were collected as 1.5 ml each fraction. Fractions 59-83 were analyzed by 12 % SDS-PAGE.

**(B)** 2 mg of His6-ArsD109 in 1 ml of buffer was separated by Superdex-75 chromatography as above. 1.5mg ovalbumin, 1.5mg carbonic anhydrase and 1.5mg ribonuclease were used as internal standards. The column was washed with 200ml of column buffer. Elutions were collected as 1.5ml each fraction. Fractions 66-102 were analyzed by 16 % SDS-PAGE.

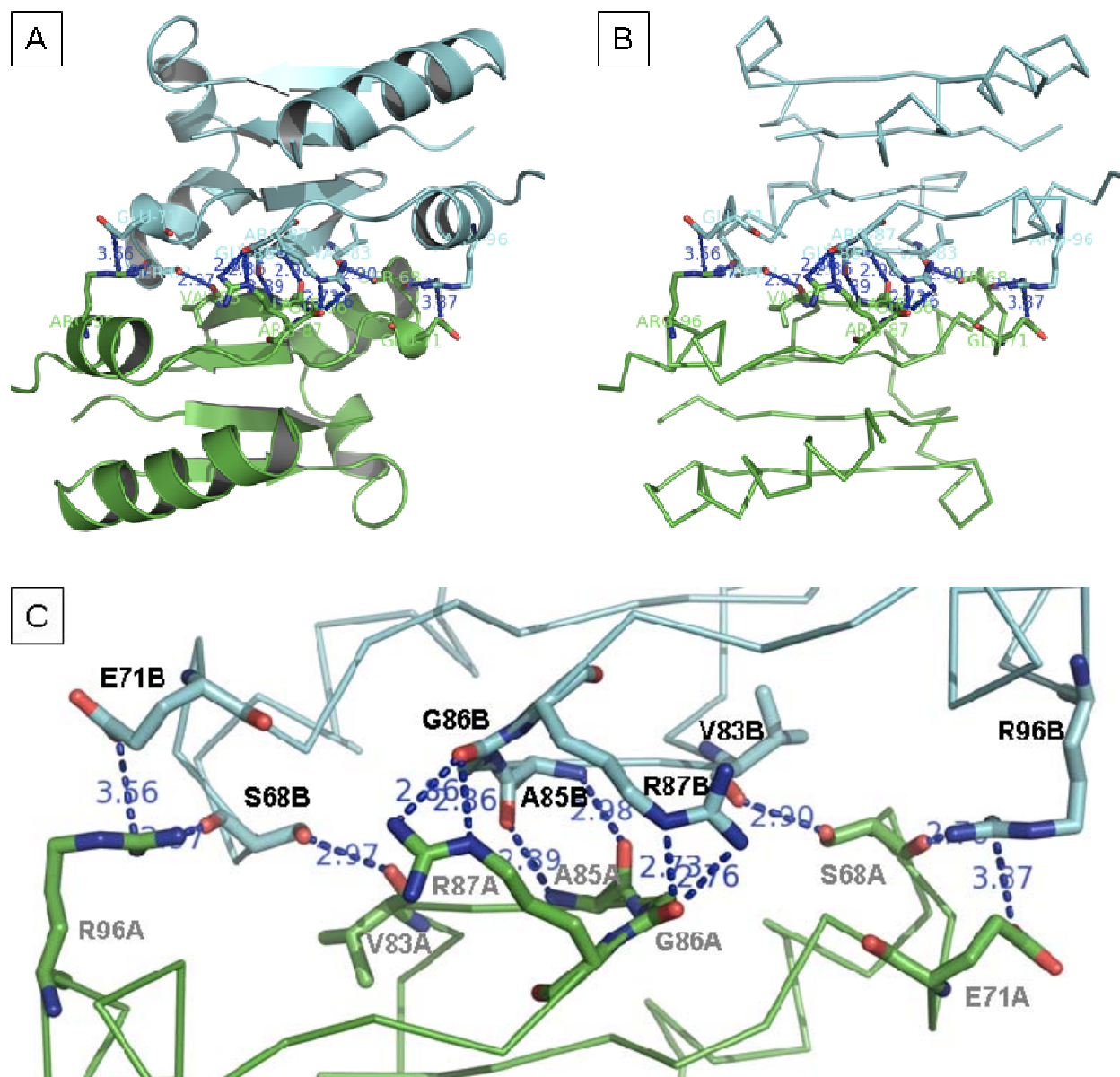


**Figure 3-3. ArsD dimerization interface in crystal structure.**

The ArsD dimerization interface was rendered with Pymol software. Subunit A is colored in green and subunit B is colored in cyan. The residues involved in potential hydrogen and salt bridge were shown in stick form and labeled. The distances of hydrogen bond and the salt bridge was measured, with distances labeled in blue. The unit for distance is Å.

**(A)** Cartoon view.

**(B)** Ribbon view.

**(C)** Ribbon view of magnified dimerization interface.

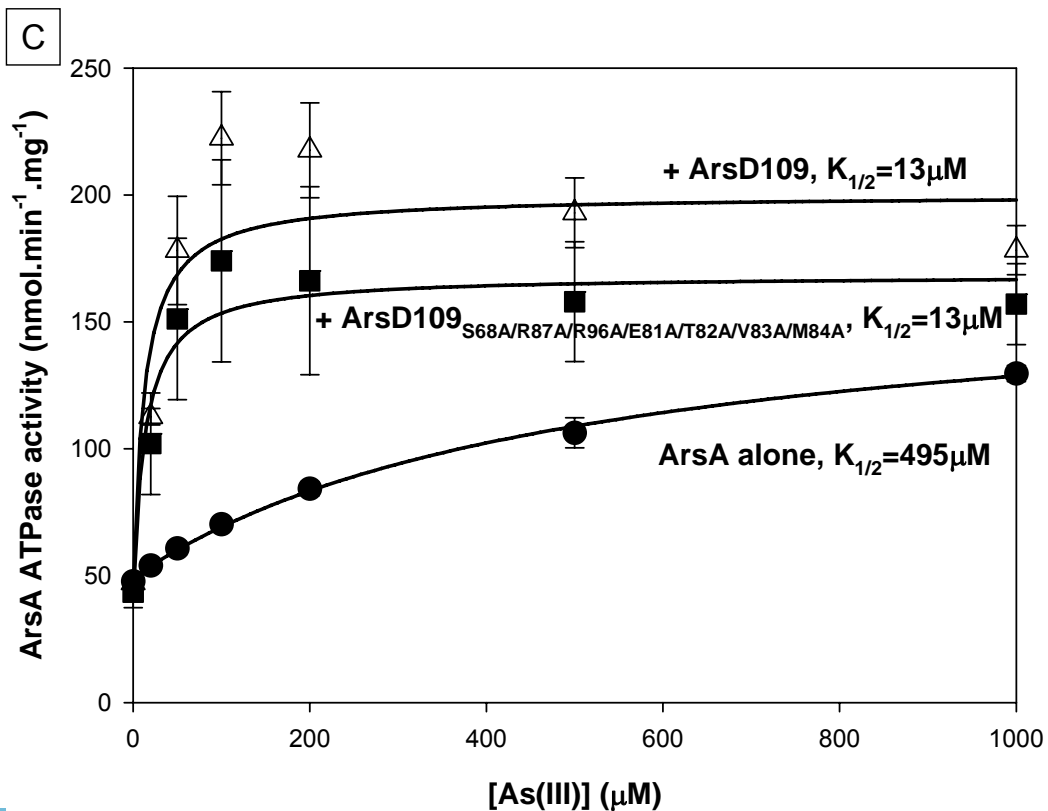
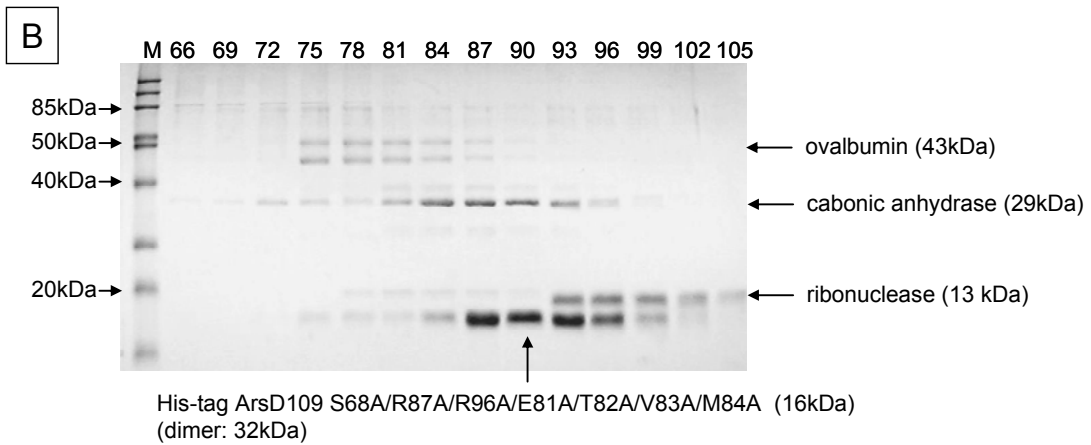
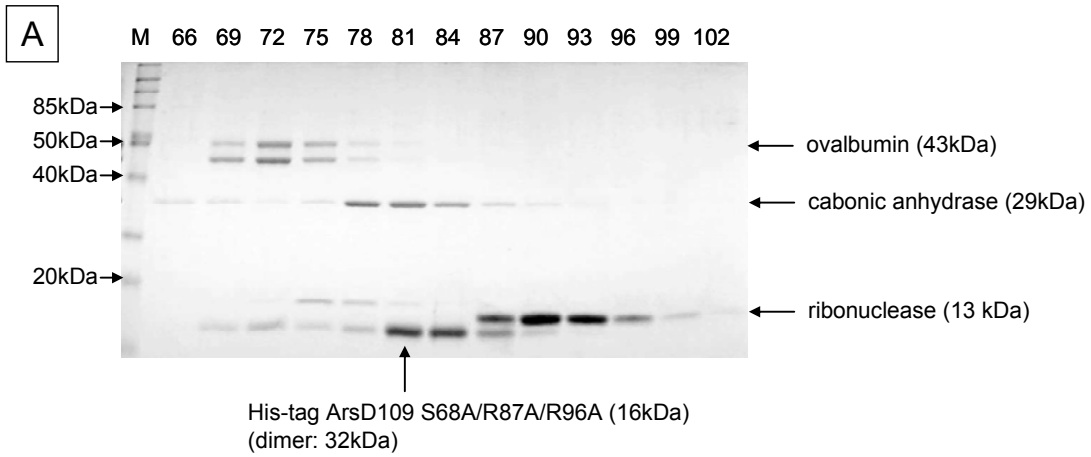


**Figure 3-4. His6-ArsD109<sub>S68A/R87A/R96A</sub> shifts equilibrium to monomer and still activates ArsA ATPase activity.**

**(A)** 2 mg His6-ArsD109<sub>S68A/R87A/R96A</sub> in 1 ml of buffer was separated by Superdex-75 gel chromatography, as described above. Fractions 66-102 were analyzed by 16% SDS-PAGE.

**(B)** 2 mg His6-ArsD109<sub>S68A/R87A/R96A/E81A/T82A/V83A/M84A</sub> in 1 ml of buffer was separated by Superdex-75 gel chromatography, as described above. Fractions 66-105 were analyzed by 16 % SDS-PAGE.

**(C)** ArsA ATPase activity was assayed at the indicated concentrations of sodium arsenite in the presence or absence of ArsD derivatives. ArsA ATPase activity was assayed as described under “Materials and Methods”. (●), no addition; (Δ), His6-ArsD109; (■), His6-ArsD109<sub>S68A/R87A/R96A/E81A/T82A/V83A/M84A</sub>. The curves were fitted using SigmaPlot 9.0, with *error bars* representing standard deviation from three assays.

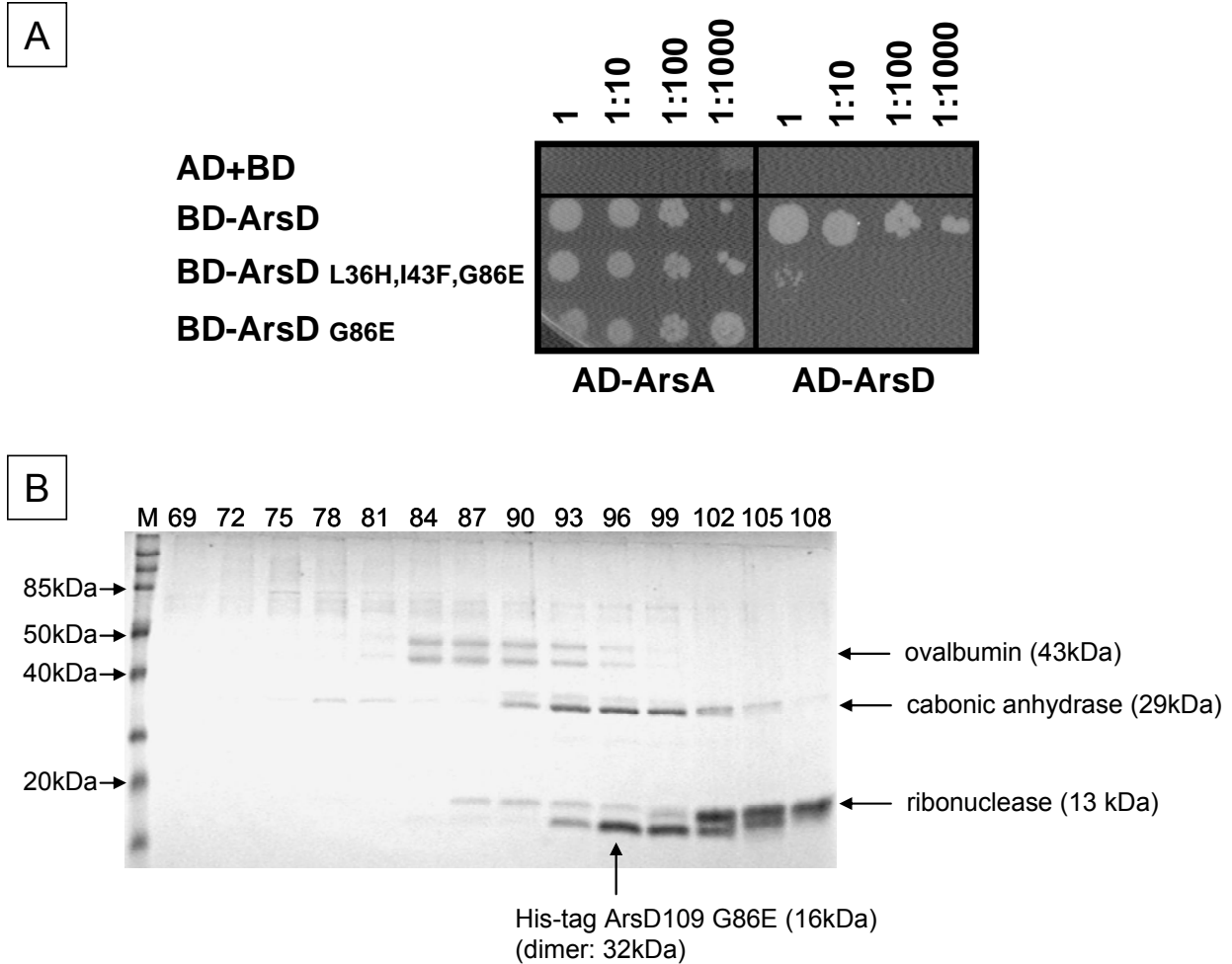


**Figure 3-5. Dimerization equilibrium of His6-ArsD109<sub>G86E</sub> shifts to monomer.**

**(A)** Yeast two-hybrid analysis was performed as described under “Materials and Methods.” *S. cerevisiae* strain AH109 bearing both GAL4 activation domain (AD) and binding domain (BD) fusion plasmids was grown in SD medium overnight and inoculated on agar plates with SD lacking histidine with 10-fold serial dilutions. The first row was cells with the empty vector serving as control. ArsD and ArsD mutants were fused to BD domain, as indicated on the left side. They are tested with ArsA fused to AD (left panel) or ArsD fused to AD (right panel).

**(B)** 2 mg His6-ArsD109<sub>G86E</sub> in 1 ml of buffer was separated by Superdex-75 gel chromatography, as described above.. Fractions 69-108 were analyzed by 16 % SDS-PAGE.

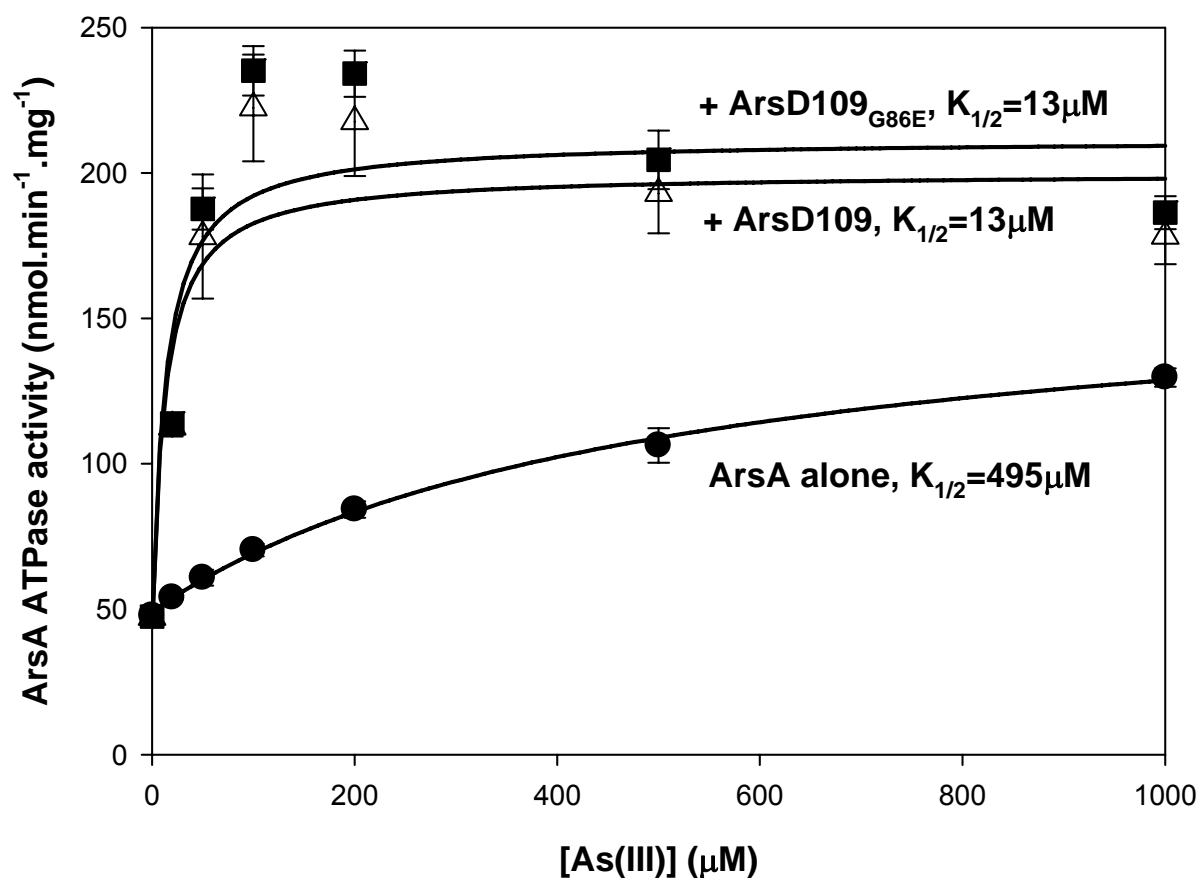


**Figure 3-6. His6-ArsD109<sub>G86E</sub> activates ArsA ATPase.**

ArsA ATPase activity was assayed at the indicated concentrations of sodium arsenite in the presence or absence of ArsD derivatives. ArsA ATPase activity was assayed as described under “Materials and Methods”. (●), no addition; (Δ), His6-ArsD109; (■), His6-ArsD109<sub>G86E</sub>. The curves were fitted using SigmaPlot 9.0, with *error bars* representing standard deviation from three assays.

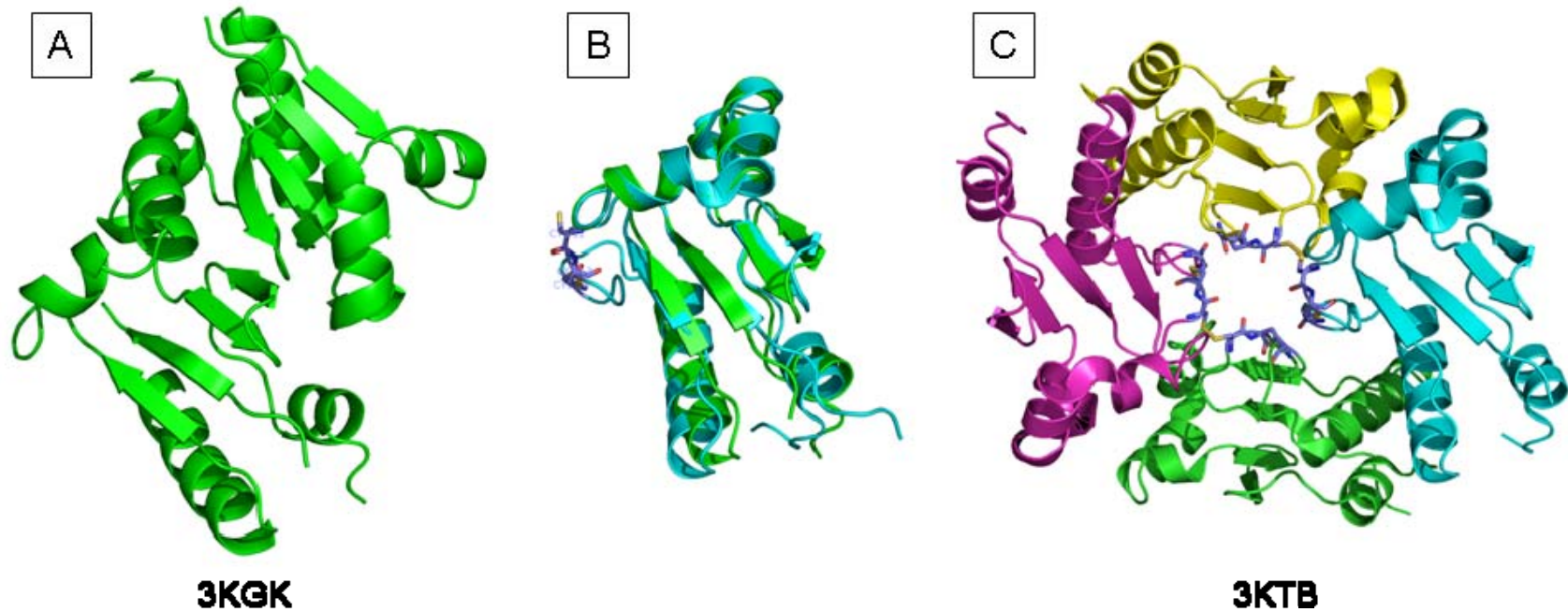


**Figure 3-7. Comparison of R773 ArsD structure and *Bacteroides vulgatus* ATCC 8482 ArsD.**

R773 ArsD structure (pdb: 3KGK) and *Bacteroides vulgatus* ATCC 8482 ArsD structure (pdb: 3KTB) were compared and presented in cartoon view with Pymol software.

**(A)** R773 ArsD structure (pdb: 3KGK) in cartoon view.

**(B)** Alignment of chain A of R773 ArsD (3KGK) with chain A of *Bacteroides vulgatus* ATCC 8482 ArsD (3KTB) with cysteine residues shown in stick.

**(C)** *Bacteroides vulgatus* ATCC 8482 ArsD structure (pdb: 3KTB) in cartoon view with cysteine residues shown in stick.



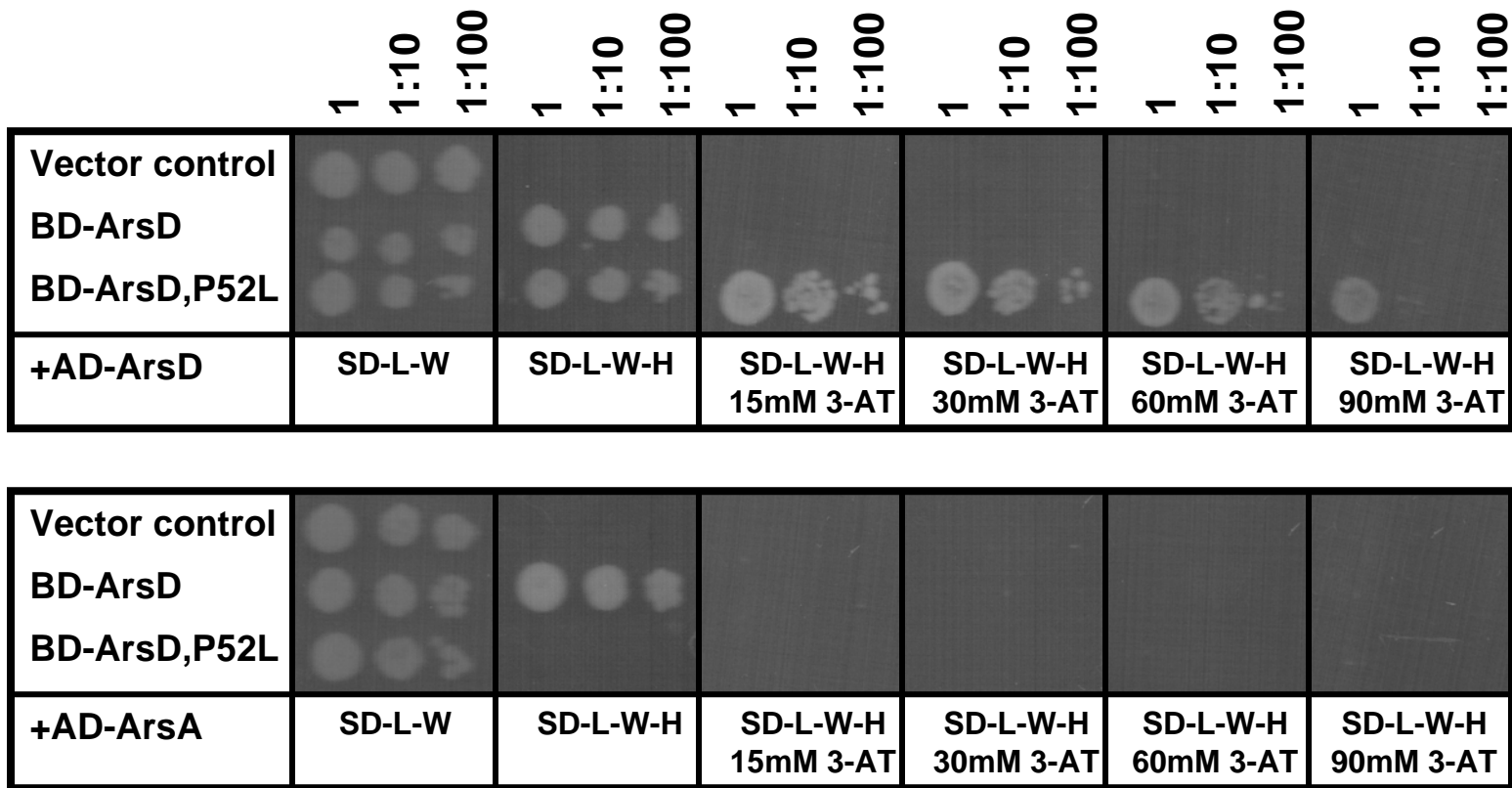


**Figure 3-8.  $ArsD_{P52L}$  dimerize more strongly with wild type  $ArsD$  in yeast two-hybrid.**

*S. cerevisiae* strain AH109 bearing both GAL4 activation domain (AD) and binding domain (BD) fusion plasmids was grown in SD medium overnight and inoculated with 10-fold serial dilutions on SD agar plates, lacking histidine and supplemented with different concentrations of 3-AT. Top panel shows wild-type  $ArsD$  and  $ArsD$  P52L fused to BD co-transformed with wild-type  $ArsD$  fused to AD. Bottom panel shows wild-type  $ArsD$  and  $ArsD$  P52L fused with BD co-transformed with wild-type  $ArsA$  fused to AD.

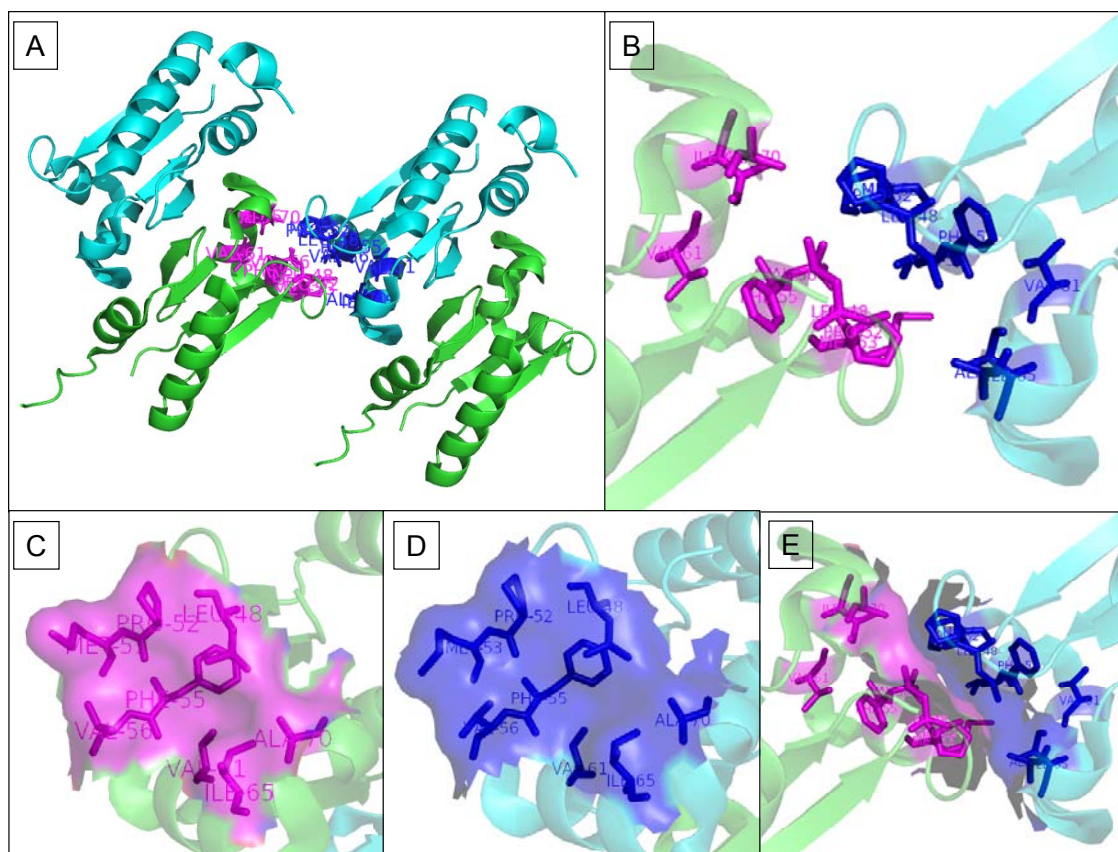


**Figure 3-9. A hypothetical dimerization interface.**

R773 ArsD structure (pdb: 3K GK) was rendered by Pymol, with backbone shown as cartoon. A patch of residues including Leu48, Phe52, Met53, Phe55, Val56, Val61, Ile66 and Ala70 was shown with stick and labeled. These residues are colored in magenta in one subunit and blue in another subunit.

**(A)** Full view of a second dimerization interface between subunits from different asymmetric units.

**(B)** Magnified view of the interface.

**(C)** and **(D)** view of the hydrophobic patch from the top.

**(E)** Interface shown with the surface of the hydrophobic patch.

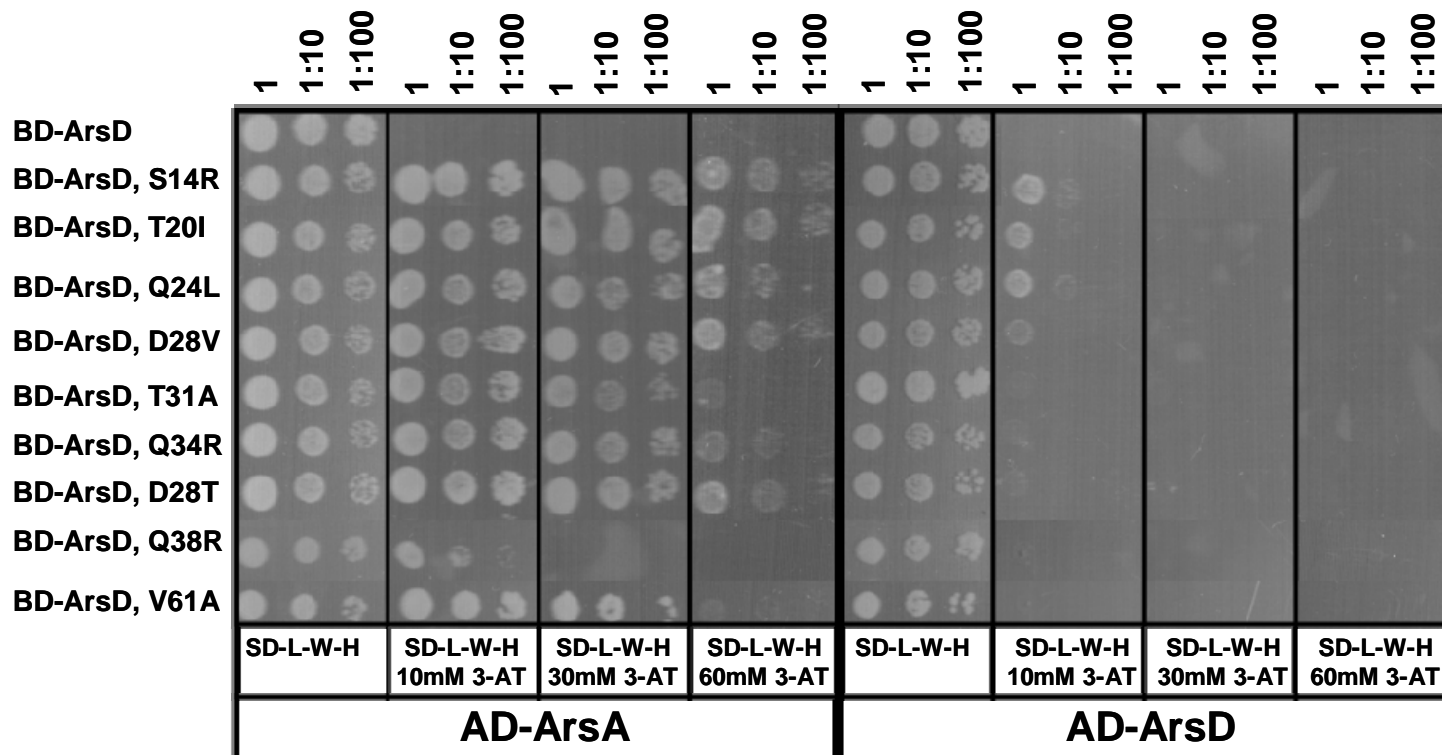
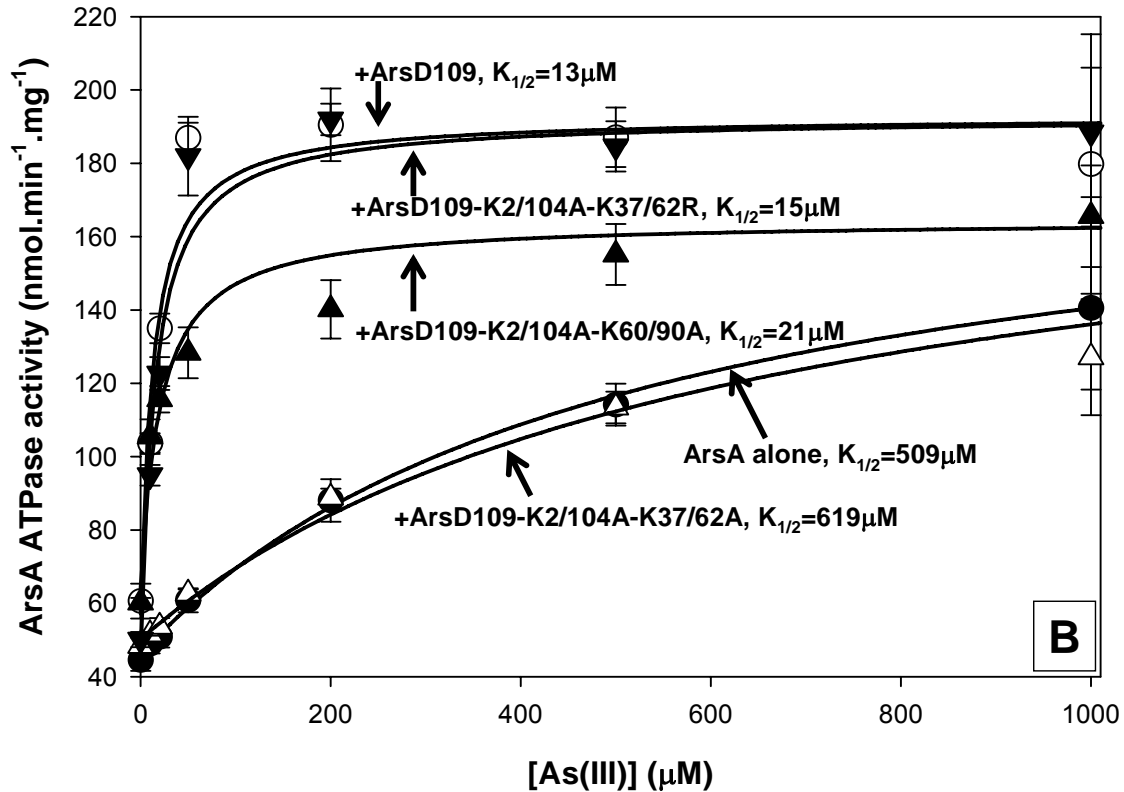
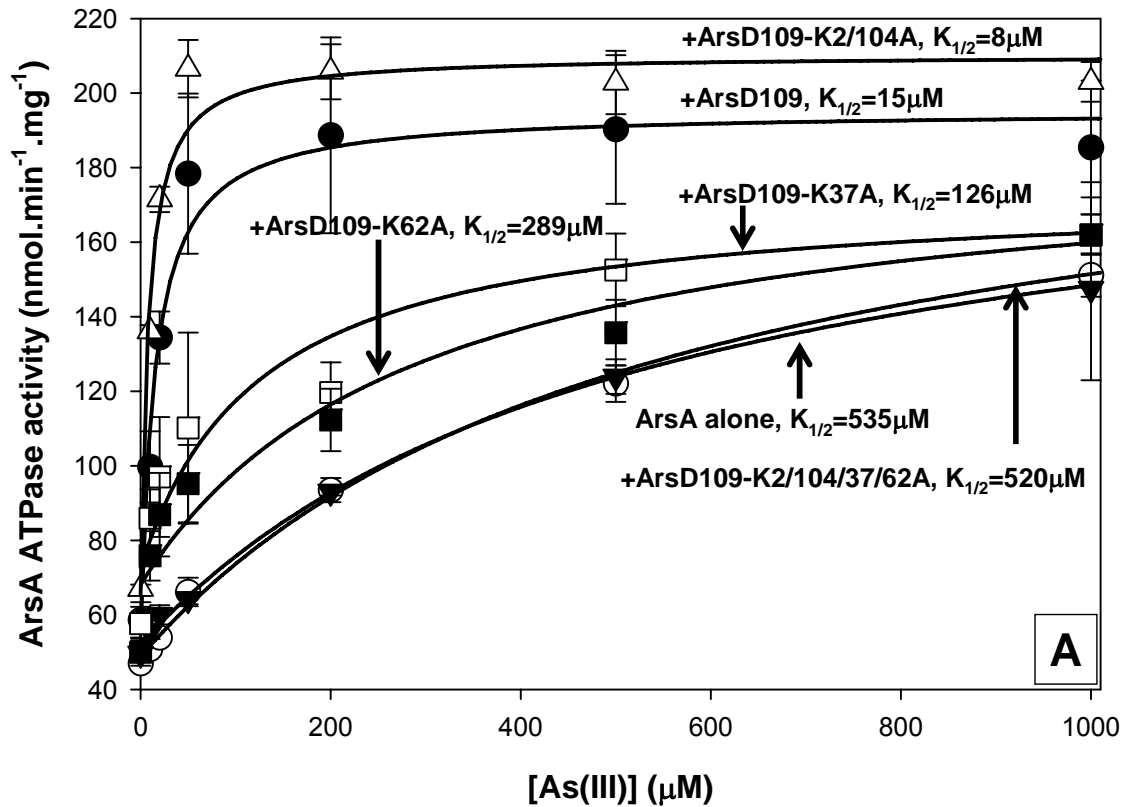


Figure 4-1. ArsD mutants showing stronger interaction with ArsA.

*S. cerevisiae* strain AH109 bearing both GAL4 activation domain (AD) and binding domain (BD) fusion plasmids was grown in SD medium overnight and inoculated with 10-fold serial dilutions on SD agar plates, lacking histidine and supplemented with different concentrations of 3-AT. Left 4 strips show wild-type ArsD or ArsD mutants fused to BD co-transformed with wild-type ArsA fused to AD. Right 4 strips show wild-type or ArsD mutants fused with BD co-transformed with wild-type ArsD fused to AD. The ArsD mutants were indicated on the left.



**Figure 4-2. Mutating Lys37 and Lys62 to alanine abolishes ArsD function as an arsenic chaperone.**

ArsA ATPase activity was assayed at the indicated concentrations of sodium arsenite in the presence or absence of ArsD derivatives. ArsA ATPase activity was assayed as described under "Materials and Methods". The curves were fitted using SigmaPlot 9.0, with *error bars* represent standard deviation.

**(A)** (○), no addition; (●), ArsD109; (▼), ArsD109<sub>K2/104A-K37/62A</sub>; (Δ), ArsD109<sub>K2/104A</sub>; (□), ArsD109<sub>K37A</sub>; (■), ArsD109<sub>K62A</sub>.

**(B)** (●), no addition; (○), ArsD109; (▲), ArsD109<sub>K2/104A-K60/90A</sub>; (Δ), ArsD109<sub>K2/104A-K37/62A</sub>; (▼), ArsD109<sub>K2/104A-K37/62R</sub>.

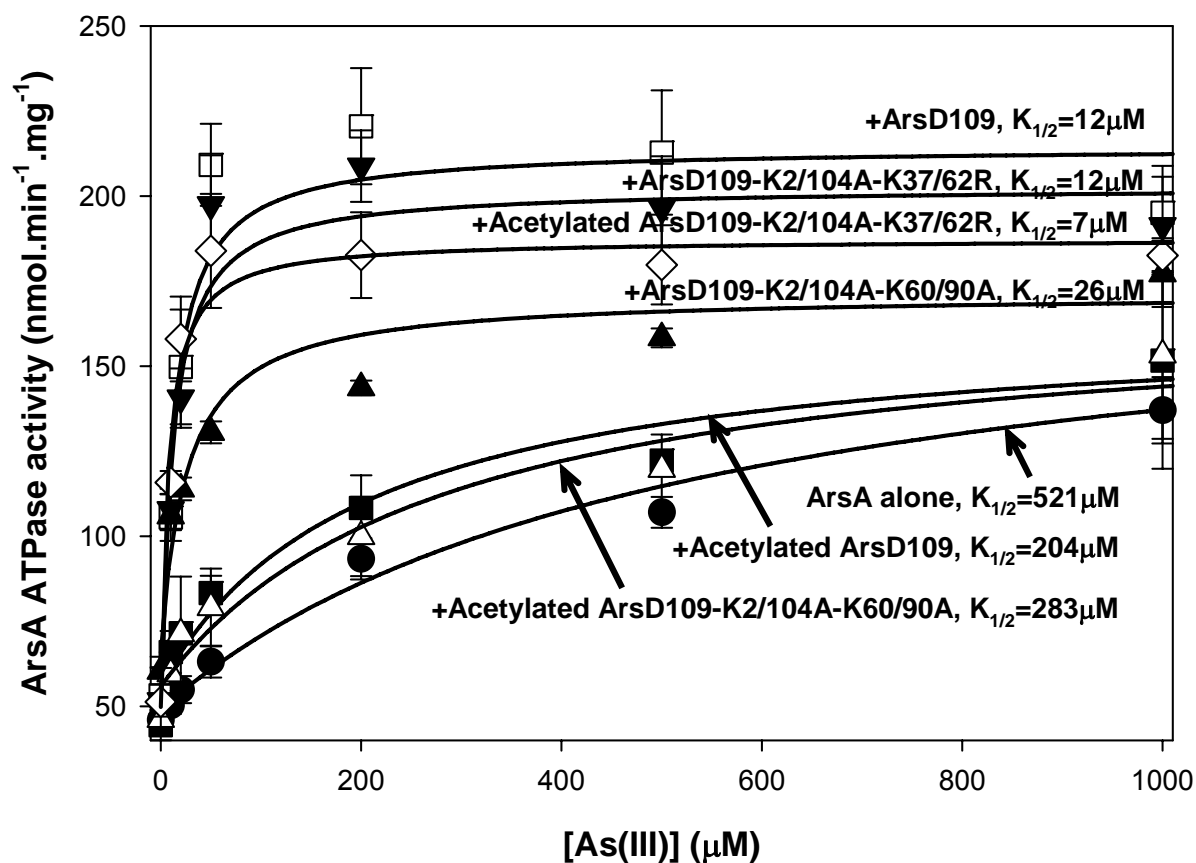


**Figure 4-3. Acetylation of Lys37 and Lys62 sabotages ArsD metallochaperone function.**

ArsA ATPase activity was assayed at the indicated concentrations of sodium arsenite in the presence or absence of ArsD derivatives. ArsA ATPase activity was assayed as described under "Materials and Methods". (●), no addition; (□), ArsD109; (■), acetylated ArsD109; (▲), ArsD109<sub>K2/104A-K60/90A</sub>; (Δ), acetylated ArsD109<sub>K2/104A-K60/90A</sub>; (▼), ArsD109<sub>K2/104A-K37/62R</sub>; (▽), acetylated ArsD109<sub>K2/104A-K37/62R</sub>. The curves were fitted using SigmaPlot 9.0, with *error bars* represent standard deviation.

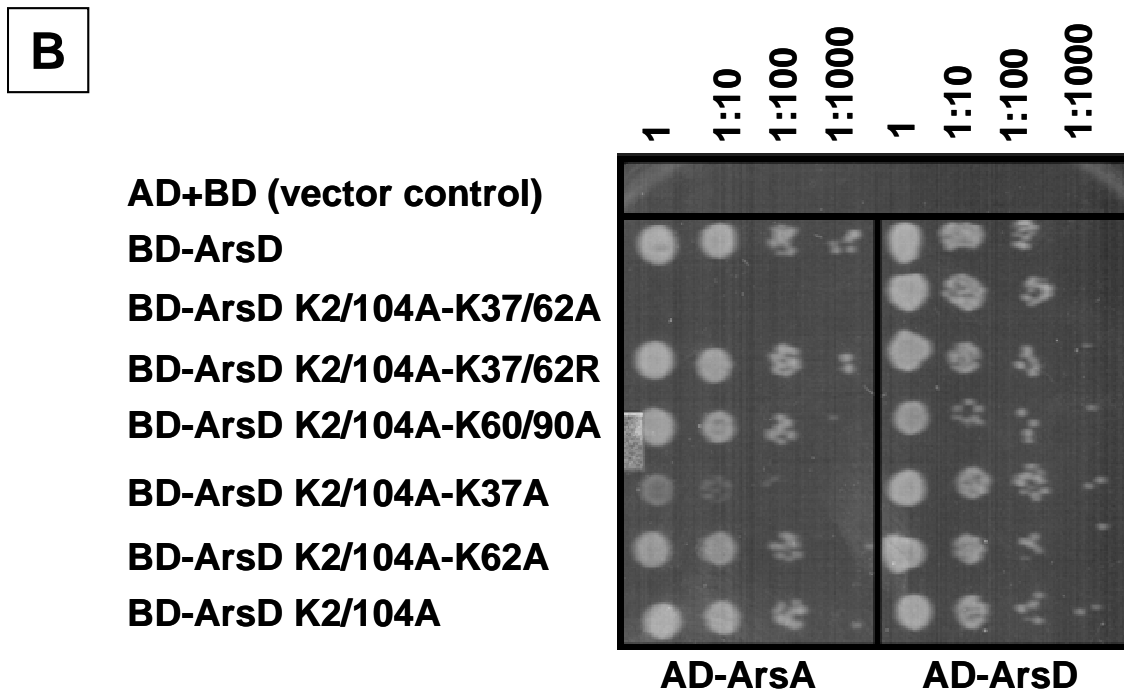
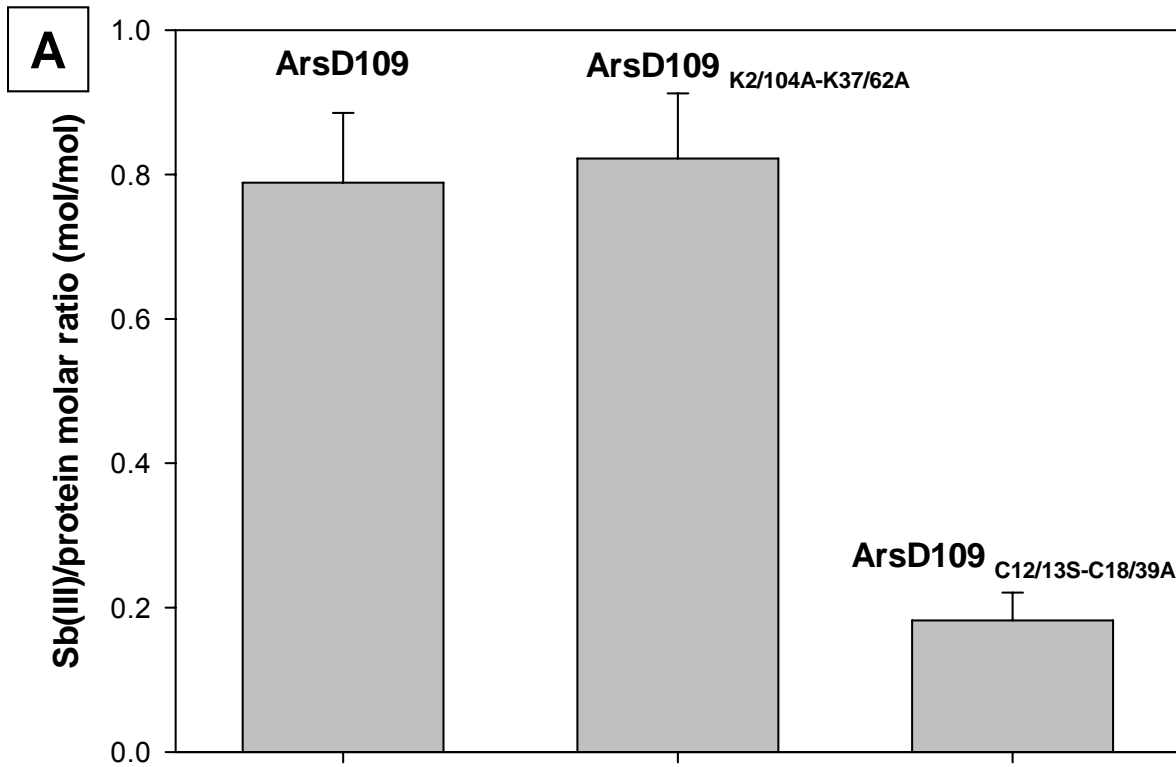


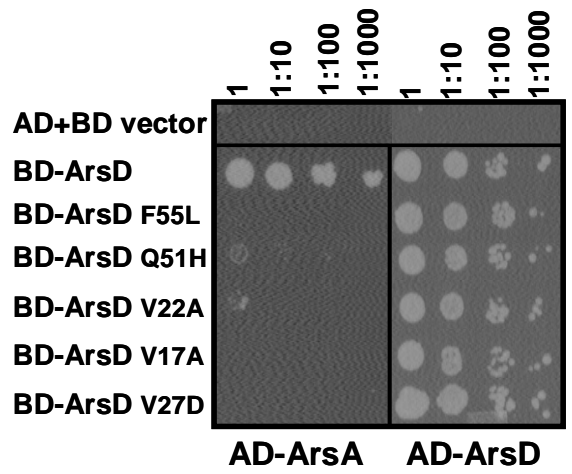
**Figure 4-4. ArsD<sub>K2/104A-K37/62A</sub> still binds As(III) but does not interact with ArsA.**

**(A)** The antimony binding ability of ArsD and ArsD mutants was measured by mixing 100  $\mu$ M of ArsD and 300  $\mu$ M of potassium antimonyl tartrate. After incubation, the mixture was passed through gel-filtration column to remove free antimony. Then protein concentration and antimony concentration was determined to get the antimony binding molar ratio. Details were described under “Materials and Methods”, and *error bars* represent standard deviation.

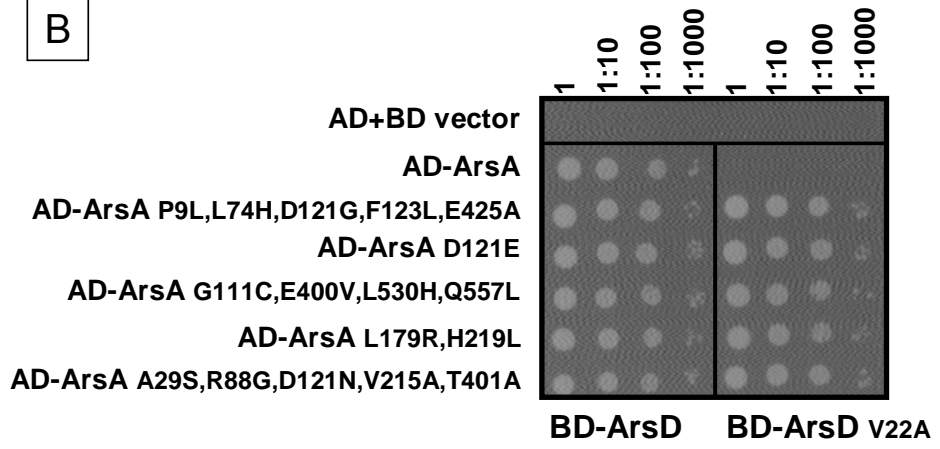
**(B)** Yeast two-hybrid analysis was performed as described under “Materials and Methods.” *S. cerevisiae* strain AH109 bearing both GAL4 activation domain (AD) and binding domain (BD) fusion plasmids was grown in SD medium overnight and inoculated on agar plates with SD lacking histidine with 10-fold serial dilutions. The first row was cells with the vector serving as control. ArsD and ArsD mutants were fused to BD domain, as indicated on the left side. They are tested with ArsA fused to AD (left panel) or ArsD fused to AD (right panel).



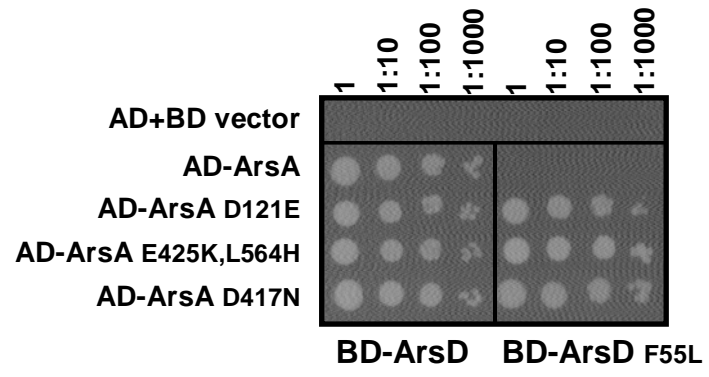
A



B



C



D

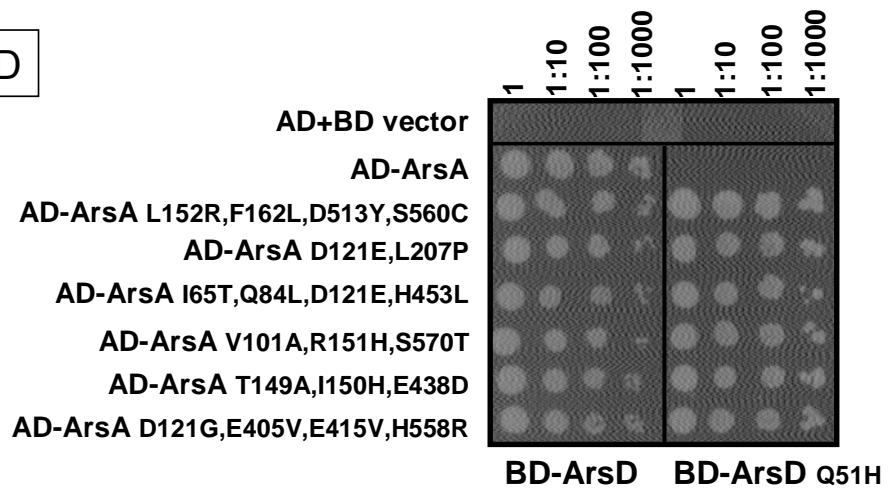
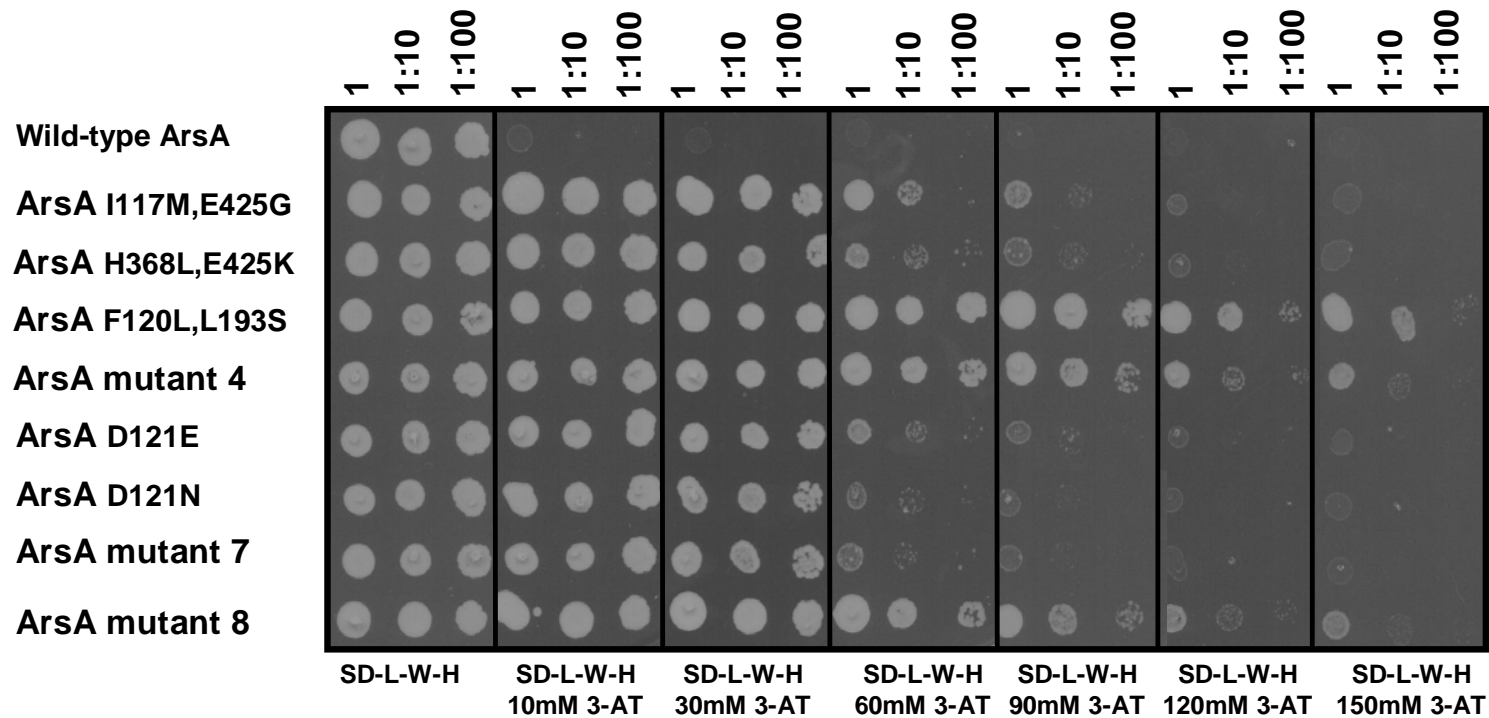


**Figure 4-5. ArsD mutants showing weaker interaction with ArsA and the corresponding complementary ArsA mutants.**

Yeast two-hybrid analysis was performed as described under “Materials and Methods.” *S. cerevisiae* strain AH109 bearing both GAL4 activation domain (AD) and binding domain (BD) fusion plasmids was grown in SD medium overnight and inoculated on agar plates with SD lacking histidine with 10-fold serial dilutions.

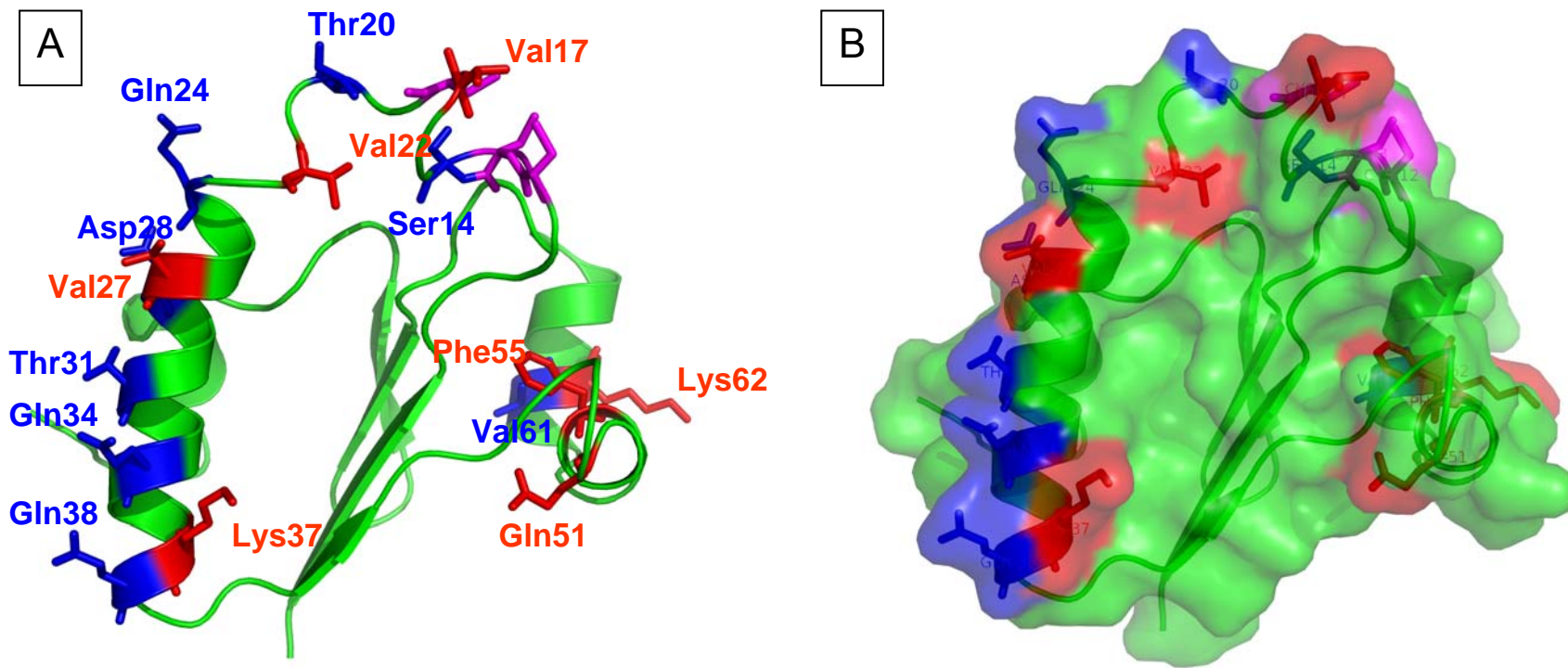
- (A)** wild-type ArsD or ArsD mutants fused with BD domain were co-transformed with AD-ArsA (ArsA fused with AD) or AD-ArsD (ArsD fused with AD). As a negative control, AD vector (pACT2) and BD vector (pGBT9) were co-transformed.
- (B)** ArsA complementary mutants restore interaction with ArsD<sub>V22A</sub>. Wild-type ArsA or ArsA mutants fused with AD domain were co-transformed with BD-ArsD (ArsD fused with BD) or BD-ArsD<sub>V22A</sub> (ArsD<sub>V22A</sub> fused with BD).
- (C)** ArsA complementary mutants restore interaction with ArsD<sub>F55L</sub>. Wild-type ArsA or ArsA mutants fused with AD domain were co-transformed with BD-ArsD (ArsD fused with BD) or BD-ArsD<sub>F55L</sub> (ArsD<sub>F55L</sub> fused with BD).
- (D)** ArsA complementary mutants restore interaction with ArsD<sub>Q51H</sub>. Wild-type ArsA or ArsA mutants fused with AD domain were co-transformed with BD-ArsD (ArsD fused with BD) or BD-ArsD<sub>Q51H</sub> (ArsD<sub>Q51H</sub> fused with BD).



- **ArsA mutant 4:** F54L, F120L, H219R, E254V, F443L, K475R, A533T
- **ArsA mutant 7:** D121G,E405V,E415V,H558R
- **ArsA mutant 8:** P9L, L74H, D121G, F123L, E425A

**Figure 4-6. ArsA mutants showing stronger interaction with ArsD.**

*S. cerevisiae* strain AH109 bearing both GAL4 activation domain (AD) and binding domain (BD) fusion plasmids was grown in SD medium overnight and inoculated with 10-fold serial dilutions on SD agar plates, lacking histidine and supplemented with different concentrations of 3-AT. Wild-type ArsA and ArsA mutants fused with AD domain were co-transformed with BD-ArsD (ArsD fused with BD domain).

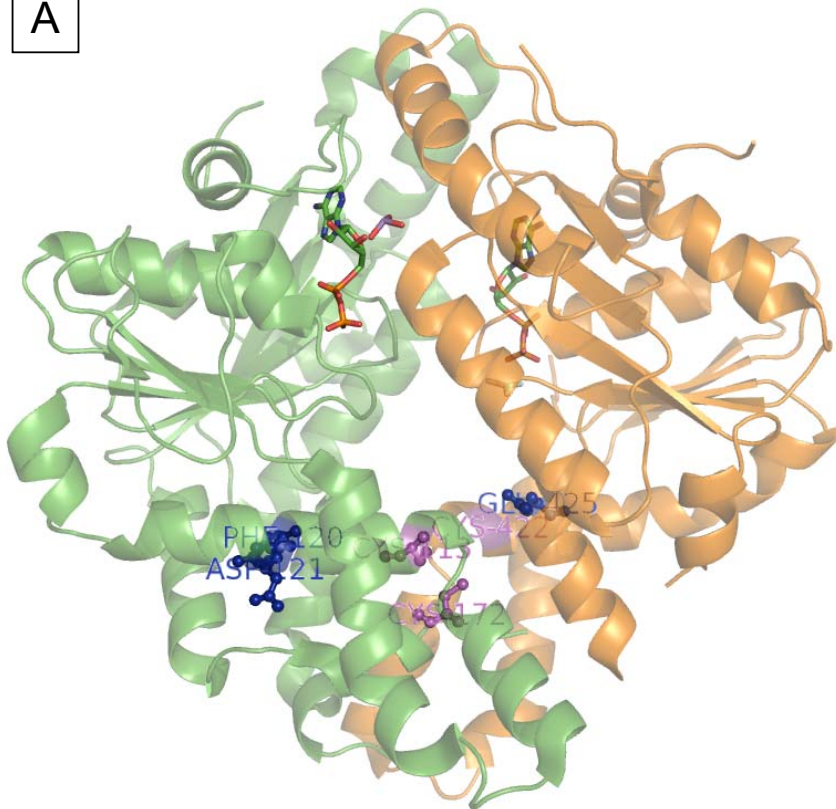
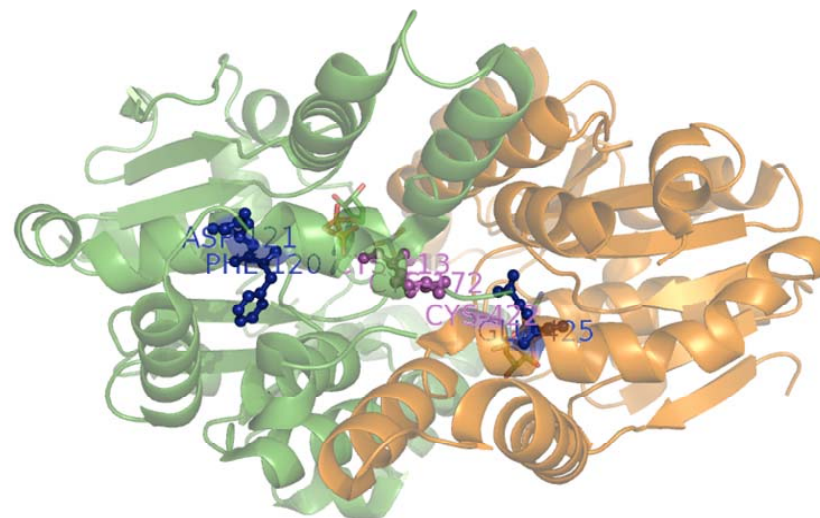


**Figure 4-7. Mapping mutations on ArsD structure.**

An ArsD structure model based on R773 ArsD structure (pdb: 3KGK) was used to show all mutations with effect on ArsA-ArsD interaction (Ye et al., 2010). The figures are generated with Pymol software. Three cysteine residues Cys12, Cys13 and Cys18 are colored in magenta. Residues Val17, Val22, Val27, Lys37, Gln51, Phe55 and Lys62, lowering down the interaction strength, are colored in red. Residues Ser14, Thr20, Gln24, Asp28, Thr31, Gln34, Gln38 and Val61, increasing interaction strength, are colored in blue. All these residues are shown with stick.

**(A)** in cartoon view.

**(B)** in cartoon view with surface.

**A****B**

**Figure 4-8. Mapping mutations on ArsA structure.**

ArsA structure (pdb: 1F48) was used to show all mutations with effect on ArsA-ArsD interaction. The figures are generated with Pymol software. ArsA-A1 part (residues 1-297) is shown in green. ArsA-A2 part (residues 308-586) is shown in orange. Three cysteine residues Cys113, Cys172 and Cys422 are colored in magenta. Residues Phe120, Asp121 and Glu425, increasing interaction strength, are colored in blue. All these residues are shown with stick.

**(A)** front view.

**(B)** bottom view.

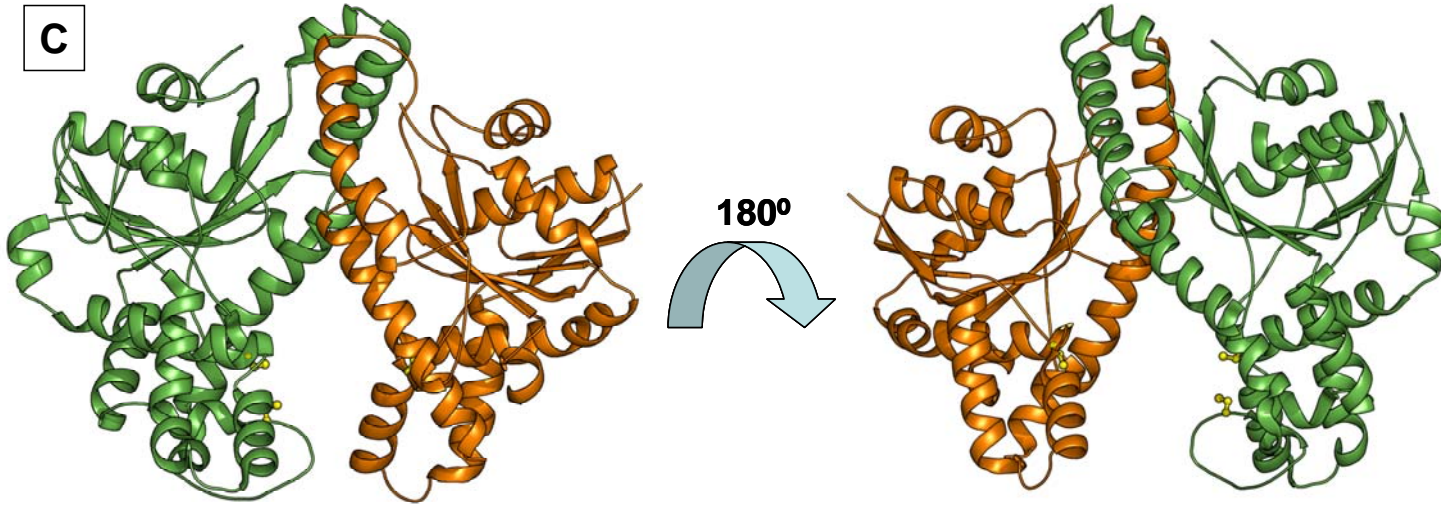
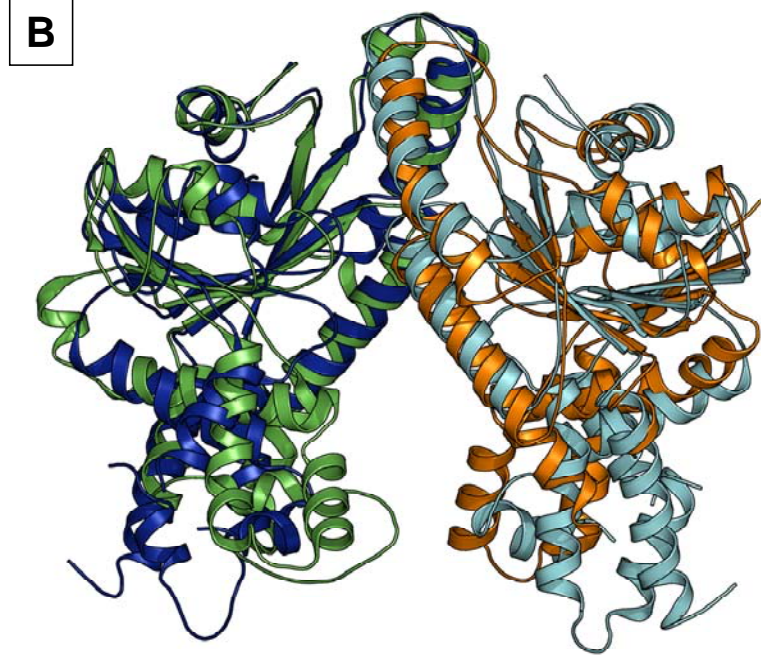
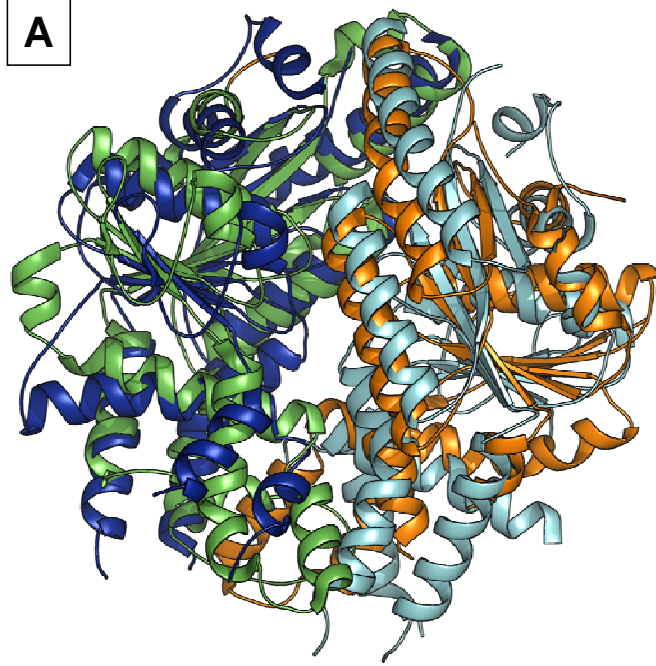


**Figure 4-9. Comparison of ArsA and Get3 structure (Ye et al., 2010).**

ArsA was superimposed with closed and open Get3.

**(A)** Superimposition of ArsA (PDB ID: 1IHU) with Get3 closed structure (PDB ID: 2WOJ). ArsA-A1 (green), ArsA-A2 (orange), Get3 monomer-1 (Blue) and Get3 monomer-2 (light-blue) are shown as cartoon.

**(B)** Superimposition of ArsA-A1 (residues 1-297) and ArsA-A2 (residues 298-583) with Get3 open structure (2WOO). ArsA-A1 (green), ArsA-A2 (orange), Get3 monomer-1 (Blue) and Get3 monomer-2 (gray) are shown as cartoon.

**(C)** ArsA open structure was modeled based on the Get3 open structure. ArsA-A1 (green) and ArsA-A2 (orange) are shown as a cartoon representation. Cysteine residues are shown in ball and stick with yellow color.

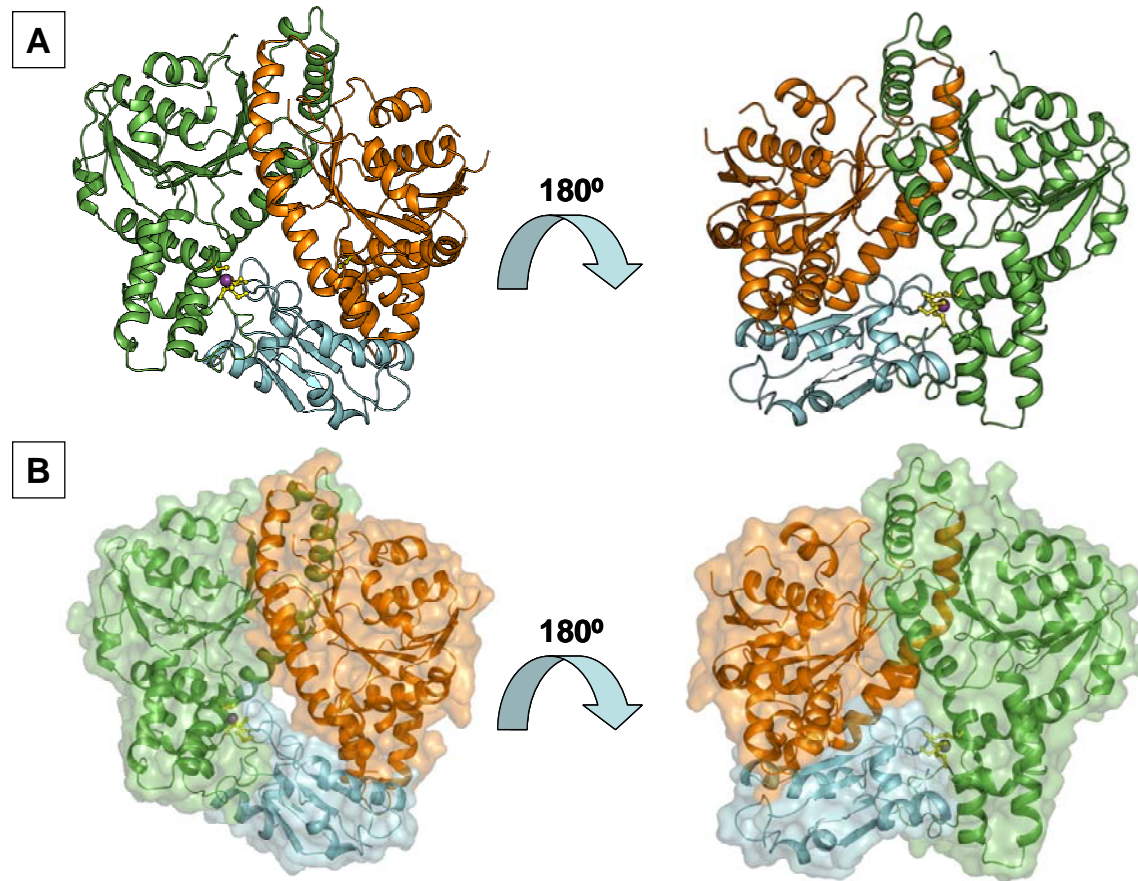


**Figure 4-10. Structure model of ArsA-ArsD complex (Ye et al., 2010).**

ArsA-ArsD model was calculated with Cluspro docking server. One of the best models is shown here. ArsA is rendered as cartoon with green and orange color. ArsD model is shown in cyan. As(III)/Sb(III) atom is shown as solid sphere in magenta color and cysteines (yellow) are shown as ball and stick.

**(A)** In cartoon view.

**(B)** Figure 8A is shown in surface representation with 40% transparency.



## REFERENCES

- Achila, D., Banci, L., Bertini, I., Bunce, J., Ciofi-Baffoni, S., and Huffman, D.L. (2006). Structure of human Wilson protein domains 5 and 6 and their interplay with domain 4 and the copper chaperone HAH1 in copper uptake. *Proceedings of the National Academy of Sciences of the United States of America* *103*, 5729-5734.
- Adams, A., Gottschling, D.E., Kaiser, C., and Stearns, T. (1998). *Methods in Yeast Genetics: A Cold Spring Harbor laboratory course manual*, (New York, Cold Spring Harbor Laboratory).
- Akter, K.F., Owens, G., Davey, D.E., and Naidu, R. (2005). Arsenic speciation and toxicity in biological systems. *Rev Environ Contam Toxicol* *184*, 97-149.
- Anderson, K.S. (1999). Fundamental mechanisms of substrate channeling. *Methods Enzymol* *308*, 111-145.
- Ankudinov, A.L., and Rehr, J.J. (1997). *Phys Rev B Condens Matter* *56*, R1712–R1715.
- Apontowiel, P., and Berends, W. (1975). Glutathione biosynthesis in *Escherichia coli* K 12. Properties of the enzymes and regulation. *Biochim Biophys Acta* *399*, 1-9.
- Arnesano, F., Banci, L., Bertini, I., and Bonvin, A.M. (2004). A docking approach to the study of copper trafficking proteins; interaction between metallochaperones and soluble domains of copper ATPases. *Structure* *12*, 669-676.
- Arnesano, F., Banci, L., Bertini, I., Cantini, F., Ciofi-Baffoni, S., Huffman, D.L., and O'Halloran, T.V. (2001). Characterization of the binding interface between the copper chaperone Atx1 and the first cytosolic domain of Ccc2 ATPase. *The Journal of biological chemistry* *276*, 41365-41376.

- Auld, K.L., Hitchcock, A.L., Doherty, H.K., Fietze, S., Huang, L.S., and Silver, P.A. (2006). The conserved ATPase Get3/Arr4 modulates the activity of membrane-associated proteins in *Saccharomyces cerevisiae*. *Genetics* 174, 215-227.
- Banci, L., Bertini, I., Cantini, F., Felli, I.C., Gonnelli, L., Hadjiliadis, N., Pierattelli, R., Rosato, A., and Voulgaris, P. (2006). The Atx1-Ccc2 complex is a metal-mediated protein-protein interaction. *Nature chemical biology* 2, 367-368.
- Banci, L., Bertini, I., Ciofi-Baffoni, S., Chasapis, C.T., Hadjiliadis, N., and Rosato, A. (2005). An NMR study of the interaction between the human copper(I) chaperone and the second and fifth metal-binding domains of the Menkes protein. *The FEBS journal* 272, 865-871.
- Bencze, K.Z., Yoon, T., Millan-Pacheco, C., Bradley, P.B., Pastor, N., Cowan, J.A., and Stemmler, T.L. (2007). Human frataxin: iron and ferroxidase binding surface. *Chemical communications (Cambridge, England)*, 1798-1800.
- Benitez, J.J., Keller, A.M., Ochieng, P., Yatsunyk, L.A., Huffman, D.L., Rosenzweig, A.C., and Chen, P. (2008). Probing transient copper chaperone-Wilson disease protein interactions at the single-molecule level with nanovesicle trapping. *Journal of the American Chemical Society* 130, 2446-2447.
- Bentley, R., and Chasteen, T.G. (2002). Microbial methylation of metalloids: arsenic, antimony, and bismuth. *Microbiol Mol Biol Rev* 66, 250-271.
- Bhattacharjee, H., Li, J., Ksenzenko, M.Y., and Rosen, B.P. (1995). Role of cysteinyl residues in metalloactivation of the oxyanion-translocating ArsA ATPase. *J Biol Chem* 270, 11245-11250.

- Bienert, G.P., Thorsen, M., Schussler, M.D., Nilsson, H.R., Wagner, A., Tamas, M.J., and Jahn, T.P. (2008). A subgroup of plant aquaporins facilitate the bi-directional diffusion of As(OH)(3) and Sb(OH)(3) across membranes. *Bmc Biol* 6, -.
- Boal, A.K., and Rosenzweig, A.C. (2009). Structural biology of copper trafficking. *Chem Rev* 109, 4760-4779.
- Bozkurt, G., Stjepanovic, G., Vilardi, F., Amlacher, S., Wild, K., Bange, G., Favaloro, V., Rippe, K., Hurt, E., Dobberstein, B., *et al.* (2009). Structural insights into tail-anchored protein binding and membrane insertion by Get3. *Proceedings of the National Academy of Sciences of the United States of America* 106, 21131-21136.
- Bradford, M.M. (1976). A rapid and sensitive method for the quantitation of microgram quantities of protein utilizing the principle of protein-dye binding. *Analytical biochemistry* 72, 248-254.
- Bruckner, A., Polge, C., Lentze, N., Auerbach, D., and Schlattner, U. (2009). Yeast two-hybrid, a powerful tool for systems biology. *Int J Mol Sci* 10, 2763-2788.
- Bulteau, A.L., O'Neill, H.A., Kennedy, M.C., Ikeda-Saito, M., Isaya, G., and Szweda, L.I. (2004). Frataxin acts as an iron chaperone protein to modulate mitochondrial aconitase activity. *Science (New York, NY)* 305, 242-245.
- Bun-Ya, M., Harashima, S., and Oshima, Y. (1992). Putative GTP-binding protein, Gtr1, associated with the function of the Pho84 inorganic phosphate transporter in *Saccharomyces cerevisiae*. *Mol Cell Biol* 12, 2958-2966.
- Bun-ya, M., Shikata, K., Nakade, S., Yompakdee, C., Harashima, S., and Oshima, Y. (1996). Two new genes, PHO86 and PHO87, involved in inorganic phosphate uptake in *Saccharomyces cerevisiae*. *Current genetics* 29, 344-351.

- Cadwell, R.C., and Joyce, G.F. (1992). Randomization of genes by PCR mutagenesis. *PCR methods and applications* 2, 28-33.
- Cassiday, L.A., and Maher, L.J., 3rd (2003). Yeast genetic selections to optimize RNA decoys for transcription factor NF-kappa B. *Proceedings of the National Academy of Sciences of the United States of America* 100, 3930-3935.
- Cebrian, M.E., Albores, A., Aguilar, M., and Blakely, E. (1983). Chronic arsenic poisoning in the north of Mexico. *Hum Toxicol* 2, 121-133.
- Challenger, F. (1945). Biological methylation. *Chem Rev* 36, 315-361.
- Chappell, W.R., Beck, B.D., Brown, K.G., Chaney, R., Cothorn, R., Cothorn, C.R., Irgolic, K.J., North, D.W., Thornton, I., and Tsongas, T.A. (1997). Inorganic arsenic: a need and an opportunity to improve risk assessment. *Environmental health perspectives* 105, 1060-1067.
- Chen, C.J., Chuang, Y.C., Lin, T.M., and Wu, H.Y. (1985). Malignant neoplasms among residents of a blackfoot disease-endemic area in Taiwan: high-arsenic artesian well water and cancers. *Cancer research* 45, 5895-5899.
- Chen, C.J., Chuang, Y.C., You, S.L., Lin, T.M., and Wu, H.Y. (1986). A retrospective study on malignant neoplasms of bladder, lung and liver in blackfoot disease endemic area in Taiwan. *Br J Cancer* 53, 399-405.
- Chen, Y., and Rosen, B.P. (1997). Metalloregulatory properties of the ArsD repressor. *The Journal of biological chemistry* 272, 14257-14262.
- Cobine, P., Wickramasinghe, W.A., Harrison, M.D., Weber, T., Solioz, M., and Dameron, C.T. (1999). The *Enterococcus hirae* copper chaperone CopZ delivers copper(I) to the CopY repressor. *FEBS letters* 445, 27-30.

- Cobine, P.A., George, G.N., Jones, C.E., Wickramasinghe, W.A., Solioz, M., and Dameron, C.T. (2002). Copper transfer from the Cu(I) chaperone, CopZ, to the repressor, Zn(II)CopY: metal coordination environments and protein interactions. *Biochemistry* 41, 5822-5829.
- Cole, S.P., Sparks, K.E., Fraser, K., Loe, D.W., Grant, C.E., Wilson, G.M., and Deeley, R.G. (1994). Pharmacological characterization of multidrug resistant MRP-transfected human tumor cells. *Cancer research* 54, 5902-5910.
- Cullen, W.R., and Reimer, K.J. (1989). Arsenic speciation in the environment. *Chem Rev* 89, 713-764.
- Culotta, V.C., Klomp, L.W., Strain, J., Casareno, R.L., Krems, B., and Gitlin, J.D. (1997). The copper chaperone for superoxide dismutase. *The Journal of biological chemistry* 272, 23469-23472.
- Deeley, R.G., Westlake, C., and Cole, S.P. (2006). Transmembrane transport of endo- and xenobiotics by mammalian ATP-binding cassette multidrug resistance proteins. *Physiol Rev* 86, 849-899.
- Delnomdedieu, M., Basti, M.M., Otvos, J.D., and Thomas, D.J. (1994a). Reduction and binding of arsenate and dimethylarsinate by glutathione: a magnetic resonance study. *Chem Biol Interact* 90, 139-155.
- Delnomdedieu, M., Basti, M.M., Styblo, M., Otvos, J.D., and Thomas, D.J. (1994b). Complexation of arsenic species in rabbit erythrocytes. *Chemical research in toxicology* 7, 621-627.

- Dey, S., Dou, D., Tisa, L.S., and Rosen, B.P. (1994). Interaction of the catalytic and the membrane subunits of an oxyanion-translocating ATPase. *Archives of biochemistry and biophysics* 311, 418-424.
- Dey, S., and Rosen, B.P. (1995). Dual mode of energy coupling by the oxyanion-translocating ArsB protein. *J Bacteriol* 177, 385-389.
- Dhankher, O.P., Rosen, B.P., McKinney, E.C., and Meagher, R.B. (2006). Hyperaccumulation of arsenic in the shoots of Arabidopsis silenced for arsenate reductase (ACR2). *Proceedings of the National Academy of Sciences of the United States of America* 103, 5413-5418.
- Dhayalan, A., Jurkowski, T.P., Laser, H., Reinhardt, R., Jia, D., Cheng, X., and Jeltsch, A. (2008). Mapping of protein-protein interaction sites by the 'absence of interference' approach. *Journal of molecular biology* 376, 1091-1099.
- Duan, G.L., Zhou, Y., Tong, Y.P., Mukhopadhyay, R., Rosen, B.P., and Zhu, Y.G. (2007). A CDC25 homologue from rice functions as an arsenate reductase. *New Phytol* 174, 311-321.
- Ellis, D.R., Gumaelius, L., Indriolo, E., Pickering, I.J., Banks, J.A., and Salt, D.E. (2006). A novel arsenate reductase from the arsenic hyperaccumulating fern *Pteris vittata*. *Plant Physiol* 141, 1544-1554.
- EPA (1988). Special report on ingested inorganic arsenic. Skin cancer; nutritional essentiality. US Environmental Protection Agency, EPA/635/633-687/-613.
- Fahey, R.C., and Sundquist, A.R. (1991). Evolution of glutathione metabolism. In *Advances in Enzymology and Related Areas of Molecular Biology*, A. Meister, ed. (New York, Wiley and Sons, Inc.), pp. 1-53.

- Field, L.S., Luk, E., and Culotta, V.C. (2002). Copper chaperones: personal escorts for metal ions. *Journal of bioenergetics and biomembranes* 34, 373-379.
- Fields, S., and Song, O. (1989). A novel genetic system to detect protein-protein interactions. *Nature* 340, 245-246.
- Francesconi, K.A. (2005). current perspectives in arsenic environmental and biological research. *Environ Chem*, 141-145.
- Fu, H.L., Meng, Y., Ordonez, E., Villadangos, A.F., Bhattacharjee, H., Gil, J.A., Mateos, L.M., and Rosen, B.P. (2009). Properties of arsenite efflux permeases (Acr3) from *Alkaliphilus metalliredigens* and *Corynebacterium glutamicum*. *The Journal of biological chemistry* 284, 19887-19895.
- Gerber, J., Muhlenhoff, U., and Lill, R. (2003). An interaction between frataxin and Isu1/Nfs1 that is crucial for Fe/S cluster synthesis on Isu1. *EMBO reports* 4, 906-911.
- Ghosh, M., Shen, J., and Rosen, B.P. (1999). Pathways of As(III) detoxification in *Saccharomyces cerevisiae*. *Proceedings of the National Academy of Sciences of the United States of America* 96, 5001-5006.
- Gill, S.C., and von Hippel, P.H. (1989). Calculation of protein extinction coefficients from amino acid sequence data. *Analytical biochemistry* 182, 319-326.
- Gonzalez-Guerrero, M., and Arguello, J.M. (2008). Mechanism of Cu<sup>+</sup>-transporting ATPases: soluble Cu<sup>+</sup> chaperones directly transfer Cu<sup>+</sup> to transmembrane transport sites. *Proceedings of the National Academy of Sciences of the United States of America* 105, 5992-5997.

- Gresser, M.J. (1981). ADP-arsenate. Formation by submitochondrial particles under phosphorylating conditions. *The Journal of biological chemistry* 256, 5981-5983.
- Hamza, I., Schaefer, M., Klomp, L.W., and Gitlin, J.D. (1999). Interaction of the copper chaperone HAH1 with the Wilson disease protein is essential for copper homeostasis. *Proceedings of the National Academy of Sciences of the United States of America* 96, 13363-13368.
- He, Y., Alam, S.L., Proteasa, S.V., Zhang, Y., Lesuisse, E., Dancis, A., and Stemmler, T.L. (2004). Yeast frataxin solution structure, iron binding, and ferrochelatase interaction. *Biochemistry* 43, 16254-16262.
- Hei, T.K., Liu, S.X., and Waldren, C. (1998). Mutagenicity of arsenic in mammalian cells: role of reactive oxygen species. *Proceedings of the National Academy of Sciences of the United States of America* 95, 8103-8107.
- Higginson, J., and DeVita, V.T., Jr. (1980). IARC monographs on the evaluation of carcinogenic risk of chemicals to humans. *Am Ind Hyg Assoc J* 41, A26, A28, A30 passim.
- Hindmarsh, J.T., and McCurdy, R.F. (1986). Clinical and environmental aspects of arsenic toxicity. *Crit Rev Clin Lab Sci* 23, 315-347.
- Hirano, S., Kobayashi, Y., Cui, X., Kanno, S., Hayakawa, T., and Shraim, A. (2004). The accumulation and toxicity of methylated arsenicals in endothelial cells: important roles of thiol compounds. *Toxicology and applied pharmacology* 198, 458-467.
- Hook, B., Bernstein, D., Zhang, B., and Wickens, M. (2005). RNA-protein interactions in the yeast three-hybrid system: affinity, sensitivity, and enhanced library screening. *RNA (New York, NY)* 11, 227-233.



- Hsu, C.M., and Rosen, B.P. (1989). Characterization of the catalytic subunit of an anion pump. *J Biol Chem* 264, 17349-17354.
- Hua, S.B., Qiu, M., Chan, E., Zhu, L., and Luo, Y. (1997). Minimum length of sequence homology required for in vivo cloning by homologous recombination in yeast. *Plasmid* 38, 91-96.
- Huffman, D.L., and O'Halloran, T.V. (2000). Energetics of copper trafficking between the Atx1 metallochaperone and the intracellular copper transporter, Ccc2. *The Journal of biological chemistry* 275, 18611-18614.
- Hughes, M.F. (2002). Arsenic toxicity and potential mechanisms of action. *Toxicol Lett* 133, 1-16.
- Hung, I.H., Casareno, R.L., Labesse, G., Mathews, F.S., and Gitlin, J.D. (1998). HAH1 is a copper-binding protein with distinct amino acid residues mediating copper homeostasis and antioxidant defense. *The Journal of biological chemistry* 273, 1749-1754.
- Ji, G., Garber, E.A., Armes, L.G., Chen, C.M., Fuchs, J.A., and Silver, S. (1994). Arsenate reductase of *Staphylococcus aureus* plasmid pI258. *Biochemistry* 33, 7294-7299.
- Ji, G., and Silver, S. (1992). Reduction of arsenate to arsenite by the ArsC protein of the arsenic resistance operon of *Staphylococcus aureus* plasmid pI258. *Proceedings of the National Academy of Sciences of the United States of America* 89, 9474-9478.
- Kala, S.V., Neely, M.W., Kala, G., Prater, C.I., Atwood, D.W., Rice, J.S., and Lieberman, M.W. (2000). The MRP2/cMOAT transporter and arsenic-glutathione complex

- formation are required for biliary excretion of arsenic. *The Journal of biological chemistry* 275, 33404-33408.
- Kaur, P. (1999). The anion-stimulated ATPase ArsA shows unisite and multisite catalytic activity. *The Journal of biological chemistry* 274, 25849-25854.
- Kim, M.J., Nriagu, J., and Haack, S. (2002). Arsenic species and chemistry in groundwater of southeast Michigan. *Environ Pollut* 120, 379-390.
- Klopotowski, T., and Wiater, A. (1965). Synergism of aminotriazole and phosphate on the inhibition of yeast imidazole glycerol phosphate dehydratase. *Archives of biochemistry and biophysics* 112, 562-566.
- Kondapalli, K.C., Kok, N.M., Dancis, A., and Stemmler, T.L. (2008). Drosophila frataxin: an iron chaperone during cellular Fe-S cluster bioassembly. *Biochemistry* 47, 6917-6927.
- Kosower, N.S., Newton, G.L., Kosower, E.M., and Ranney, H.M. (1980). Bimane fluorescent labels. Characterization of the bimane labeling of human hemoglobin. *Biochim Biophys Acta* 622, 201-209.
- Kuroda, M., Dey, S., Sanders, O.I., and Rosen, B.P. (1997). Alternate energy coupling of ArsB, the membrane subunit of the Ars anion-translocating ATPase. *The Journal of biological chemistry* 272, 326-331.
- Kwok, E.Y., Severance, S., and Kosman, D.J. (2006). Evidence for iron channeling in the Fet3p-Ftr1p high-affinity iron uptake complex in the yeast plasma membrane. *Biochemistry* 45, 6317-6327.
- Laemmli, U.K. (1970). Cleavage of structural proteins during the assembly of the head of bacteriophage T4. *Nature* 227, 680-685.

- Lagunas, R. (1980). Sugar-arsenate esters: thermodynamics and biochemical behavior. *Archives of biochemistry and biophysics* 205, 67-75.
- Lamb, A.L., Torres, A.S., O'Halloran, T.V., and Rosenzweig, A.C. (2000). Heterodimer formation between superoxide dismutase and its copper chaperone. *Biochemistry* 39, 14720-14727.
- Lamb, A.L., Torres, A.S., O'Halloran, T.V., and Rosenzweig, A.C. (2001). Heterodimeric structure of superoxide dismutase in complex with its metallochaperone. *Nature structural biology* 8, 751-755.
- Larin, D., Mekios, C., Das, K., Ross, B., Yang, A.S., and Gilliam, T.C. (1999). Characterization of the interaction between the Wilson and Menkes disease proteins and the cytoplasmic copper chaperone, HAH1p. *The Journal of biological chemistry* 274, 28497-28504.
- Legare, D., Richard, D., Mukhopadhyay, R., Stierhof, Y.D., Rosen, B.P., Haimeur, A., Papadopoulou, B., and Ouellette, M. (2001). The Leishmania ATP-binding cassette protein PGPA is an intracellular metal-thiol transporter ATPase. *The Journal of biological chemistry* 276, 26301-26307.
- Leier, I., Jedlitschky, G., Buchholz, U., Cole, S.P., Deeley, R.G., and Keppler, D. (1994). The MRP gene encodes an ATP-dependent export pump for leukotriene C4 and structurally related conjugates. *The Journal of biological chemistry* 269, 27807-27810.
- Leipe, D.D., Wolf, Y.I., Koonin, E.V., and Aravind, L. (2002). Classification and evolution of P-loop GTPases and related ATPases. *Journal of molecular biology* 317, 41-72.

- Li, J., and Rosen, B.P. (2000). The linker peptide of the ArsA ATPase. *Mol Microbiol* 35, 361-367.
- Li, S., Chen, Y., and Rosen, B.P. (2001). Role of vicinal cysteine pairs in metalloid sensing by the ArsD As(III)-responsive repressor. *Molecular microbiology* 41, 687-696.
- Li, S., Rosen, B.P., Borges-Walmsley, M.I., and Walmsley, A.R. (2002). Evidence for cooperativity between the four binding sites of dimeric ArsD, an As(III)-responsive transcriptional regulator. *J Biol Chem* 277, 25992-26002.
- Lieberman, R.L., Kondapalli, K.C., Shrestha, D.B., Hakemian, A.S., Smith, S.M., Telser, J., Kuzelka, J., Gupta, R., Borovik, A.S., Lippard, S.J., *et al.* (2006). Characterization of the particulate methane monooxygenase metal centers in multiple redox states by X-ray absorption spectroscopy. *Inorg Chem* 45, 8372-8381.
- Lin, Y.F., Walmsley, A.R., and Rosen, B.P. (2006). An arsenic metallochaperone for an arsenic detoxification pump. *Proc Natl Acad Sci U S A* 103, 15617-15622.
- Lin, Y.F., Yang, J., and Rosen, B.P. (2007a). ArsD residues Cys12, Cys13, and Cys18 form an As(III)-binding site required for arsenic metallochaperone activity. *J Biol Chem* 282, 16783-16791.
- Lin, Y.F., Yang, J., and Rosen, B.P. (2007b). ArsD: an As(III) metallochaperone for the ArsAB As(III)-translocating ATPase. *Journal of bioenergetics and biomembranes* 39, 453-458.

- Liu, X.P., Narla, R.K., and Uckun, F.M. (2003). Organic phenyl arsonic acid compounds with potent antileukemic activity. *Bioorganic & medicinal chemistry letters* *13*, 581-583.
- Liu, Z., Boles, E., and Rosen, B.P. (2004a). Arsenic trioxide uptake by hexose permeases in *Saccharomyces cerevisiae*. *The Journal of biological chemistry* *279*, 17312-17318.
- Liu, Z., Carbrey, J.M., Agre, P., and Rosen, B.P. (2004b). Arsenic trioxide uptake by human and rat aquaglyceroporins. *Biochemical and biophysical research communications* *316*, 1178-1185.
- Liu, Z., Sanchez, M.A., Jiang, X., Boles, E., Landfear, S.M., and Rosen, B.P. (2006a). Mammalian glucose permease GLUT1 facilitates transport of arsenic trioxide and methylarsonous acid. *Biochemical and biophysical research communications* *351*, 424-430.
- Liu, Z., Shen, J., Carbrey, J.M., Mukhopadhyay, R., Agre, P., and Rosen, B.P. (2002). Arsenite transport by mammalian aquaglyceroporins AQP7 and AQP9. *Proceedings of the National Academy of Sciences of the United States of America* *99*, 6053-6058.
- Liu, Z., Styblo, M., and Rosen, B.P. (2006b). Methylarsonous acid transport by aquaglyceroporins. *Environmental health perspectives* *114*, 527-531.
- Martin, P., DeMel, S., Shi, J., Gladysheva, T., Gatti, D.L., Rosen, B.P., and Edwards, B.F. (2001). Insights into the structure, solvation, and mechanism of ArsC arsenate reductase, a novel arsenic detoxification enzyme. *Structure* *9*, 1071-1081.

- Mateja, A., Szlachcic, A., Downing, M.E., Dobosz, M., Mariappan, M., Hegde, R.S., and Keenan, R.J. (2009). The structural basis of tail-anchored membrane protein recognition by Get3. *Nature* 461, 361-366.
- McDermott, J.R., Jiang, X., Beene, L.C., Rosen, B.P., and Liu, Z. (2010). Pentavalent methylated arsenicals are substrates of human AQP9. *Biometals* 23, 119-127.
- Meharg, A.A., and Jardine, L. (2003). Arsenite transport into paddy rice (*Oryza sativa*) roots. *New Phytol* 157, 39-44.
- Meng, Y.L., Liu, Z., and Rosen, B.P. (2004). As(III) and Sb(III) uptake by GlpF and efflux by ArsB in *Escherichia coli*. *The Journal of biological chemistry* 279, 18334-18341.
- Messens, J., Hayburn, G., Desmyter, A., Laus, G., and Wyns, L. (1999). The essential catalytic redox couple in arsenate reductase from *Staphylococcus aureus*. *Biochemistry* 38, 16857-16865.
- Mukhopadhyay, R., and Rosen, B.P. (2002). Arsenate reductases in prokaryotes and eukaryotes. *Environmental health perspectives* 110 Suppl 5, 745-748.
- Mukhopadhyay, R., Rosen, B.P., Phung, L.T., and Silver, S. (2002). Microbial arsenic: from geocycles to genes and enzymes. *FEMS microbiology reviews* 26, 311-325.
- Mukhopadhyay, R., Shi, J., and Rosen, B.P. (2000). Purification and characterization of ACR2p, the *Saccharomyces cerevisiae* arsenate reductase. *The Journal of biological chemistry* 275, 21149-21157.
- Multhaup, G., Strausak, D., Bissig, K.D., and Solioz, M. (2001). Interaction of the CopZ copper chaperone with the CopA copper ATPase of *Enterococcus hirae*

- assessed by surface plasmon resonance. *Biochemical and biophysical research communications* 288, 172-177.
- Niu, C., Yan, H., Yu, T., Sun, H.P., Liu, J.X., Li, X.S., Wu, W., Zhang, F.Q., Chen, Y., Zhou, L., *et al.* (1999). Studies on treatment of acute promyelocytic leukemia with arsenic trioxide: remission induction, follow-up, and molecular monitoring in 11 newly diagnosed and 47 relapsed acute promyelocytic leukemia patients. *Blood* 94, 3315-3324.
- Odermatt, A., and Solioz, M. (1995). Two trans-acting metalloregulatory proteins controlling expression of the copper-ATPases of *Enterococcus hirae*. *The Journal of biological chemistry* 270, 4349-4354.
- Ordóñez, E., Letek, M., Valbuena, N., Gil, J.A., and Mateos, L.M. (2005). Analysis of genes involved in arsenic resistance in *Corynebacterium glutamicum* ATCC 13032. *Appl Environ Microbiol* 71, 6206-6215.
- Ordóñez, E., Thiyagarajan, S., Cook, J.D., Stemmler, T.L., Gil, J.A., Mateos, L.M., and Rosen, B.P. (2008). Evolution of metal(loid) binding sites in transcriptional regulators. *J Biol Chem* 283, 25706-25714.
- Peter, C., Laliberte, J., Beaudoin, J., and Labbe, S. (2008). Copper distributed by Atx1 is available to copper amine oxidase 1 in *Schizosaccharomyces pombe*. *Eukaryotic cell* 7, 1781-1794.
- Peters, G.R., McCurdy, R.F., and Hindmarsh, J.T. (1996). Environmental aspects of arsenic toxicity. *Crit Rev Clin Lab Sci* 33, 457-493.

- Pufahl, R.A., Singer, C.P., Peariso, K.L., Lin, S.J., Schmidt, P.J., Fahrni, C.J., Culotta, V.C., Penner-Hahn, J.E., and O'Halloran, T.V. (1997). Metal ion chaperone function of the soluble Cu(I) receptor Atx1. *Science (New York, NY)* **278**, 853-856.
- Qin, J., Fu, H.L., Ye, J., Bencze, K.Z., Stemmler, T.L., Rawlings, D.E., and Rosen, B.P. (2007). Convergent evolution of a new arsenic binding site in the ArsR/SmtB family of metalloregulators. *J Biol Chem* **282**, 34346-34355.
- Qin, J., Lehr, C.R., Yuan, C., Le, X.C., McDermott, T.R., and Rosen, B.P. (2009). Biotransformation of arsenic by a Yellowstone thermoacidophilic eukaryotic alga. *Proceedings of the National Academy of Sciences of the United States of America* **106**, 5213-5217.
- Qin, J., Rosen, B.P., Zhang, Y., Wang, G., Franke, S., and Rensing, C. (2006). Arsenic detoxification and evolution of trimethylarsine gas by a microbial arsenite S-adenosylmethionine methyltransferase. *Proceedings of the National Academy of Sciences of the United States of America* **103**, 2075-2080.
- Rae, T.D., Schmidt, P.J., Pufahl, R.A., Culotta, V.C., and O'Halloran, T.V. (1999). Undetectable intracellular free copper: the requirement of a copper chaperone for superoxide dismutase. *Science (New York, NY)* **284**, 805-808.
- Rahman, M.M., Ng, J.C., and Naidu, R. (2009). Chronic exposure of arsenic via drinking water and its adverse health impacts on humans. *Environ Geochem Health* **31 Suppl 1**, 189-200.
- Ramirez-Solis, A., Mukopadhyay, R., Rosen, B.P., and Stemmler, T.L. (2004). Experimental and theoretical characterization of arsenite in water: insights into the coordination environment of As-O. *Inorganic chemistry* **43**, 2954-2959.



- Rosen, B.P. (1999). Families of arsenic transporters. *Trends in microbiology* 7, 207-212.
- Rosen, B.P. (2002). Biochemistry of arsenic detoxification. *FEBS letters* 529, 86-92.
- Rosenberg, H., Gerdes, R.G., and Chegwidan, K. (1977). Two systems for the uptake of phosphate in *Escherichia coli*. *Journal of bacteriology* 131, 505-511.
- Rosenzweig, A.C. (2002). Metallochaperones: bind and deliver. *Chem Biol* 9, 673-677.
- Ruan, X., Bhattacharjee, H., and Rosen, B.P. (2006). Cys-113 and Cys-422 form a high affinity metalloid binding site in the ArsA ATPase. *The Journal of biological chemistry* 281, 9925-9934.
- Ruan, X., Bhattacharjee, H., and Rosen, B.P. (2008). Characterization of the metalloactivation domain of an arsenite/antimonite resistance pump. *Molecular microbiology* 67, 392-402.
- Sambrook, J., Fritsch, E.F., and Maniatis, T. (1989). *Molecular cloning, a laboratory manual* ( New York., Cold Spring Harbor Laboratory).
- Sanders, O.I., Rensing, C., Kuroda, M., Mitra, B., and Rosen, B.P. (1997). Antimonite is accumulated by the glycerol facilitator GlpF in *Escherichia coli*. *Journal of bacteriology* 179, 3365-3367.
- Sato, T., and Kobayashi, Y. (1998). The ars operon in the skin element of *Bacillus subtilis* confers resistance to arsenate and arsenite. *Journal of bacteriology* 180, 1655-1661.
- Scheindlin, S. (2005). The duplicitous nature of inorganic arsenic. *Mol Interv* 5, 60-64.
- Shi, H., Bencze, K.Z., Stemmler, T.L., and Philpott, C.C. (2008). A cytosolic iron chaperone that delivers iron to ferritin. *Science (New York, NY)* 320, 1207-1210.

- Shi, W., Dong, J., Scott, R.A., Ksenzenko, M.Y., and Rosen, B.P. (1996). The role of arsenic-thiol interactions in metalloregulation of the *ars* operon. *J Biol Chem* 271, 9291-9297.
- Shin, H., Shin, H.S., Dewbre, G.R., and Harrison, M.J. (2004). Phosphate transport in Arabidopsis: Pht1;1 and Pht1;4 play a major role in phosphate acquisition from both low- and high-phosphate environments. *Plant J* 39, 629-642.
- Smedley, P.L., and Kinniburgh, D.G. (2002). A review of the source, behaviour and distribution of arsenic in natural waters. *Applied Geochemistry* 17, 517-568.
- Smith, A.H., Hopenhayn-Rich, C., Bates, M.N., Goeden, H.M., Hertz-Picciotto, I., Duggan, H.M., Wood, R., Kosnett, M.J., and Smith, M.T. (1992). Cancer risks from arsenic in drinking water. *Environmental health perspectives* 97, 259-267.
- Sneader, W. (1985). *Drug discovery: The evolution of modern medicines*. (Chichester, England, John Wiley & Sons).
- Spuches, A.M., Kruszyna, H.G., Rich, A.M., and Wilcox, D.E. (2005). Thermodynamics of the As(III)-thiol interaction: arsenite and monomethylarsenite complexes with glutathione, dihydrolipoic acid, and other thiol ligands. *Inorg Chem* 44, 2964-2972.
- Szinicz, L., and Forth, W. (1988). Effect of As<sub>2</sub>O<sub>3</sub> on gluconeogenesis. *Arch Toxicol* 61, 444-449.
- Tamerler, C., Oren, E.E., Duman, M., Venkatasubramanian, E., and Sarikaya, M. (2006). Adsorption kinetics of an engineered gold binding Peptide by surface plasmon resonance spectroscopy and a quartz crystal microbalance. *Langmuir* 22, 7712-7718.

- Thomas, D.J., Waters, S.B., and Styblo, M. (2004). Elucidating the pathway for arsenic methylation. *Toxicology and applied pharmacology* 198, 319-326.
- Torres, A.S., Petri, V., Rae, T.D., and O'Halloran, T.V. (2001). Copper stabilizes a heterodimer of the yCCS metallochaperone and its target superoxide dismutase. *J Biol Chem* 276, 38410-38416.
- Tripathi, R.D., Srivastava, S., Mishra, S., Singh, N., Tuli, R., Gupta, D.K., and Maathuis, F.J. (2007). Arsenic hazards: strategies for tolerance and remediation by plants. *Trends Biotechnol* 25, 158-165.
- Tseng, W.P. (1977). Effects and dose--response relationships of skin cancer and blackfoot disease with arsenic. *Environmental health perspectives* 19, 109-119.
- Valentine, J.L., Campion, D.S., Schluchter, M.D., and Massey, F.J. (1982). Arsenic effects on human nerve conduction. (New York, Springer-Verlag).
- van Dongen, E.M., Klomp, L.W., and Merkx, M. (2004). Copper-dependent protein-protein interactions studied by yeast two-hybrid analysis. *Biochemical and biophysical research communications* 323, 789-795.
- Verstovsek, S., and Estrov, Z. (2004). Arsenic derivatives as therapeutic agents for hematologic malignancies. *Leuk Res* 28, 901-903.
- Vidal, M., Brachmann, R.K., Fattaey, A., Harlow, E., and Boeke, J.D. (1996). Reverse two-hybrid and one-hybrid systems to detect dissociation of protein-protein and DNA-protein interactions. *Proceedings of the National Academy of Sciences of the United States of America* 93, 10315-10320.

- Vogel, G., and Steinhart, R. (1976). ATPase of *Escherichia coli*: purification, dissociation, and reconstitution of the active complex from the isolated subunits. *Biochemistry* 15, 208-216.
- Walmsley, A.R., Zhou, T., Borges-Walmsley, M.I., and Rosen, B.P. (1999). The ATPase mechanism of ArsA, the catalytic subunit of the arsenite pump. *The Journal of biological chemistry* 274, 16153-16161.
- Walmsley, A.R., Zhou, T., Borges-Walmsley, M.I., and Rosen, B.P. (2001). A kinetic model for the action of a resistance efflux pump. *The Journal of biological chemistry* 276, 6378-6391.
- Wanibuchi, H., Yamamoto, S., Chen, H., Yoshida, K., Endo, G., Hori, T., and Fukushima, S. (1996). Promoting effects of dimethylarsinic acid on N-butyl-N-(4-hydroxybutyl)nitrosamine-induced urinary bladder carcinogenesis in rats. *Carcinogenesis* 17, 2435-2439.
- Williams, P.N., Price, A.H., Raab, A., Hossain, S.A., Feldmann, J., and Meharg, A.A. (2005). Variation in arsenic speciation and concentration in paddy rice related to dietary exposure. *Environ Sci Technol* 39, 5531-5540.
- Willsky, G.R., and Malamy, M.H. (1980). Effect of arsenate on inorganic phosphate transport in *Escherichia coli*. *Journal of bacteriology* 144, 366-374.
- Winski, S.L., and Carter, D.E. (1998). Arsenate toxicity in human erythrocytes: characterization of morphologic changes and determination of the mechanism of damage. *J Toxicol Environ Health A* 53, 345-355.

- Wu, J., and Rosen, B.P. (1993). The *arsD* gene encodes a second trans-acting regulatory protein of the plasmid-encoded arsenical resistance operon. *Mol Microbiol* 8, 615-623.
- Wu, M.M., Kuo, T.L., Hwang, Y.H., and Chen, C.J. (1989). Dose-response relation between arsenic concentration in well water and mortality from cancers and vascular diseases. *Am J Epidemiol* 130, 1123-1132.
- Wysocki, R., Bobrowicz, P., and Ulaszewski, S. (1997). The *Saccharomyces cerevisiae* ACR3 gene encodes a putative membrane protein involved in arsenite transport. *The Journal of biological chemistry* 272, 30061-30066.
- Wysocki, R., Chery, C.C., Wawrzycka, D., Van Hulle, M., Cornelis, R., Thevelein, J.M., and Tamas, M.J. (2001). The glycerol channel Fps1p mediates the uptake of arsenite and antimonite in *Saccharomyces cerevisiae*. *Molecular microbiology* 40, 1391-1401.
- Xu, X.Y., McGrath, S.P., Meharg, A.A., and Zhao, F.J. (2008). Growing rice aerobically markedly decreases arsenic accumulation. *Environ Sci Technol* 42, 5574-5579.
- Yager, J.W., and Wiencke, J.K. (1993). Enhancement of chromosomal damage by arsenic: implications for mechanism. *Environmental health perspectives* 101 Suppl 3, 79-82.
- Yager, J.W., and Wiencke, J.K. (1997). Inhibition of poly(ADP-ribose) polymerase by arsenite. *Mutat Res* 386, 345-351.
- Ye, J., Ajees, A.A., Yang, J., and Rosen, B.P. (2010). The 1.4 Å Crystal Structure of the ArsD Arsenic Metallochaperone Provides Insights into Its Interaction with the ArsAATPase. *Biochemistry*.

- Yehiayan, L., Pattabiraman, M., Konstantinos, K., Wang, X., Boise, L.H., and Cai, Y. (2009). Speciation, formation, stability and analytical challenges of human arsenic metabolites. *J Anal At Spectrom* 24, 1397-1405.
- Yoon, T., and Cowan, J.A. (2003). Iron-sulfur cluster biosynthesis. Characterization of frataxin as an iron donor for assembly of [2Fe-2S] clusters in ISU-type proteins. *Journal of the American Chemical Society* 125, 6078-6084.
- Zakharyan, R., Wu, Y., Bogdan, G.M., and Aposhian, H.V. (1995). Enzymatic methylation of arsenic compounds: assay, partial purification, and properties of arsenite methyltransferase and monomethylarsonic acid methyltransferase of rabbit liver. *Chemical research in toxicology* 8, 1029-1038.
- Zaman, G.J., Lankelma, J., van Tellingen, O., Beijnen, J., Dekker, H., Paulusma, C., Oude Elferink, R.P., Baas, F., and Borst, P. (1995). Role of glutathione in the export of compounds from cells by the multidrug-resistance-associated protein. *Proceedings of the National Academy of Sciences of the United States of America* 92, 7690-7694.
- Zavala, Y.J., and Duxbury, J.M. (2008). Arsenic in rice: I. Estimating normal levels of total arsenic in rice grain. *Environ Sci Technol* 42, 3856-3860.
- Zegers, I., Martins, J.C., Willem, R., Wyns, L., and Messens, J. (2001). Arsenate reductase from *S. aureus* plasmid pI258 is a phosphatase drafted for redox duty. *Nature structural biology* 8, 843-847.
- Zhang, X.W., Yan, X.J., Zhou, Z.R., Yang, F.F., Wu, Z.Y., Sun, H.B., Liang, W.X., Song, A.X., Lallemand-Breitenbach, V., Jeanne, M., *et al.* (2010). Arsenic trioxide

controls the fate of the PML-RARalpha oncoprotein by directly binding PML. Science (New York, NY 328, 240-243.

Zhou, T., Radaev, S., Rosen, B.P., and Gatti, D.L. (2000). Structure of the ArsA ATPase: the catalytic subunit of a heavy metal resistance pump. *Embo J* 19, 4838-4845.

Zhou, T., Radaev, S., Rosen, B.P., and Gatti, D.L. (2001). Conformational changes in four regions of the *Escherichia coli* ArsA ATPase link ATP hydrolysis to ion translocation. *The Journal of biological chemistry* 276, 30414-30422.

Zhou, T., and Rosen, B.P. (1997). Tryptophan fluorescence reports nucleotide-induced conformational changes in a domain of the ArsA ATPase. *The Journal of biological chemistry* 272, 19731-19737.

Zhou, T., Shen, J., Liu, Y., and Rosen, B.P. (2002). Unisite and multisite catalysis in the ArsA ATPase. *The Journal of biological chemistry* 277, 23815-23820.

Zhou, Y., Bhattacharjee, H., and Mukhopadhyay, R. (2006). Bifunctional role of the leishmanial antimonate reductase LmACR2 as a protein tyrosine phosphatase. *Molecular and biochemical parasitology* 148, 161-168.

**ABSTRACT****CHARACTERIZATION OF ArsD: AN ARSENIC  
CHAPERONE FOR ArsAB AS(III)-TRANSLOCATING ATPase**

by

**JIANBO YANG****August 2010****Advisor:** Dr. Barry P. Rosen**Major:** Biochemistry and Molecular Biology**Degree:** Doctor of Philosophy

Arsenic is a metalloid toxicant that is widely distributed throughout the earth's crust and causes a variety of health and environment problems. As an adaptation to arsenic-contaminated environments, organisms have developed resistance systems. In bacteria and archaea various *ars* operons encode ArsAB ATPases that pump the trivalent metalloids As(III) or Sb(III) out of cells. In these operons, an *arsD* gene is almost always adjacent to the *arsA* gene, suggesting a related function. ArsA is the catalytic subunit of the pump that hydrolyzes ATP in the presence of arsenite or antimonite. ArsB is a membrane protein which containing arsenite-conducting pathway. ArsA forms complex with ArsB, therefore ATP hydrolysis is coupled to extrusion of As(III) or Sb(III) through ArsB.

Most transition and heavy metal ions do not exist as free ions in the cytosol but are sequestered by a variety of proteins called metal ion chaperones, scaffolds or intracellular carriers. ArsD was recently shown to be a chaperone for transfer of cytosolic As(III) to the 583-residue ArsA ATPase, the catalytic subunit of the efflux pump. ArsD is a 120-residue protein with three conserved cysteine residues, Cys12, Cys13 and Cys18 required for chaperone activity. ArsA exhibits a low, basal rate of ATPase



activity in the absence of As(III) or Sb(III) and a higher, activated rate in their presence. ArsA has a high affinity metalloid binding site composed of Cys113 and Cys422 and a third residue, Cys172, which participates in high affinity binding and activation of ATP hydrolysis. By directly transferring As(III) to ArsA, ArsD also increased ArsA ATPase activity at environmental concentrations of arsenic. Therefore, ArsAB pump efficiency is increased and less As(III) will be accumulated in the cells. In analogy with the mechanism of copper transfer from chaperones to copper pumps or enzymes, a step-wise transfer of As(III) from the cysteines of ArsD to the cysteines of ArsA, was proposed.

The properties of As(III) binding by ArsD and subsequent transfer to ArsA were examined. X-ray absorption spectroscopy was used to show that As(III) is coordinated with three sulfur atoms, consistent with Cys12, Cys13 and Cys18 forming the As(III) binding site. An assay using intrinsic protein fluorescence was developed as a probe of metalloid binding to ArsD. Two single tryptophan derivatives of ArsD were constructed by changing either Thr15 or Val17 to tryptophan in a tryptophan-free background. Both exhibited quenching of fluorescence upon binding of As(III) or Sb(III), from which the apparent affinity for metalloid could be estimated. Since it is likely that cytosolic As(III) is bound to reduced glutathione (GSH), the effect of GSH on binding to ArsD was examined. GSH greatly increased the rate of binding As(III) to ArsD, suggesting that ArsD accepts metalloid from the As(GS)<sub>3</sub> complex. In contrast, GSH did not affect the As(III)-stimulated ArsA ATPase activity, suggesting that As(III) is directly transferred from ArsD to ArsA, as opposed to release from ArsD, binding to GSH and then interaction of ArsA with the As(GS)<sub>3</sub> complex. To differentiate between these two

possibilities, the effect of the As(III) chelator dimercaptosuccinic acid (DMSA) was examined. The chelator did not affect transfer, indicating channeling of As(III) from ArsD to ArsA. Transfer occurs only under conditions where ArsA hydrolyzes ATP, suggesting that ArsD transfer As(III) to an ArsA conformation transiently formed during catalysis and not simply to the closed conformation that ArsA adopts when As(III) and MgATP are bound.

R773 ArsD was shown to be a dimer in crystal structure. Whether the dimerization form is a physiological one existing in the solution, was studied by mutagenesis. Residues, Ser68, Arg87 and Arg96, involved in dimerization were mutated to alanine. ArsD dimerization equilibrium was shifted to the monomer direction by mutating these residues to alanine, but not totally a monomeric form. One mutant  $ArsD_{G86E}$  was selected from reverse yeast two-hybrid analysis, showing no dimerization with wild-type ArsD. Gel-filtration chromatography confirmed mutation G86E shifts ArsD dimerization equilibrium to the monomer direction, but not totally change ArsD to a monomeric form. Since Gly86 sits on the dimerization interface in the crystal structure, it is most likely the crystallographic ArsD dimer forms in the solution. All these mutants still retain the ability to stimulate ArsA ATPase activity, suggesting dimerization is not strictly required for ArsD metallochaperone function.

ArsA and ArsD crystal structure have been solved individually. But little is known about ArsA-ArsD interaction interface. Yeast two-hybrid and reverse yeast two-hybrid are combined to select for totally 14 ArsD mutants with weaker or stronger interaction with ArsA. Additionally, Lys37 and Lys62 were shown to be important for ArsD function by site-directed mutagenesis. ArsD loses function when Lys37 and Lys62 were mutated

to alanine as well as acetylated by Sulfo-NHS acetate. The charge carried by Lys37 and Lys6 was shown to be important since protein is still active when they are mutated to arginine. Yeast two-hybrid confirmed mutating Lys37 and Lys62 to alanine has effect on ArsA-ArsD interaction. Mapping all the mutations on ArsD structure gives us information on ArsA-ArsD interaction interface. Four residues, Ser14, Val17, Thr20 and Val22, are in the loop containing the important metal binding site Cys12-Cys13-Cys18. This suggests the metal binding site may be directly involved in the interaction with ArsA. Seven residues, Gln24, Val27, Asp28, Thr31, Gln34, Lys37 and Gln38 are located on helix  $\alpha$ 1. They are aligned at one side of helix  $\alpha$ 1 and solvent exposed, suggesting this region might be directly involved in interaction. A structure model of ArsA-ArsD complex was generated by docking. The model suggested an extensive interaction interface at multiple directions, consistent with most of the yeast two-hybrid results.

## AUTOBIOGRAPHICAL STATEMENT

### Jianbo Yang

5324 Scott Hall, 540 E. Canfield Ave.  
School of Medicine, Wayne State University  
Detroit, MI 48201  
jiyang@med.wayne.edu

### EDUCATION

---

- |           |   |
|-----------|---|
| 2005-2010 | Wayne State University, School of Medicine<br>Detroit, MI, USA<br><b>PhD</b> in Biochemistry and Molecule Biology, Aug 2010       |
| 2002-2005 | Nanjing University, School of Life Science<br>Nanjing, Jiangsu, China<br><b>MS</b> in Biochemistry and Molecule Biology, Jun 2005 |
| 1998-2002 | Nanjing University, School of Life Science<br>Nanjing, Jiangsu, China<br><b>BS</b> , Jul 2002                                     |

### HONORS & AWARDS

---

- |           |   |
|-----------|---|
| 2006      | Thomas C. Rumble Fellowship                             |
| 2004      | Guanghua Scholarship, Second Prize                      |
| 1999-2001 | People's Scholarship for Excellent Student, Third Prize |

### PUBLICATIONS

---

**Yang J**, Rosen BP. Mapping ArsD-ArsA interaction interface by genetic analysis. *In preparation*.

Ye, J., Abdul Ajees, A., **Yang, J.** and Rosen, B.P. The 1.4 Å crystal structure of the ArsD arsenic metallochaperone provides insights into its interaction with the ArsA ATPase. *Biochemistry*. 2010, *In press*.

**Yang J**, Rawat S, Stemmler T and Rosen BP. Arsenic binding and transfer by the ArsD As(III) metallochaperone. *Biochemistry*. 2010 May 4;49(17):3658-3666.

Lin YF, **Yang J**, Rosen BP. ArsD: an As(III) metallochaperone for the ArsAB As(III)-translocating ATPase. *J Bioenerg Biomembr*. 2007 Dec;39(5-6):453-458.

Lin YF, **Yang J**, Rosen BP. ArsD residues Cys12, Cys13, and Cys18 form an As(III)-binding site required for arsenic metallochaperone activity. *J Biol Chem*. 2007 Jun 8;282(23):16783-16791.

**Yang J**, Yao J, Chen L, Yang J. The Amino-terminal domain of integrin beta3 functions as a transcriptional activator in yeast. *Mol Cell Biochem*. 2006 Aug;288(1-2):1-5.